Continuous Tubular Crystallizer for the Preparation of Active Pharmaceutical Ingredients

Dissertation

to obtain the academic degree of ‘Doktor der technischen Wissenschaften’ at the
Graz University of Technology
by Dipl.-Ing. Rafael Johannes-Paul Eder
Graz, 2012

Institute for Process and Particle Engineering
Graz University of Technology
Graz, Austria
Research Center Pharmaceutical Engineering GmbH
Graz, Austria

Rafael Johannes-Paul Eder

Continuous Tubular Crystallizer for the Preparation
of Active Pharmaceutical Ingredients

Dissertation

First assessor and supervisor
Univ.-Prof. Dipl.-Ing. Dr.techn. Johannes G. Khinast
Institute for Process and Particle Engineering
Graz University of Technology
and
Research Center Pharmaceutical Engineering GmbH

Second assessor
Univ.-Prof. Dipl.-Ing. Dr.techn. Karl Gatterer
Institute of Physical and Theoretical Chemistry
Graz University of Technology

STATUTORY DECLARATION

I declare that I have authored this thesis independently, that I have not used other than the declared sources/resources, and that I have explicitly marked all material which has been quoted either literally or by content from the used sources.

April, 2012 ……..

Dipl.-Ing. Rafael Johannes-Paul Eder

EIDESSTATTLICHE ERKLÄRUNG

Ich erkläre an Eides statt, dass ich die vorliegende Arbeit selbstständig verfasst, andere als die angegebenen Quellen/Hilfsmittel nicht benutzt, und die den benutzten Quellen wörtlich und inhaltlich entnommenen Stellen als solche kenntlich gemacht habe.

April, 2012 ……..

Dipl.-Ing. Rafael Johannes-Paul Eder

Abstract

A tubular continuous-flow crystallizer has been developed in which the crystallization of active pharmaceutical ingredients (APIs) can be performed under controlled conditions. The tubular shape of the 15 to 25 m-long crystallizer with an inner diameter of 2 mm enables narrow residence time distribution of the crystals in the pipe and excellent temperature control in the radial direction and along the tubing. To completely minimize the residence time distribution a segmented air bubble – slurry flow was implemented in the process. Crystals entering the crystallizer simultaneously have identical growth conditions along the tubing and about the same time for crystal growth. Thus, high quality bulk product with narrow crystal size distributions was achieved.

The effects of varying flow rates, hence residence times, different seed loadings, as well as differently sized seeds on the product crystals have been investigated for the model substance acetylsalicylic acid crystallized from the corresponding ethanolic solution via cooling. All experiments resulted in considerably larger product crystals in comparison to the seeds despite short crystallization times of approximately 3 min.

Seeds were taken from storage vessels or were generated in situ in the tubing via ultrasound irradiation. Optionally, temperature cycling was employed to dissolve the large amount of fine crystals generated due to the direct precipitation. This allowed to yield larger product crystals.

Additionally to the experiments, simulations regarding the temperature, the supersaturation and the crystal growth were performed in order to get a better understanding of the process.

Kurzfassung

Der auf dem Wachstum von Impfkristallen in einem Rohr basierende Prozess ist ein vielseitiges, kontinuierliches Kristallisationskonzept. Es zeichnet sich vor allem dadurch aus, dass schnell und einfach in den Kristallisationsprozess eingegriffen werden kann. Zu den kritischen Prozessparametern, die je nach Bedarf angepasst werden können, gehören unter anderem die Beladung an Impfkristallen, die Konzentration und Temperatur der Wirkstofflösung, der Temperaturverlauf über die Länge, sowie die Fließgeschwindigkeit der Suspension durch das Rohr.

Als Modellsubstanz wurden Acetylsalicylsäure aus Ethanol durch Kühlen auskristallisiert. Impfkristalle werden entweder aus einem gerührten Vorratsbehälter entnommen oder mit Hilfe von Ultraschall im Rohr in Situ hergestellt. Optional können Temperatursprünge entlang des Rohres genutzt werden, um Feinstkristallanteile wie sie bei der direkten Prezipitation entstehen aufzulösen. Auf diese Art können größere Produktkristalle erzielt werden. Aufgrund des kleinen Rohrdurchmessers (wenige Millimeter) ist es möglich, die Temperatur längs des Rohres genau zu kontrollieren, und so einzustellen, dass ständig eine moderate Übersättigung der Lösung für das Kristallwachstum besteht. Darüber hinaus sorgt eine enge Verweilzeitverteilung der Kristalle im Rohr für eine schmale Korngrößenverteilung (KGV) der Produkte. Um diese Verweilzeitverteilung auf ein absolutes Minimum zu reduzieren wurde ein segmentierter Luftblasen-Suspensionsstrom im Rohr verwirklicht. In den Versuchen konnte trotz der kurzen Verweilzeiten von wenigen Minuten ein deutliches Wachstum der Impfkristalle erzielt werden. Mit temperierten Wasserbädern wurden flache Kühlverläufe eingestellt, wodurch Übersättigungsspitzen abgefangen werden konnten. Dadurch wurde Kristallneubildung aufgrund von Nukleation erfolgreich verhindert, welche aus hoher Übersättigung resultieren könnte. Zusammen mit der Vermeidung von Kristallabrieb (keine beweglichen Teile im Rohr) wurde dieserart die Entstehung von Feinstkristallen unterdrückt und eine hohe Produktgüte mit einer engen KGV erzielt. Unabhängiges Variieren einzelner kritischer Prozessparameter (Flussrate, Impfkristallbeladung, Temperaturgradient etc.) erlaubte es, deren Einfluss auf die Produktkristallgröße individuell zu bestimmen.

Um den Prozess besser verstehen und optimieren zu können, wurden Simulationen bezüglich des Temperaturverlaufs, der Übersättigung und des Kristallwachstums durchgeführt.

Danksagung

Ich bedanke mich für die wissenschaftliche Leitung und Betreuung durch Prof. Johannes Khinast und bei Prof. Gatterer für die zweite Beurteilung der Arbeit.
Weiters bedanke ich mich bei Michaela Cibulka und Silvia Heissenberger für die zahlreichen Hilfestellungen bei administrativen Notwendigkeiten.
Ich bedanke mich bei meinen Diplomandinnen und der gesamten Arbeitsgruppe für die gemeinsam verlebte Zeit -speziell für die nach der eigentlichen Kernzeit am Institut.
Besonderer Dank gilt meinen Eltern, Geschwistern und Verwandten, sowie engen Freunden für die Unterstützung und vor allem für die charmante Ablenkung von forschungs- und universitätsbezogenen Themen.

Rafael Eder
Graz, April 2012

Contents

1 Intorduction[a]

1.1 Bulk Crystallization from Solution

Crystallization is the formation of a solid phase from a solution, a melt, or from the gaseous phase.[1-3] The driving force for the generation of crystal nuclei (birth of nuclei) and the growth of crystals is supersaturation which is the difference between the thermodynamic equilibrium solubility of a solute in the solvent at a given set of conditions and the actual concentration.[4] Supersaturation can be achieved via evaporation of solvent, cooling, changing the solution composition (e.g., antisolvent: solvent that lowers the solubility of the solute and is miscible with the original solvent; addition of ions: common ion effect; addition of other components that lower the solubility of the solute.), and by forming a product with lower solubility than the starting material (reactive crystallization).[1-3]

The steps that lead to the solid crystal products from the solution are the generation of supersaturation followed by nucleation, crystal growth, and if necessary the stabilization of the crystals followed by filtration and drying.

Crystallization is a common unit operation for solid-liquid phase separation and purification in many industrial areas[5-8] and of course it is also a widespread process in the production lines of fine chemicals and the pharmaceutical industry.[6;9-13] Next to purity[14] further quality attributes of interest are crystal size and shape as well as the corresponding distributions,[15] the distinct crystal form[16;17] that denotes the regular arrangement of the molecules in the crystal lattice and in the broader sense also the incorporation of solvent molecules into the lattice (i.e., solvates). Clearly, the crystal shape[18;19] and the size distribution (CSSD)[18;20] have an important influence on downstream processes[21-23] such as filtering,[22;24] centrifugation, washing, drying[21;22;24] and shelf life stability.[22] Flowability,[21] dusting,[21] agglomeration, and blending characteristics[25] are affected by the crystal quality. Also granulation,[25] compaction,[25] and coating properties are dependent on particle shape and PSD (Particle Size Distribution).

The distinct crystal form may affect physical, chemical and mechanical material properties[26] such as solubility -thus bioavailability-,[27] density[27] and mechanical

[a] The chapter 1 of this work is to some extend based on the FWF proposal 'Development of a versatile continuous-flow crystallizer' by Khinast, Eder and Kutschera. Here it has to be acknowledged that the scientific part was mainly written by the author of this thesis and that the FWF proposal itself is based on two publications of which the author of this thesis was the principle writer (Eder et al. 2010 & 2011).

strength which are very important for handling and storage of the product. Furthermore, the distinct crystal form may have and influence on the morphology of a crystal[28] and therefore may readily compromise downstream efficiency after the crystallization.

Since the formation of particles from solution is influenced by many factors (i.e., pH, temperature and temperature gradients, concentration and gradients, solvents, surfactants, impurities, agitation etc.) that can have impact on size, shape, polymorphism, and imperfections,[1-3] crystallization is a complex unit operation.

Getting things right in the crystallization process has great impact on the downstream process efficiency and the product quality!

Thus, it is important to tightly control a crystallization process.

1.2 Motivation

Highly purified solid organic particles are important products of many industries, including the fine-chemical, pharmaceutical and food industry.[29;30] In the fine-chemical and pharmaceutical industry, products are typically synthesized in the liquid phase, using multiple steps. The main goal of crystallization is to produce – as the final step of the synthesis - solid particles with defined shape and size in an efficient, high-yield process.[29;31-34] Other objectives include the (i) purification of the product,[2;5-7;9;10] (ii) polymorphism control,[27;35] and (iii) tailoring of the compounds' particle properties as well as stability.[31]

In this context size-, shape- and polymorphism-control is designated "crystal engineering", a field that is increasingly receiving attention. For example, the shape of particles has a major impact on the flowability of the powder, which (in case of the pharmaceutical industry) determines if particles can be used for direct compression or if complex particle control steps, such as agglomeration, are required prior to compression. In this example, crystal engineering would focus on the production of close-to-spherical crystals, as they exhibit a better flowability compared to their non-spherical counterparts (e.g., needles and plates).[36] Other properties – such as polymorphic modification – may be engineered as well and need to be addressed in the development of crystallization processes. Clearly, all of the above-mentioned crystal properties (shape, size,[37] crystal structure modification,[38] etc.) have a major impact on the final product's quality attributes (QAs). In the case of the pharmaceutical industry the products are granulates or tablets, where the QAs

include the dissolution and disintegration rate.[21] Other important QAs are the storage stability or the compactibility or tabletability of granules, all of which depend to a various degree on the crystal properties.[39] In addition, the costs and the efficiency of down-stream processes[20;40] (e.g., filtration and drying[6]) depend on the crystal quality.

Table 1-1. Economic significance of crystallized substances

Product	Area	Production Rate [t/a]	Value [Mio. €]
Sodium Chloride	EU	38,348,000	2300.1
Sugar	EU	15,000,000	6280.5
Caprolactam	Worldwide	3,5000,000	3850.0
Potassium Chloride	EU	4,150,000	450.7
Isomaltulose	Worldwide	50,000	100.0

Thus, it is essential to ensure both - excellent product quality and high yields.[29] Tight process control and optimized process conditions are a pre-requisite for this.

As indicated above, a vast number of solid products with varying bulk properties are produced via crystallization. Table 1-1 shows yearly production rates and the economic relevance of a few common substances. Compared to active pharmaceutical ingredients (APIs) these products have a low price per ton but huge yearly production rates. Table 1-2[b] summarizes the total yearly sales of a few blockbuster drugs (i.e., drugs that have yearly sales exceeding 1 billion US$). The APIs in Table 1-2 are crystalline solids. Generally over 90% of the APIs are crystalline.[41;42] Thus, it is evident that crystallization in the pharmaceutical industry is of high economic importance.

Table 1-2. Crystalline blockbuster drugs

Brand Name	Drug Substance	Value [Billion. US$]
Lipitor	Atrovastatin Ca	6.26
Effexor	Venlafaxine HCl	2.4
Zoloft	Sertraline HCl	2.14
Pravachol	Pravastatin Na	~2.5
Zithromax	Azithromycin	~2.0
Protonix	Pantoprazole Na	~2.2

1.2.1 Continuous vs. Batch Manufacturing

Several advantages are associated with batch processing for high-value added products, including the flexible way of implementing and maintaining equipment, the suitability for toxic or viscous substances, and – in case of crystallization - the

[b] Data stems from the APV-course on crystallization in the pharmaceutical industry (Berlin, 2010).

possibility to obtain larger crystals[43] for systems that exhibit slow crystal growth.[44] Nevertheless, continuous processes offer significant benefits, including:

- better control of the process conditions, effectively eliminating batch-to-batch variability[41]
- increased equipment use (over-all asset effectiveness, currently being at around 10-30%)
- faster throughput times (production to market time: currently 100-300 days vs. a few days in continuous manufacturing)
- no need for scale-up steps in development, as even bench-top continuous systems can often produce the desired quantities or scale-up is done by numbering up.[29]

In Figure 1-1, the advantages and disadvantages of continuous manufacturing are summarized.

Figure 1-1. Comparison of batch vs. continuous

In recent years, significant efforts towards continuous manufacturing have been initiated by pharmaceutical companies. For example, in 2007 Novartis provided the Massachusetts Institute of Technology (MIT) with a $ 65 Million grant to develop continuous processes for pharmaceutical manufacturing.[42] Further drivers for the implementation of continuous manufacturing in the pharmaceutical industry are the Process Analytical Technology (PAT) initiative of the Federal Drug Administration (FDA) and the Quality-by-Design (QbD) approach by the International Conference of Harmonization (ICH, Q8-Q10).

While the synthesis in continuous reactors (e.g., continuously stirred tanks, slurry reactors, plug-flow reactors, fixed-bed reactors, static mixers, spinning-disc reactors, micro-reactor systems and many more) has been at the forefront of scientific interest for years, comparably little efforts have been devoted towards continuous crystallization and continuous crystal engineering. Similarly, in secondary manufacturing, i.e., the manufacturing steps that turn an API into a drug product, continuous manufacturing (i.e., compaction, capsule filling, roller compaction, packaging) has been established for many years (blending, feeding, coating and wet granulation may be the exception). Evidently, continuous crystallization constitutes a

gap between continuous primary and secondary manufacturing. Thus, this step – which is the last step in primary drug manufacturing – is the focus of the proposed work.

1.2.2 Background on Continuous API Crystallization

In the industrial practice, a vast number of active pharmaceutical ingredients (APIs) with varying desired bulk properties are produced via crystallization. As a consequence, countless crystallizer types and methods are available.[45] A classification can either be based on how super-saturation is created (i.e., by evaporation, cooling, reaction, change of solvent composition, etc.) or on the processes characteristics (i.e., batch or continuous operation).[29] Like in other fields of chemical process engineering, continuous processing is also becoming a trend in crystallization,[45] as there are several disadvantages of batch crystallizers. These include the difficulty of integrating batch crystallizers in a continuous synthesis environment, the need to scale-up, the changing conditions during the crystallization, leading to batch-to-batch variability and others. Continuous crystallization, in combination with sophisticated process-analytical tools, allows the precise control of crystallization conditions, and thus, control of the size, shape and polymorphism. Therefore enhanced reproducibility is possible.[46]

In addition, economic pressure has become a dominant driver in the pharmaceutical industry. As continuous processes are often less cost-intensive compared to their batch counterparts (operating and capital cost reductions of up to 70% have been reported), research focusing on continuous crystal production and control is of significant interest to the scientific community and the industry. One example for the continuous production of active pharmaceutical ingredient (API) particles is impinging jet precipitation for the generation of micro-particles, e.g., by Midler et al.[47] and Brenek et al.[48] In addition, micro-reactor technology has been shown to have several benefits (e.g., scale-up via numbering up and a tight reaction control)[42] and was therefore adopted for the continuous production of particles. However, the application of micro-systems for the production of solid products has, so far, almost exclusively been limited to inorganic nanoparticles.[42] Exceptions are the patents of Myerson[49] on organic nano-particles and the work by Su et al.,[50] as well as the reports by Dombrowski et al. (alpha-lactose monohydrate),[51] and Gerdts et al.[52] (proteins) where organic particles have been formed in micro-structured channels. Raphael et al.[53] described the precipitation of sunflower proteins, Riviera et al.[54] of

pentaerythritol tetranitrate and Stahl et al.[55] of benzoic acid in a tubular device with an inner diameter in the milimeter range. A patent by Schiewe and Zierenberg (Boehringer Ingelheim AG)[56] describes the continuous production of inhalable drug particles in a size range from 0.3-20 µm. These particles are precipitated in tube-like channels similar to a segmented flow tubular reactor,[57-59] where a stream of alternating segments of a solution and transport medium (e.g., gas or oil), which is not miscible with the solution, is produced in order to achieve a very narrow residence time distribution. In addition, Méndez del Rio and Rousseau[60] reported the use of a tubular device for tubular-batch crystallization. The tubing was used to rapidly cool the solution. After primary nucleation the paracetamol crystals grew in the stirred receiving vessel. Other approaches include the crystallization in stirred tank cascades, for example at Novartis.

Lately, new crystallization equipment has been described in literature, such as the continuous baffled crystallizer,[61] or the recent work on continuous plug flow crystallization for drug compounds by Alvarez and Myerson[41] and the laminar flow device by Eder et al.[29;31-34] This underlines that continuous crystallization in pharmaceutical applications is a research area of increasing interest and is critical for implementation of over-all continuous API manufacturing.

1.3 Objective of this Thesis

The thesis encompasses the development and study of a flexible, continuously operated crystallizer system, which is based on the growth of seeds to product particles in a tubular flow system, featuring precise control of the temperature trajectory, supersaturation profile, residence time (e.g., by segmented gas-liquid flow) and solute concentration.

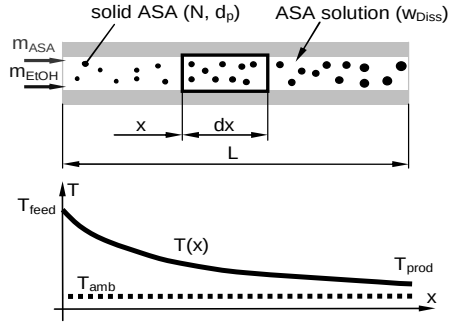

Figure 1-2. Schematic of the crystal growth in the tubular crystallizer and the temperature profile. *Ref*: Eder et al., Crystal Growth & Design, 2010

The principle has successfully been demonstrated for acetylsalicylic acid (ASA) (Eder et al.[29;31-34]). In Figure 1-2 the continuous tubular crystallizer (CTC) is shown schematically. The ASA seed crystals enter the tubing with a defined amount of solid particles (N) with the diameter (d_p) and a defined mass fraction of dissolved ASA (w_{Diss}). The driving force for crystal growth is supersaturation, which is created due to cooling of the feed-suspension (magma) from the feed temperature (T_{feed}) to the

product temperature (T_{prod}) along the temperature gradient T_x. Thus, the particles grow while moving through the tubular reactor.

1.4 References

(1) Myerson, A. S. *Handbook of Industrial Crystallization*; Butterworth-Heinemann: Boston Oxford Johannesburg Melbourne New Delhi Singapore, 2002.

(2) Mullin, J. W. *Crystallization*; Butterworth-Heinemann: Oxford Boston Johannesburg Melbourne New Delhi Singapore, 1992.

(3) Hofmann Guenter *Kristallisation in der Industriellen Praxis*; Wiley-VCH: Weinheim, 2004.

(4) Ward, J. D.; Mellichamp, D. A.; Doherty, M. F. Choosing an operating policy for seeded batch crystallization. *Aiche Journal* **2006**, *52*, 2046-2054.

(5) Ulrich, J. Solution crystallization - Developments and new trends. *Chemical Engineering & Technology* **2003**, *26*, 832-835.

(6) Barrett, P.; Smith, B.; Worlitschek, J.; Bracken, V.; O'Sullivan, B.; O'Grady, D. A review of the use of process analytical technology for the understanding and optimization of production batch crystallization processes. *Organic Process Research & Development* **2005**, *9*, 348-355.

(7) Lindenberg, C.; Krattli, M.; Cornel, J.; Mazzotti, M.; Brozio, J. Design and Optimization of a Combined Cooling/Antisolvent Crystallization Process. *Crystal Growth & Design* **2009**, *9*, 1124-1136.

(8) Simon, L. L.; Oucherif, K. A.; Nagy, Z. K.; Hungerbuhler, K. Histogram Matching, Hypothesis Testing, and Statistical Control-Chart-Assisted Nucleation Detection Using Bulk Video Imaging for Optimal Switching between Nucleation and Seed Conditioning Steps. *Industrial & Engineering Chemistry Research* **2010**, *49*, 9932-9944.

(9) Hammond, R. B.; Pencheva, K.; Ramachandran, V.; Roberts, K. J. Application of grid-based molecular methods for modeling solvent-dependent crystal growth morphology: Aspirin crystallized from aqueous ethanolic solution. *Crystal Growth & Design* **2007**, *7*, 1571-1574.

(10) Togkalidou, T.; Braatz, R. D.; Johnson, B. K.; Davidson, O.; Andrews, A. Experimental design and inferential modeling in pharmaceutical crystallization. *Aiche Journal* **2001**, *47*, 160-168.

(11) Simon, L. L.; Nagy, Z. K.; Hungerbuhler, K. Endoscopy-Based in Situ Bulk Video Imaging of Batch Crystallization Processes. *Organic Process Research & Development* **2009**, *13*, 1254-1261.

(12) Shekunov, B. Y.; York, P. Crystallization processes in pharmaceutical technology and drug delivery design. *Journal of Crystal Growth* **2000**, *211*, 122-136.

(13) Fevotte, G. New perspectives for the on-line monitoring of pharmaceutical crystallization processes using in situ infrared spectroscopy. *International Journal of Pharmaceutics* **2002**, *241*, 263-278.

(14) Lekhal, A.; Girard, K. P.; Brown, M. A.; Kiang, S.; Khinast, J. G.; Glasser, B. J. The effect of agitated drying on the morphology of L-threonine (needle-like) crystals. *International Journal of Pharmaceutics* **2004**, *270*, 263-277.

(15) Lekhal, A.; Girard, K. P.; Brown, M. A.; Kiang, S.; Glasser, B. J.; Khinast, J. G. Impact of agitated drying on crystal morphology: KCl-water system. *Powder Technology* **2003**, *132*, 119-130.

(16) Woo, X. Y.; Nagy, Z. K.; Tan, R. B. H.; Braatz, R. D. Adaptive Concentration Control of Cooling and Antisolvent Crystallization with Laser Backscattering Measurement. *Crystal Growth & Design* **2009**, *9*, 182-191.

(17) bu Bakar, M. R.; Nagy, Z. K.; Rielly, C. D. Seeded Batch Cooling Crystallization with Temperature Cycling for the Control of Size Uniformity and Polymorphic Purity of Sulfathiazole Crystals. *Organic Process Research & Development* **2009**, *13*, 1343-1356.

(18) Eggers, J.; Kempkes, M.; Mazzotti, M. Measurement of size and shape distributions of particles through image analysis. *Chemical Engineering Science* **2008**, *63*, 5513-5521.

(19) Kempkes, M.; Vetter, T.; Mazzotti, M. Measurement of 3D particle size distributions by stereoscopic imaging. *Chemical Engineering Science* **2010**, *65*, 1362-1373.

(20) Shekunov, B. Y.; Chattopadhyay, P.; Tong, H. H. Y.; Chow, A. H. L. Particle size analysis in pharmaceutics: Principles, methods and applications. *Pharmaceutical Research* **2007**, *24*, 203-227.

(21) Oullion, M.; Puel, F.; Fevotte, G.; Righini, S.; Carvin, P. Industrial batch crystallization of a plate-like organic product. In situ monitoring and 2D-CSD modelling. Part 2: Kinetic modelling and identification. *Chemical Engineering Science* **2007**, *62*, 833-845.

(22) Fujiwara, M.; Nagy, Z. K.; Chew, J. W.; Braatz, R. D. First-principles and direct design approaches for the control of pharmaceutical crystallization. *Journal of Process Control* **2005**, *15*, 493-504.

(23) bu Bakar, M. R.; Nagy, Z. K.; Saleemi, A. N.; Rielly, C. D. The Impact of Direct Nucleation Control on Crystal Size Distribution in Pharmaceutical Crystallization Processes. *Crystal Growth & Design* **2009**, *9*, 1378-1384.

(24) Lung-Somarriba, B. L. M.; Moscosa-Santillan, M.; Porte, C.; Delacroix, A. Effect of seeded surface area on crystal size distribution in glycine batch cooling crystallization: a seeding methodology. *Journal of Crystal Growth* **2004**, *270*, 624-632.

(25) Kim, S.; Lotz, B.; Lindrud, M.; Girard, K.; Moore, T.; Nagarajan, K.; Alvarez, M.; Lee, T.; Nikfar, F.; Davidovich, M.; Srivastava, S.; Kiang, S. Control of the

particle properties of a drug substance by crystallization engineering and the effect on drug product formulation. *Organic Process Research & Development* **2005**, *9*, 894-901.

(26) Zhang, G. G. Z.; Law, D.; Schmitt, E. A.; Qiu, Y. H. Phase transformation considerations during process development and manufacture of solid oral dosage forms. *Advanced Drug Delivery Reviews* **2004**, *56*, 371-390.

(27) Doki, N.; Yokota, M.; Kido, K.; Sasaki, S.; Kubota, N. Reliable and selective crystallization of the metastable alpha-form glycine by seeding. *Crystal Growth & Design* **2004**, *4*, 103-107.

(28) Spruijtenburg, R. Examples of the selective preparation of a desired crystal modification by an appropriate choice of operating parameters. *Organic Process Research & Development* **2000**, *4*, 403-406.

(29) Eder, R. J. P.; Radl, S.; Schmitt, E.; Innerhofer, S.; Maier, M.; Gruber-Woelfler, H.; Khinast, J. G. Continuously Seeded, Continuously Operated Tubular Crystallizer for the Production of Active Pharmaceutical Ingredients. *Crystal Growth & Design* **2010**, *10*, 2247-2257.

(30) Tavare, N. S.; Matsuoka, M.; Garside, J. Modelling a continuous column crystallizer: Dispersion and growth characteristics of a cooling section. *Journal of Crystal Growth* **1990**, 1151-1155.

(31) Eder, R. J. P.; Schmitt, E. K.; Grill, J.; Radl, S.; Gruber-Woelfler, H.; Khinast, J. G. Seed loading effects on the mean crystal size of acetylsalicylic acid in a continuous-flow crystallization device. *Crystal Research and Technology* **2011**, *46*, 227-237.

(32) Eder, R. J. P.; Schmitt, E.; Grill, J.; Maier, M.; Innerhofer, S.; Radl, S.; Gruber-Wölfler, H.; Khinast, J. G. Crystallization of APIs in a Continuously Seeded Tubular Crystallizer. *Scientia Pharmaceutica* **2010**, *78*, 664.

(33) Eder, R. J. P.; Gruber-Woelfler, H.; Khinast, J. G. Kontinuierliche Kristallisation in einem Rohrkristallisator. *Chemie Ingenieur Technik* **2009**, *81*, 1171.

(34) Eder, R. J. P.; Schmitt, E.; Grill, J.; Radl, S.; Gruber-Wölfler, H.; Khinast, J. G. Kontinuierliches Wachstum von API Impf- zu Produktkristallen in einem Rohrkristallisator. *Chemie Ingenieur Technik* **2010**, *82*, 1469-1470.

(35) Chow, K.; Tong, H. H. Y.; Lum, S.; Chow, A. H. L. Engineering of pharmaceutical materials: An industrial perspective. *Journal of Pharmaceutical Sciences* **2008**, *97*, 2855-2877.

(36) Goczo, H.; Szabo-Revesz, P.; Farkas, B.; Hasznos-Nezdei, M.; Serwanis, S. F.; Pintye-Hodi, K.; Kasa, P.; Eros, I.; Antal, I.; Marton, S. Development of spherical crystals of acetylsalicylic acid for direct tablet-making. *Chemical & Pharmaceutical Bulletin* **2000**, *48*, 1877-1881.

(37) Barrett, P.; Glennon, B. In-line FBRM monitoring of particle size in dilute agitated suspensions. *Particle & Particle Systems Characterization* **1999**, *16*, 207-211.

(38) Wang, J.; Loose, C.; Baxter, J.; Cai, D. W.; Wang, Y. L.; Tom, J.; Lepore, J. Growth promotion by H2O in organic solvent-selective isolation of a target polymorph. *Journal of Crystal Growth* **2005**, *283*, 469-478.

(39) Winn, D.; Doherty, M. F. Modeling crystal shapes of organic materials grown from solution. *Aiche Journal* **2000**, *46*, 1348-1367.

(40) Sarkar, D.; Rohani, S.; Jutan, A. Multi-objective optimization of seeded batch crystallization processes. *Chemical Engineering Science* **2006**, *61*, 5282-5295.

(41) Alvarez, A. j.; Myerson, A. S. Continuous Plug Flow Crystallization of Pharmaceutical Compounds. *Crystal Growth & Design* **2010**, *10*, 2219-2228.

(42) Variankaval, N.; Cote, A. S.; Doherty, M. F. From form to function: Crystallization of active pharmaceutical ingredients. *Aiche Journal* **2008**, *54*, 1682-1688.

(43) Mersmann, A. Crystallization and precipitation. *Chemical Engineering and Processing* **1999**, *38*, 345-353.

(44) Oullion, M.; Puel, F.; Fevotte, G.; Righini, S.; Carvin, P. Industrial batch crystallization of a plate-like organic product. In situ monitoring and 2D-CSD modelling: Part 1: Experimental study. *Chemical Engineering Science* **2007**, *62*, 820-832.

(45) Gros, H.; Kilpio, T.; Nurmi, J. Continuous cooling crystallization from solution. *Powder Technology* **2001**, *121*, 106-115.

(46) Chen, J.; Sarma, B.; Evans, J. M. B.; Myerson, A. S. Pharmaceutical Crystallization. *Crystal Growth & Design* **2011**, *11*, 887-895.

(47) Midler, M. Jr.; Liu, P. D.; Paul, E. L.; Futran, M.; Whittington, E. F. A crystallization method to improve crystal structure and size. *EP* **1991**, *0461930A1*.

(48) Brenek, S. J.; AM Ende, D. J. Crystallization method and apparatus using and impinging plate assembly. *US Patent* **4 A.D.**, *0040098839*.

(49) Myerson, A. S. Molecular crystals of controlled size. *US Patent* **2003**, *0030170999*.

(50) Su, Y. F.; Kim, H.; Kovenklioglu, S.; Lee, W. Y. Continuous nanoparticle production by microfluldic-based emulsion, mixing and crystallization. *Journal of Solid State Chemistry* **2007**, *180*, 2625-2629.

(51) Dombrowski, R. D.; Litster, J. D.; Wagner, N. J.; He, Y. Crystallization of alpha-lactose monohydrate in a drop-based microfluidic crystallizer. *Chemical Engineering Science* **2007**, *62*, 4802-4810.

(52) Gerdts, C. J.; Tereshko, V.; Yadav, M. K.; Dementieva, I.; Collart, F.; Joachimiak, A.; Stevens, R. C.; Kuhn, P.; Kossiakoff, A.; Ismagilov, R. F. Time-controlled microfluidic seeding in nL-volume droplets to separate nucleation and growth stages of protein crystallization. *Angewandte Chemie-International Edition* **2006**, *45*, 8156-8160.

(53) Raphael, M.; Rohani, S.; Sosulski, F. Isoelectric Precipitation of Sunflower Protein in A Tubular Precipitator. *Canadian Journal of Chemical Engineering* **1995**, *73*, 470-483.

(54) Rivera, T.; Randolph, A. D. Model for Precipitation of Pentaerythritol Tetranitrate (Petn). *Industrial & Engineering Chemistry Process Design and Development* **1978**, *17*, 182-188.

(55) Stahl, M.; Alund, B. L.; Rasmuson, A. C. Reaction crystallization kinetics of benzoic add. *Aiche Journal* **2001**, *47*, 1544-1560.

(56) Schiewe, J.; Zierenberg, B. Process and apparatus for producing inhalable medicaments. *US Patent* **2003**, *2003/0015194A1*.

(57) Guillemet-Fritsch, S.; oun-Habbache, M.; Sarrias, J.; Rousset, A.; Jongen, N.; Donnet, M.; Bowen, P.; Lemaitre, J. High-quality nickel manganese oxalate powders synthesized in a new segmented flow tubular reactor. *Solid State Ionics* **2004**, *171*, 135-140.

(58) Vacassy, R.; Lemaitre, J.; Hofmann, H.; Gerlings, J. H. Calcium carbonate precipitation using new segmented flow tubular reactor. *Aiche Journal* **2000**, *46*, 1241-1252.

(59) Jones, A.; Rigopoulos, S.; Zauner, R. Crystallization and precipitation engineering. *Computers & Chemical Engineering* **2005**, *29*, 1159-1166.

(60) Méndez del Rio, J. R.; Rousseau, R. W. Batch and tubular-batch crystallization of paracetamol: Crystal size distribution and polymorph formation. *Crystal Growth & Design* **2006**, *6*, 1407-1414.

(61) Lawton, S.; Steele, G.; Shering, P.; Zhao, L. H.; Laird, I.; Ni, X. W. Continuous Crystallization of Pharmaceuticals Using a Continuous Oscillatory Baffled Crystallizer. *Organic Process Research & Development* **2009**, *13*, 1357-1363.

2 Continuously Seeded, Continuously Operated Tubular Crystallizer for the Production of Active Pharmaceutical Ingredients[c]

Abstract. A continuously operated tubular crystallizer system with an inner diameter of 2.0 mm has been successfully operated. It allows the crystallization of active pharmaceutical ingredients (APIs) under controlled conditions. Acetylsalicylic acid (ASA) which was crystallized from ethanol (EtOH), was used as the model substance. An ethanolic suspension of ASA-seeds was fed into the tubular crystallizer system, where it was mixed with a slightly undersaturated ASA-EtOH solution that was kept at an elevated temperature in its storage vessel. Supersaturation was created via cooling and the seeds grew to form the product crystals. This chapter mainly focuses on the proof-of-concept and on the impact of the flow rates on the product crystals and the crystal size distribution (CSD). All other parameters including, concentrations, temperatures, and loading of seeds were kept constant. Higher flow velocities generally resulted in reduced number and volume mean diameters, due to reduced tendency of agglomeration and decreased time for crystal growth due to shorter residence times of the suspension in the tube. Generally, all experiments unmistakably led to shifting of volume density distributions towards significantly larger values for product crystals in comparison to the seeds and were capable of yielding product masses in a g/min scale.

[c] This chapter is based on a journal article by Eder et al. in Crystal Growth and Design in 2010.

2.1 Introduction

Highly purified organic materials are essential in various fields, including the fine-chemical, pharmaceutical and food industry.[1;2] Crystallization from solution is a common unit operation for phase separation and the purification of solid particles[3-9] due to the high efficiency and the relatively low capital and operating costs.[6] Other objectives of a crystallization process include polymorphism control,[10;11] control of the crystal size and shape distribution,[11] and the stability of the compounds. These factors need to be addressed in the development of crystallization processes.[12] Clearly, all of the above mentioned parameters have a major impact on the product quality attributes. In the case of a drug product these quality attributes include dissolution and disintegration rate.[13] Furthermore, properties such as flowability, storage characteristics, segregation phenomena, dusting,[13;14] compactibility or tabletability are a function of the aforementioned properties.[15] In addition, the costs and the efficiency of down-stream processes[16;17] (e.g., filtration and drying[6;18]) depend on the crystal quality. Therefore, tight process control and optimized process conditions are essential to ensure excellent product quality and high yields.

In the industrial practice, a vast number of solid products with varying desired bulk properties are produced via crystallization. As a consequence, countless crystallizer types and methods are available.[19] A classification can either be based on how super-saturation is created (i.e., by evaporation, cooling, reaction, change of solvent composition, etc.), or on the processes characteristics (i.e., batch or continuous operation).

Several advantages are associated with batch processing for high-value added products, including the flexible way of implementing and maintaining equipment, the suitability for toxic or viscous substances, and the possibility to obtain larger crystals for systems that exhibit slow crystal growth.[14] However, like in other fields of chemical process engineering, continuous processing is a trend in crystallization,[19] as continuous processes offer significant benefits, including:

- better control of the optimal process conditions, effectively eliminating batch-to-batch variability,
- shorter down times, and the
- lack of scale-up problems, since even bench-top continuous systems can often produce the desired quantities required in the pharmaceutical or fine-chemicals industry.

In some cases, smaller equipment size may be an advantage, although this may be offset by additional facilities and instrumentation. However, in pharmaceutical manufacturing implementation of continuous processes is still held back due to the regulatory framework. One of the few examples for the continuous production of active pharmaceutical ingredient (API) particles are impinging jet precipitations for the generation of micro-particles, as described by Midler et al.[20] and Brenek et al.[21] In addition, micro-reactor technology has been shown to have several benefits (e.g., scale-up via numbering up and a tight reaction control)[22] and was adopted for the continuous production of particles. However, the application of micro-systems for the production of solid products has, so far, almost exclusively been limited to inorganic nanoparticles.[22] Exceptions for example are the patents of Myerson[23] on organic nano-particles and Su,[24] as well as the reports by Dombrowski et al. (alpha-lactose monohydrate),[25] and Gerdts et al. (proteins)[26] where organic particles have been formed in micro-structured channels. Another patent by Schiewe et al.[27] describes the continuous production of inhalable drug particles in a size range from 0.3-20 μm. These particles are precipitated in tube-like channels, where a stream of alternating segments of a solution and transport medium (e.g., gas or oil), which is not miscible with the solution, is produced in order to achieve a very narrow residence time distribution and to prevent the pipe from plugging. In addition, Méndez del Rio and Rousseau[28] reported the use of a tubular device for tubular-batch crystallization. The tubing was used to rapidly cool the solution. After primary nucleation the crystals grew in the stirred receiving vessel. Several other publications exist on continuous crystallization, e.g., the work by Lawton et al.[29]

In this work, we present a novel continuously seeded, continuously operated tubular crystallizer system, in which seeded particles grow inside the tubular reactor to product crystals with a narrow PSD. In an industrial setting the seeds would be produced by recycling, milling and classifying a small fraction of the product stream. In this study, however, seeds are pre-prepared and fed to the tubular crystallizer. This system can be used for the continuous production of engineered crystals and can be, if combined with additional reactor segments, used to develop multi-layer or coated crystals with highly defined properties.

As a model system the crystallization of acetylsalicylic acid (ASA) from an ASA-EtOH solution was chosen, as the solubility in EtOH increases strongly with the temperature. Thus, by changing the temperature trajectory of the tubular crystallizer,

the crystallization process can be controlled in a straightforward manner. ASA crystallizes under most circumstances as one polymorph (Form I), even though a form II[30] and intergrowth of the two forms have been reported.[31] The suspended ASA seeds (in EtOH) are introduced into the continuous tubular crystallizer at a temperature around 25 [℃], upon which they are mixed in a Y-fitting with a heated, highly concentrated ASA-EtOH solution. The continuous tubular crystallizer developed in our work is robust and allows us to vary *independently* various parameters that have an influence on the crystal growth, including the (i) solution concentration and the temperature of the ASA-EtOH solution, (ii) the amount of seeds and (iii) the residence time of the crystals in the crystallizer.

Furthermore, the tubular design allows for tight temperature control. Due to the large surface-to-volume ratio of the system the heat of crystallization can be removed immediately. Thus, temporal or spatial temperature oscillations that would lead to uncontrolled growth conditions can be avoided.[27] Additionally, the temperature trajectories can be adjusted to yield products of optimal quality and to optimize the whole process. Furthermore, a narrow residence time distribution of the crystals in the tubing leads to a narrow crystal size distribution.

In summary, in our work a novel continuous tubular crystallizer has been developed and studied by varying the flow rates. The length of the crystallizer is 15 m, its width 2 mm. The influence of varying flow rates on the product crystals has been assessed. All other parameters (i.e., temperatures, seed to solution ratio, concentration etc.) were kept constant. The results of our study show that this system has significant potential for industrial implementation, as it enables an independent control of all relevant parameters, allowing for true crystal engineering.

2.2 Materials and Methods

Materials: Acetylsalicylic acid (ASA) (99.0%, M = 180.16 [g/mol]) was purchased from Sigma Life Science. Ethanol (EtOH) (99.8%, M = 46.07 [g/mol], denaturized with 1.0% Methyl Ethyl Ketone) was purchased from Roth (Lactan).

Equipment: The tubular crystallizer consists of a polysiloxane tubing with an inner diameter (d_{inner}) of 2.0 [mm] and an outer diameter (d_{outer}) of 4.0 [mm]. A peristaltic pump, later referred to as pump I (PI) (Ismatec BVP- Process IP 65 - 3/6), equipped with a PHARMED® tubing (d_{inner} = 1.6 [mm], d_{outer} = 4.8 [mm]) was used to pump the ASA-EtOH solution into the Y-fitting (PTFE, d_{inner} = 2.0 [mm]) mixing zone of the

tubular crystallizer. A second peristaltic pump (PII) (Ismatec Reglo Digital MS 2/6V 1.13C, PHARMED® tubing d_{inner} = 2.8 [mm], d_{outer} = 5.0 [mm]) pumped the seed suspension into the crystallizer. PTFE (Polytetrafluorethylene) pipes (L = 0.03 [m]; d_{inner} = 1.0 [mm], d_{outer} = 3.0 [mm]) connected this Pharmmed® tubing of pump II (d_{inner} = 2.8 [mm], d_{outer} = 5.0 [mm]) with a piece of polysiloxane tubing (d_{inner} = 2.0 [mm], d_{outer} = 4.0 [mm]) in order to transport the seeds to the Y-fitting.

For particle size characterization a Leica DM 4000 microscope equipped with a Leica DFC 290 camera was employed. Approximately 1000 crystals of each sample were analyzed. ImageJ, an open source program, was used to determine the projected areas of the particles under the microscope and to estimate the circle equivalent diameters (CED) of the particles. The pictures of the crystals were processed and manually checked twice in order to exclude particles that were cut on the edges, as well as overlapped particles. The particle statistic data, as well as the volume density distribution graphs, were generated in Matlab. Quantification of agglomeration events based on optical methods can be found in literature (e.g. Faria et al.[32] and Vivier et al.[33]). In this work, however, agglomeration effects have been quantified based on the difference between model and experiment.

Set-up: Figure 2-1 shows a schematic of the crystallizer system.

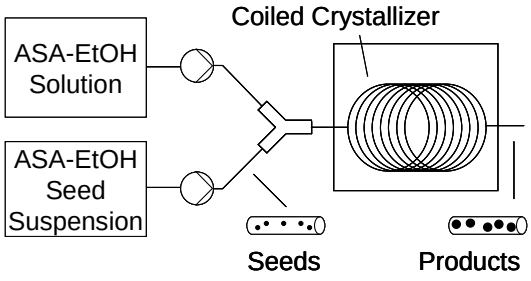

Figure 2-1. Schematic of the coiled, tubular crystallizer apparatus, including the ASA-EtOH solution feed, the seed-suspension supply, the Y-mixing zone and the crystallizer tubing. The housing of the tubular crystallizer is flushed with pressurized air to control the ambient temperature.

The storage vessels for the seed-suspension and the ASA-EtOH solution had a volume of 1.0 liter each. The solution was kept at 62.0 ± 0.2 [°C] (T_{sol}), whereas the seeds were kept at 24.6 ± 0.2 [°C] (T_{seed}). In an experiment, the pumps feed the ASA-EtOH solution (PI) and the ASA seeds (PII) into the crystallizer that is coiled on a pipe (d = 0.1 [m]) formed from grid-structured material that ensured good heat transfer with the surrounding air. The crystallizer is kept in a box (length 0.41 [m], height 0.24 [m], width 0.26 [m]) that is flushed with pressurized air (3 [m^3/h]) to keep the temperature in this box (T_{amb}) at 24.3 ± 1 [°C].

Figure 2-2 displays a schematic of the growth of crystals in the tubular crystallizer due to super-saturation caused by cooling, assuming that no new nuclei are formed and neglecting particle breakage, as well as agglomeration. A narrow CSD of the seeds together with a narrow residence time distribution lead to similarly sized product crystals.

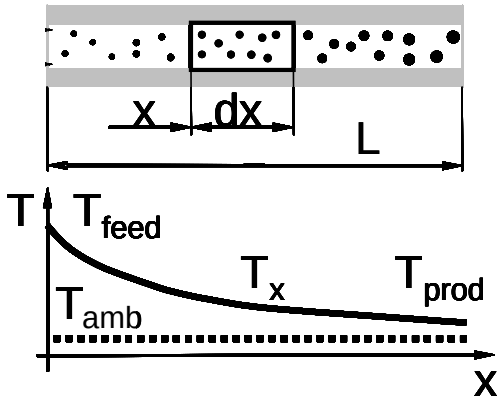

Figure 2-2. Cooling rate and growth of crystals in the tubular crystallizer, if neither nucleation, nor agglomeration occur and ideal flow conditions are assumed.

The feed stream (T_{feed}) approaches the ambient temperature in the box (T_{amb}) along the temperature trajectory T_x. The heat of crystallization lowers the cooling rate, but has only a small influence on the product stream temperature (T_{prod}), as shown below (Figure 2-9). Due to the small inner dimensions of the crystallizer, radial temperature gradients can be neglected in our analysis. Thus, the crystals entering the tubular crystallizer at the same time find the identical growth conditions on their path through the tube.

Procedure: In order to prepare the seed suspension 0.050 [kg] ASA were mixed with 0.100 [kg] ethanol and vigorously stirred (magnetic stirrer and stir bar) for at least 48 hours at a constant temperature (24.6 ± 0.2 [℃]). Thus, the solid and the liquid phase were in equilibrium. Dissolution and mechanical effects (including impeller-particle and particle-particle collisions) yielded seeds between 5 and 200 [µm]. The ASA-EtOH solution with an ASA mole fraction (X_{ASA}) of 0.113 (c_{ASA} ~ 2.19 [mol/l]) was prepared by dissolving 0.050 [kg] ASA per 0.100 [kg] ethanol while continuously stirring the solutions at 62.0 ± 0.2 [℃] for appro ximately 30 minutes.

Eq. (2-1) gives the mole fraction of the solution.

$$X_{ASA} = \frac{n_{ASA}}{n_{ASA} + n_{EtOH}} \qquad \text{Eq. (2-1)}$$

Here n [mol] represents the moles of either ASA or EtOH respectively according to the indices and X_{ASA} is the mole fraction.

The mole fraction (X_{ASA}) in the product and in the feed stream (seed suspension and ASA-EtOH feed solution) were determined by removing the seeds and the product crystals respectively by filtration, followed by weighting the solutions and the ASA-residue after evaporation of the ethanol.

Experimental data from prior publications[34] and the Nývlt-Model (Eq. 2-2) were used to establish the solubility of ASA in EtOH at a given temperature.

$$\log X_{ASA} = N_1 + \frac{N_2}{T} + N_3 \log(T) \qquad \text{Eq. (2-2)}$$

For the solvent ethanol the parameters in Eq. (2-2) are N_1 = 27.769, N_2 = -2500.906, and N_3 = -8.323.[34] The temperature T in Eq. (2-2) has the units Kelvin [K].

At 63.4 [℃] Maia [34] measured a dissolved mole fraction of X_{ASA} = 0.204, and at 60.2 [℃] of X_{ASA} = 0.187, respectively. The Nývlt-Model predicts mole fractions of dissolved ASA of X_{ASA} = 0.195 at 62.0 [℃]. Thus, the ASA-EtOH solution (X_{ASA} = 0.113), that was prepared for our experiments was under-saturated at 62.0 [℃].

Prior to each experiment warm ethanol (40 [℃]) was used to flush the system with PI and PII in order to rinse the tubing. Subsequently, PII was switched to the seed suspension supply vessel and a sample of the seeds was collected by filtration for 60 seconds in order to analyze their PSD in each experiment. The collected seed crystals were washed with cold cyclohexane, an antisolvent, for analysis. After collection, seeds were fed to the crystallizer (PII) together with warm ethanol (PI). Shortly after the Y-fitting all of the seeds were dissolved in EtOH. Finally, PI was switched from pure ethanol to the concentrated ASA-EtOH solution. This start-up procedure guaranteed that some seeds were in the crystallizer when the ASA-EtOH solution entered the tubing. Absence of seeds at any time led to excessive primary nucleation and immediate blockage of the tube. Typically, about 5 minutes were needed in order to reach steady-state conditions. An experiment was performed for 15 minutes, before the pumps where switched again to warm ethanol in order to rinse the tubing. During an experiment, two product samples were taken at the end of the crystallizer at different times. For that purpose the product stream was filtered for 30 seconds. Again the collected crystals were washed with cold cyclohexane. The weight of the sample was then measured and the crystal size distribution (CSD) was analyzed.

Four different *total* flow rates (i.e., ASA + seeded solution), i.e., 11.4 [ml/min], 17.2 [ml/min], 22.8 [ml/min] and 25.2 [ml/min] were tested in a 15m tubing. Other parameters, including the temperatures of the ASA-EtOH solution and seed suspension, the concentrations of the ASA-EtOH solution, the solids loading of the seed-suspension, and the ratio of the seed suspension to the ASA-EtOH solution, were kept constant. In order to avoid excessive nucleation in the tubular crystallizer, leading to the formation of small crystals and the risk of blockage of the tubing, the seed loading was relatively high. However, the high seed loading, the high concentration of ASA and the absence of any moving parts in the crystallizer (e.g., stirrer) increases agglomeration and crystal inter-growth as shown below. Higher flow rates above 17.2 [ml/min] and the associated higher local shear rates reduced this effect and the tubular crystallizer could be operated without blockage.

Thus, it can be concluded that a safe and reproducible operation of the system is possible, while avoiding agglomeration, for suitable sets of operation parameters.

2.3 Results and Discussion

Figure 2-3 shows the volume density distributions $q_3(x)$ of the seeds and the two product samples of the experiment for a flow rate of 11.4 [ml/min], together with microscope pictures of the seeds and the product crystals (sample 2) and the number density distribution $q_0(x)$ of the product (sample 2).

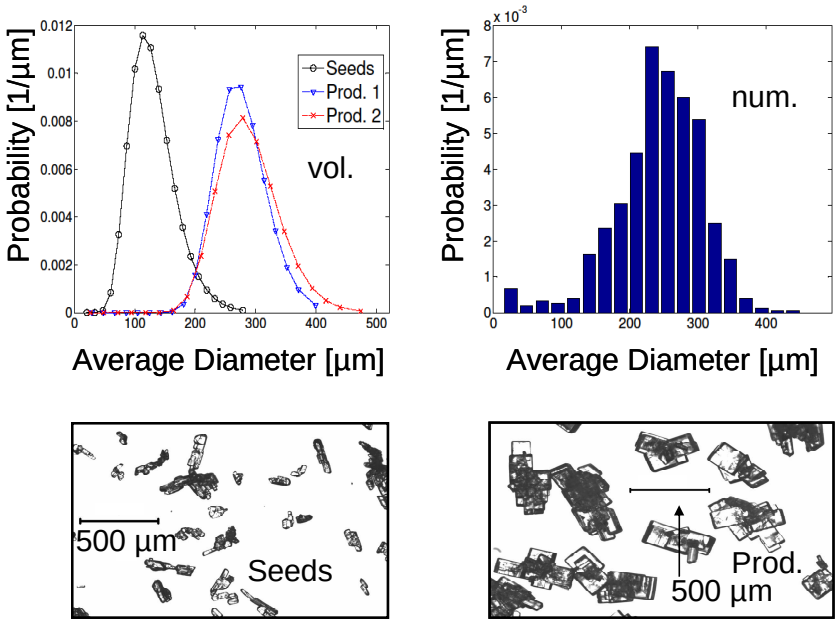

Figure 2-3. Crystallization with an ASA-EtOH solution flow of 8.9 [ml/min] (PI) and 2.5 [ml/min] of the seed suspension (PII). Top left corner: volume-density distributions of the seeds and two product samples. Top right corner: number density distribution of product (sample 2). Bottom: photos of seed and product crystals.

As can be seen from Fig. 2-3 the CSD of the seeds is relatively narrow, as is the CSD of the product crystals. Both, sample 1 and 2 give about the same distribution, which is still within the limits of statistical fluctuations. Clearly, the seeds grew significantly during their residence time in the tubular crystallizer. This is due to crystal growth, although agglomeration and crystal intergrowth have amplified this effect, as can be seen in the microscopic pictures. However, even some of the seed crystals were agglomerated, and thus, some of the larger agglomerated crystals of the product were generated due to growth of the individual crystallites, which have clearly grown in size. Furthermore, the number density distribution of the product shown in Fig. 2-3 establishes that no fines were produced in the tubular crystallizer. In summary, crystals with narrow CSDs have been produced in the crystallizer.

Figures 2-4 and 2-5 show the results for the flow rates of 17.2 [ml/min] and, 22.8 [ml/min], respectively.

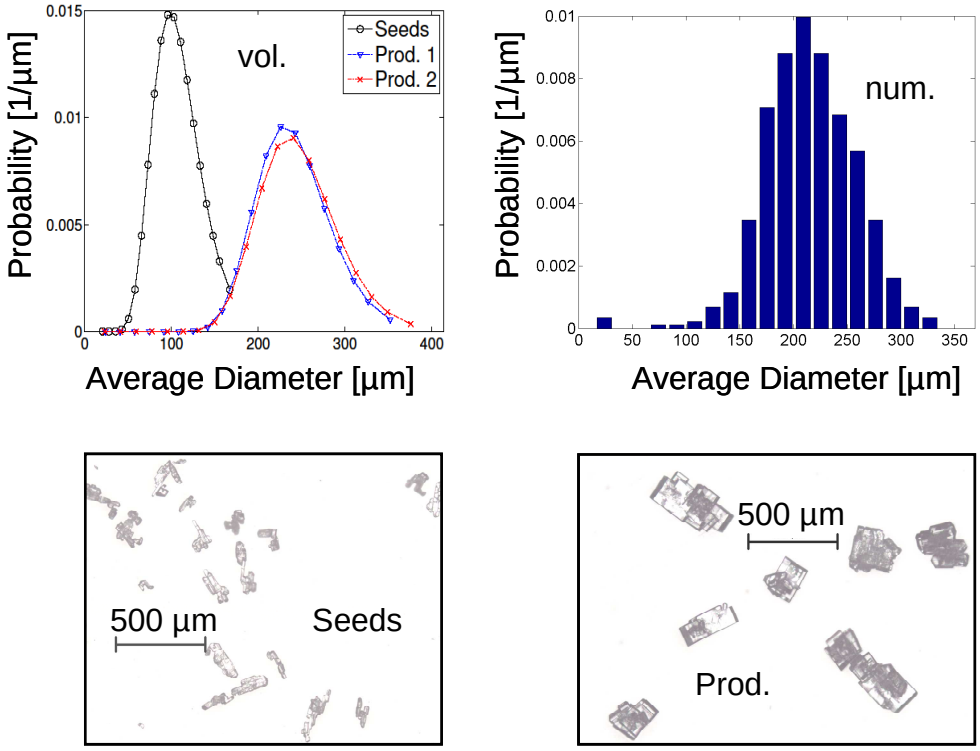

Figure 2-4. Crystallization with an ASA-EtOH solution flow of 13.4 [ml/min] (PI) and 3.8 [ml/min] of the seed suspension (PII). Top left corner: volume-density distributions of the seeds and two product samples. Top right corner: number density distribution of product (sample 2). Bottom: photos of seed and product crystals.

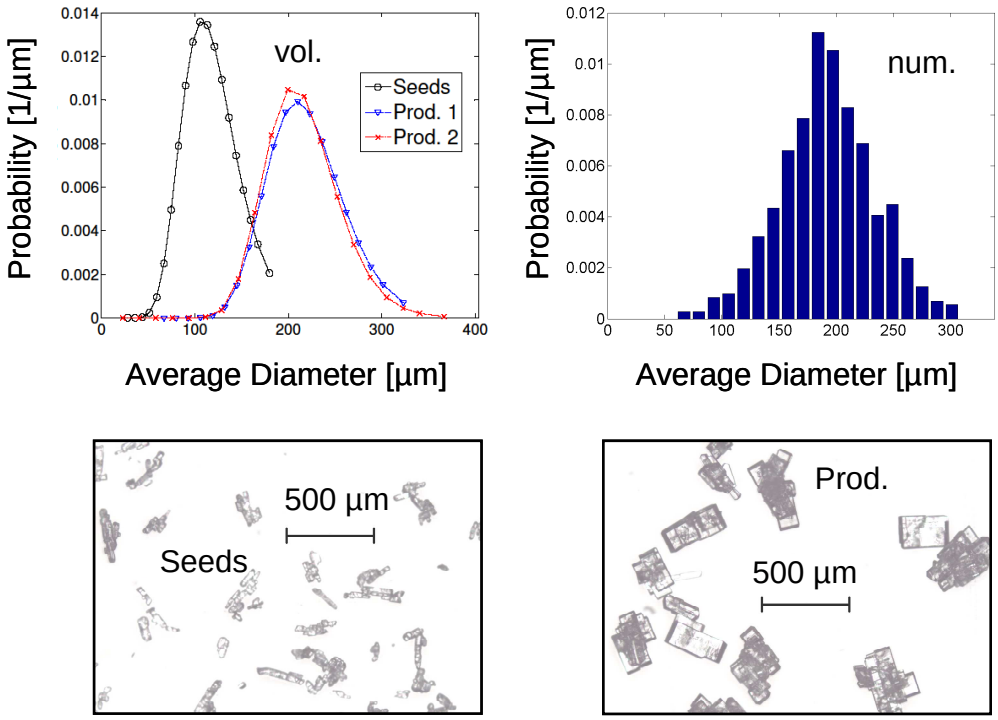

Figure 2-5. Crystallization with an ASA-EtOH solution flow of 17.8 [ml/min] (PI) and 5.0 [ml/min] of the seed suspension (PII). Top left corner: volume-density distributions of the seeds and two product samples. Top right corner: number density distribution of product (sample 2). Bottom: photos of seed and product crystals.

Again, significant growth and well-defined crystals were obtained. The agreement between sample 1 and 2 is even better for these two cases. Figure 2-6 shows the data of the experiment for a flow rate of 25.2 [ml/min]. Once more, significant growth is obtained, although the CSD is shifted to the left as the residence time is decreased.

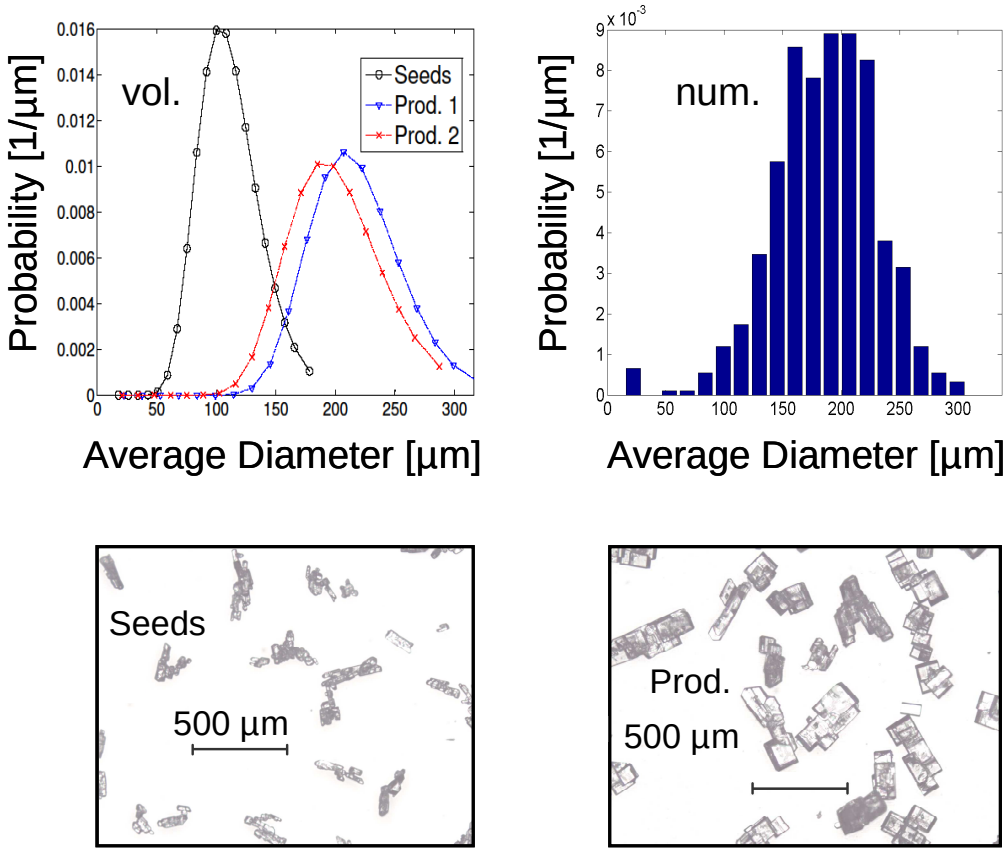

Figure 2-6. Crystallization with an ASA-EtOH solution flow of 19.7 [ml/min] (PI) and 5.5 [ml/min] of the seed suspension (PII). Top left corner: volume-density distributions of the seeds and two product samples. Top right corner: number density distribution of product (sample 2). Bottom: photos of seed and product crystals.

In summary, for all flow rates crystals with well defined shape and size have been obtained. The product crystals in Fig. 2-3 seem to be clusters of multiple crystal parts that are agglomerated and have grown together. The products in Fig. 2-4, 2-5 and 2-6 also seem to be intergrown crystals and agglomerates. However, they are more compact and already display the defined crystal shapes of slightly elongated cuboids. This suggests that at higher flow rates (starting with about 17.2 [ml/min]) product crystals with better quality are obtained.

Typically, continuous crystallization processes, such as MSMPR or Oslo-crystallizer, require significant time until they reach steady state operation,[19] up to 10 times the mean residence time of the suspension in the crystallizer. In our case, sampling of two product crystal fractions from the tubular crystallizer was done within 15 minutes after starting the process. As shown, above in all cases the CSDs of the two product samples were almost identical. Therefore, it is evident that steady-state conditions were achieved in a short period of time.

Table 2-1 comprises data of four continuous crystallization experiments, including the flow rates, the sample intervals, the mass gained during crystallization, the average diameters of the seeds and the products (both number and volume-averages) as well as the standard deviations (σ_{vol} and σ_{nmd}). The ratios of the seed-to-ASA-solution (i.e., PI/PII) and other parameters including the concentrations and temperatures of the solution and the seed-suspension were not varied.

In Table 2-1 the resulting volume mean diameters ($\overline{d}_{p,vol}$ [µm]) have been established using the logarithmic normal fitting function in Eq. 2-3, i.e.,

$$f(d_{p,vol}) = \frac{1}{\sigma_{vol} \cdot d_{p,vol} \cdot \sqrt{2\pi}} \cdot \exp\left[-\frac{1}{2} \cdot \left(\frac{\ln\left(d_{p,vol} / \overline{d}_{p,vol} \right)}{\sigma_{vol}} \right)^2 \right]. \qquad \text{Eq. (2-3)}$$

The arithmetic number-mean diameters of the particles were established directly from the microscopic images using Eq. 2-4

$$\overline{d}_{p,nmd} = \frac{1}{N} \sum_{i=1}^{n} d_{p,i} \,, \qquad \text{Eq. (2-4)}$$

where N is the total number of particles, $\overline{d}_{p,nmd}$ [µm] is the number mean diameter, and $d_{p,i}$ [µm] is the circle equivalent diameter (CED) of the i-th particle.

Table 2-1. Results for varying flow rates in a 15 m long tubular crystallizer. Sampling time (t_{sample}), mass flow of solid ASA particles ($\dot{m}_{ASA}$), number and volume mean diameter ($\overline{d}_{p,nmd}$, $\overline{d}_{p,vol}$), standard deviation of volume and number mean diameters σ_{vol} and σ_{nmd}.

Sample	PI [ml/min] (ASA-EtOH)	PII [ml/min] (seeds)	t_{sample} [min]	$\dot{m}_{ASA}$ [g/min]	$\overline{d}_{p,nmd}$ [µm]	σ_{nmd} [µm]	$\overline{d}_{p,vol}$ [µm]	σ_{vol} [-]
$1\text{-}1_{Seeds}$	-	2.5	-	0.26	90	38	125	0.29
$1\text{-}2_{Product\ 1}$	8.9	2.5	9	1.48	233	62	274	0.15
$1\text{-}3_{Product\ 2}$			15	1.48	243	65	284	0.17
$2\text{-}1_{seeds}$	-	3.8	-	0.43	81	26	106	0.26
$2\text{-}2_{Product\ 1}$	13.4	3.8	7	2.51	215	43	238	0.18
$2\text{-}3_{Product\ 2}$			11	2.53	214	50	244	0.18
$3\text{-}1_{Seeds}$	-	5.0	-	0.54	91	27	116	0.26
$3\text{-}2_{Product\ 1}$	17.8	5.0	6	3.33	192	41	217	0.19
$3\text{-}3_{Product\ 2}$			9	3.11	183	49	212	0.18
$4\text{-}1_{Seeds}$	-	5.5	-	0.63	85	29	109	0.23
$4\text{-}2_{Product\ 1}$	19.7	5.5	5	3.44	186	44	215	0.18
$4\text{-}3_{Product\ 2}$			9	3.07	166	45	198	0.20

Table 2-2 reports the mass increase by crystallization (expressed as mass gain r_m), the theoretical mass gain ($r_{m,theor}$), the residence time (t_{res}), the Reynolds number of the flow in the system, the mass ASA per ml seed suspension, the measured temperatures at the Y-fitting (T_{feed}) and at the end of the crystallizer (T_{prod}), as well as the volume mean diameters of the experiments and the calculations. The model is described in chapter 2-4.

Table 2-2. Mass gain (r_m) and the theoretical mass gain ($r_{m,theor}$) of the product to seed crystal masses, Re-numbers, mass of solid ASA per ml seed-suspension, residence times (t_{res}), temperatures in the Y-fitting (T_{feed}) and the product temperature (T_{prod}) as well as the volume mean diameter ($\overline{d}_{p,vol}$) of the experiment and the calculated crystal diameter ($d_{p,calc}$) and their difference.

Flow rate [ml/min]	t_{res} [s]	Re [-]	$m_{seed}/ml_{see\ d\text{-}susp}$ [g/ml]	$r_{m,theor}$ [%]	r_m [%]	T_{feed} [° C]	T_{prod} [° C]	$\overline{d}_{p,vol}$ [µm]	$d_{p,calc}$ [µm]	$\Delta d_{p,calc}$ [µm]
11.4	248	10.8	0.10	655	569	34.4	24.6	279	189	90
17.2	164	16.3	0.11	617	588	39.7	24.2	241	189	52
22.8	124	21.7	0.11	615	595	39.9	25.3	215	185	30
25.2	112	24.0	0.11	562	517	40.5	26.3	207	184	23

The mass gain r_m, i.e., the mass increase in [%], is given by

$$r_m = \frac{\dot{\overline{m}}_{prod}}{\dot{m}_{seed}} \cdot 100 \quad \text{and} \quad r_{m,theor} = \frac{\Delta\dot{m}_{sol,theor} + \dot{m}_{seed} + \Delta\dot{m}_{seed,theor}}{\dot{m}_{seed}} \cdot 100 \qquad \text{Eq. (2-5)}$$

r_m was computed by dividing the arithmetic mean mass flow of the product crystals ($\dot{\overline{m}}_{prod}$ [g/min]) by the mass of the seeds ($\dot{m}_{seed}$ [g/min]) of each run. From Table 2-2 it can be seen that the mass gain was between 500 and 600 [%] for each run. $r_{m,theor}$ was calculated according to Eq. 2-5 under the assumption that equilibrium is reached and that the theoretically possible changes in solid ASA mass for the solution- ($\Delta\dot{m}_{sol,theor}$) and the seed-suspension stream were achieved ($\Delta\dot{m}_{seed,theor}$) at the given temperatures (T_{prod}). As can be seen the achieved mass gain is close to the theoretical one. For the lowest flow rate (11.4 [ml/min]) the difference is slightly increased due to feeding a supersaturated solution to the Y-mixer, which may have led to crystallization in the mixer and hence to a reduced solid ASA mass flow. Differences between r_m and $r_{m,theor}$ for flow rates of 17.2 and 22.8 [ml/min] are almost

constant. The difference increases for a flow velocity of 25.2 [ml/min]. This suggests that the reduced time for crystallization results in higher degrees of supersaturation at the end of the tubing.

Furthermore Table 2-2 compares the computed final diameters ($d_{p,calc}$) based on an average mean diameter of the seeds for all experiments with the final volume mean diameters obtained from the experiments ($\overline{d}_{p,vol}$). It can be seen that there is a significant deviation between experiments and the idealized model (which neglects agglomeration, see chapter 2-4). Thus, it becomes evident that agglomeration, together with crystal growth, is also responsible for the size increase in the experiments. However, for higher flow rates (and increased shear) in the tubular crystallizer, the difference between computed and experimental diameters becomes marginal. Thus, for these conditions agglomeration evidently does not dominate the crystallization process.

The Reynolds number is defined as

$$\mathrm{Re} = \frac{\rho_{susp} v d_{inner}}{\mu}. \qquad \text{Eq. (2-6)}$$

The dynamic viscosity (μ = 0.01 [Pa·s]) of the suspension has been measured with a rheometer at 25.0 [°C] (Physica – Anton Paar, MCR 3 00). In Eq. 2-6 v denotes the mean velocity of the suspension. v = 0.06, 0.09, 0.12 and 0.13 [m/s] for the four flow rates reported in Table 2-2. ρ_{susp} is the density of the suspension (898 [kg/m^3] at 40 [°C]), and d_{inner} is the inner diameter of the tubing (d_{inner} = 0.002 [m]). From Table 2-2 it can be seen that the Reynolds numbers are between 10 and 25. Thus, the flow is well below the critical Reynolds number (Re_{crit} = 2000) for the transition to the turbulent regime.

From the r_m-data in Table 2-2 the gain of crystal mass can be assessed. From the shift of the q_3 distribution and the microscopic images it is clear that the increase in mass was due to crystal growth (and not due to nucleation). Despite the short crystallization (or residence) time in the reactor of only a few minutes (Table 2-2), all volume density distributions and the pictures of the seed and product crystals (Figs. 2-3 to 2-6) clearly display a shift to larger sizes, of product crystals. The number density distributions generally suggest absence of excessively large amounts of fines. This is probably due to reduced secondary nucleation and friction effects by crystal-crystal and crystal-wall interactions in the tubular crystallizer.

As outlined above, the $q_3(x)$ distribution shifted to the right during the crystallization run. Figure 2-7 correlates the extent of this shift with the flow rate (i.e., inversely proportional to the residence time) in the reactor for multiple experiments. In Fig. 2-7 we plot the average diameter increase $\Delta\overline{d}_{p,vol}$, which is the difference between the average seed and product diameters (an average of product sample 1 and 2 was taken), as a function of the flow rate. The squares and dots are based on data from different experiments and show the same trends. Data for the flow rate of 11.4 [ml/min] together with the data for the experiments represented by the dots (Fig. 2-7) are summarized in Table 2-1. Data referring to the rest of the squares are not shown in Table 2-1, as they are similar to "dot-data".

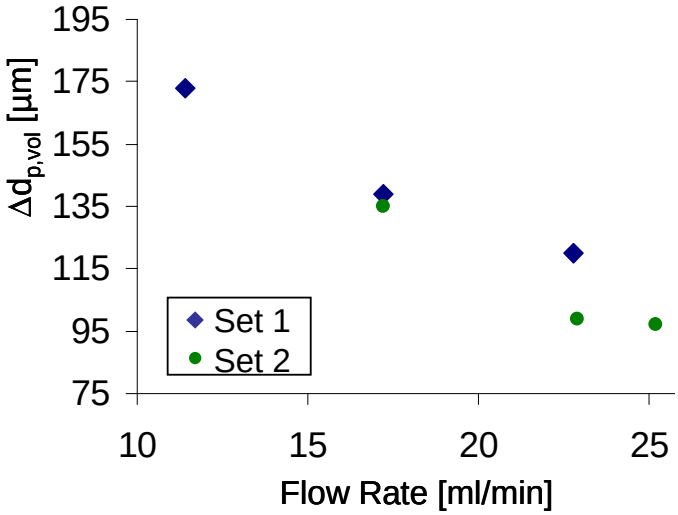

Figure 2-7. The average increase in diameter during crystallization as a function of flow rate. The mean value of two product samples has been used. Note that the squares and the dots are based on data from different sets of experiments.

As can be seen, the average increase in diameter $\Delta\overline{d}_{p,vol}$ is a strong function of the flow rate. In fact, almost a linear correlation can be established for the set of operating conditions. Note, that this linear dependence is rather a coincidence and should not be the case in general. The decrease of $\Delta\overline{d}_{p,vol}$ with flow rate may be due to three effects: (i) the decreasing residence time (see Table 2-2), (ii) the slightly elevated temperature T_{prod} for increased flow rates (see Table 2-2) and thus the reduced crystallization rate at higher flow rates, and (iii) the reduced tendency of agglomeration with increasing flow rates, significantly contributes to this effect of decreasing $\Delta\overline{d}_{p,vol}$. In the following paragraphs this effect is discussed in more detail.

In order to assess the theoretical yield of the crystallization by observing the dissolved ASA, the measured mole fraction X_{ASA} of the liquid phase and the

theoretical solubility for the respective temperature (according to the Nývlt model, see section 2-2) are plotted for both the feed (i.e., the mix of solution and seed suspension) and the product stream as a function of the flow rate. This plot is shown in Figure 2-8.

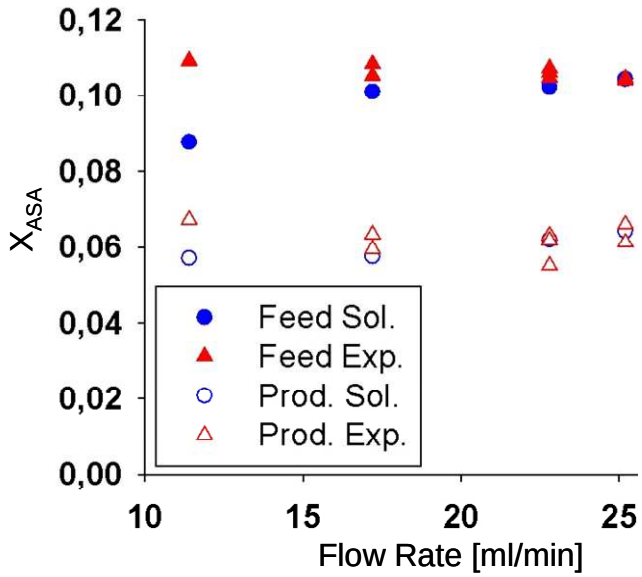

Figure 2-8. Theoretical solubility (according to the Nývlt model, Sol.) and measured mole fraction (Exp.) of dissolved ASA (X_{ASA}) of the feed and the product stream as a function of the flow rate.

As can be seen from Fig. 2-8, the feed stream, i.e., a mixture of the seed suspension (PII) and the ASA-EtOH solution (PI), entered the crystallizer close to saturation in most experiments. For the lowest flow rate (11.4 [ml/min]) the temperature was lower, and thus, the solution was supersaturated, increasing the risk of excessive nucleation and tube-blockage. Furthermore, Fig. 2-8 shows that the product stream was close to equilibrium in all experiments.

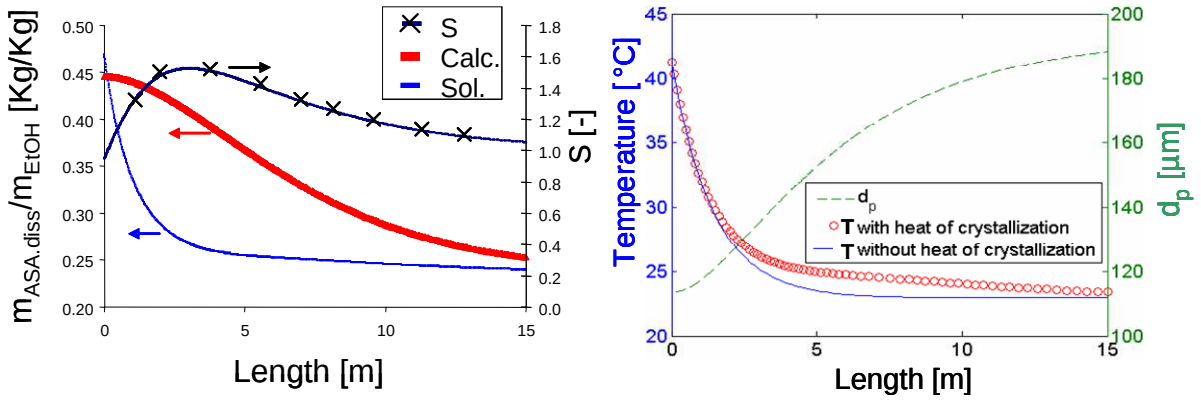

Figure 2-9. Left: ASA solubility according to Nývlt (Sol.), dissolved ASA computed according to the model presented in chapter 2-4 (Calc.) and the resulting supersaturation ratio (S) vs. length. Right: Temperature (T) with and without heat of crystallization and the increase of the particle diameter (d_p) versus the length of the crystallizer (flow rate = 22.8 [ml/min]).

Supersaturation, the driving force for crystal growth, was generated via cooling. In Figure 2-9 a computed temperature trajectory and the corresponding increase in crystal size are shown together with the solubility (see Nývlt model in section 2-2), the actual ASA concentration and the resulting supersaturation expressed as ratio S of the dissolved ASA concentration and the solubility. These data (all based on the model) are shown for a representative case, i.e., a flow rate of 22.8 [ml/min]. The outer heat transfer coefficient α_{outer} of the tubular pipe has been measured using deionized water that was kept at 75.0 [℃] in a sto rage vessel and pumped at different flow rates through the crystallizer system. The resulting heat transfer coefficient of α_{outer} = 70 [W/m^{2}K] was used in the calculations. The models used to calculate the temperature distribution and the increase of particle size (Fig. 2-9, Fig. 2-10) in the tubular reactor are detailed in chapter 2-4.

In Figure 2-9 (top) the feed stream is slightly undersaturated when entering the tubing. Cooling leads to supersaturation and particle growth consumes dissolved ASA until the liquid phase approaches equilibrium towards the end of the crystallizer. Slower cooling could be employed to avoid high levels of supersaturation (e.g., for polymorphism control). This would also reduce the risk of pipe plugging and impurity inclusion/incorporation. However, the time needed for crystallization, and thus the length of the crystallizer, would increase. Hence, by adjusting the temperature trajectory, an optimum can be found.

The temperature trajectory in Figure 2-9 shows that there is no significant difference whether the heat of crystallization is taken into account or not. In both cases the final

temperatures are very close to each other and are almost equal to the ambient temperature (T_{amb}). Furthermore, the temperature drops relatively quickly, and about 2/3 of the reactor have a very similar temperature. Thus, due to the small diameter of the tubing the heat transfer is very fast in our crystallizer.

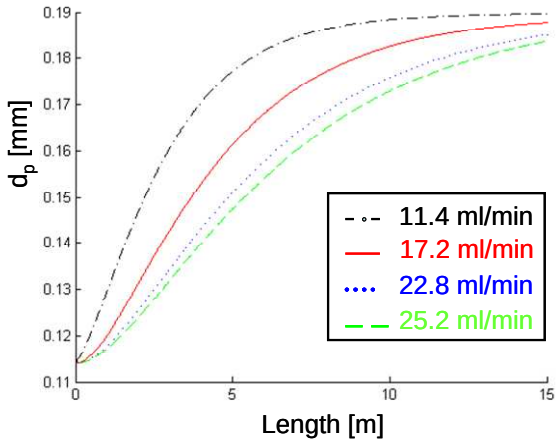

Figure 2-10. Growth of particles vs. crystallizer length. An average of the mean seed diameters was used. Lines show the modeled increase of d_p.

Figure 2-10 shows the modelled increase of a single particle size for a typical overall mass transfer coefficient of $K_g = 1.0 \cdot 10^{-5}$ [m/s] based on the arithmetic mean of the volume mean diameters of the seeds of all experiments (i.e., $d_{av,seed} = 114$ µm). Note, that the model is non-isothermal, i.e., temperature variations are accounted for.

Due to the steep cooling gradient at the feed end of the tubing fast build up of supersaturation at the beginning of the pipe ensures rapid crystal growth. After the supersaturation passes a maximum a reduction of the supersaturation occurs towards the end of the crystallizer (Fig. 2-9). For flow rates of 25.2 and 22.8 [ml/min] the growth slowed significantly down after the suspension passed the first ~8-9 meters of the pipe. For a flow rate of 17.2 [ml/min] a similar behavior was observed at around 7 and for 11.4 [ml/min] at approximately 4.5 meters. As conjectured above, the final computed diameter of the crystals is rather similar, as in all cases a state close to equilibrium is obtained. Note that agglomeration is not taken into account in that model.

2.4 Model

Here a model for predicting the temperature, as well as the particle size and the dissolved ASA mass fraction in a tubular crystallizer is presented. The major assumption for this model is that we describe the particle population at each position x in the crystallizer with a single particle size d_p [m]. Also, we neglect agglomeration,

as well as breakage, in the crystallizer. Thus, we assume a constant particle (number) concentration in the reactor, which significantly simplifies the governing equations for mass and energy. A sketch of the tubular crystallizer is given in Figure 2-11. Agglomeration and breakage effects have not been included in the model but could be included by combining our model with a population balance equation (PBE) approach.[35] The models here are used to assess supersaturation and temperature trajectories and the particle growth without agglomeration effects.

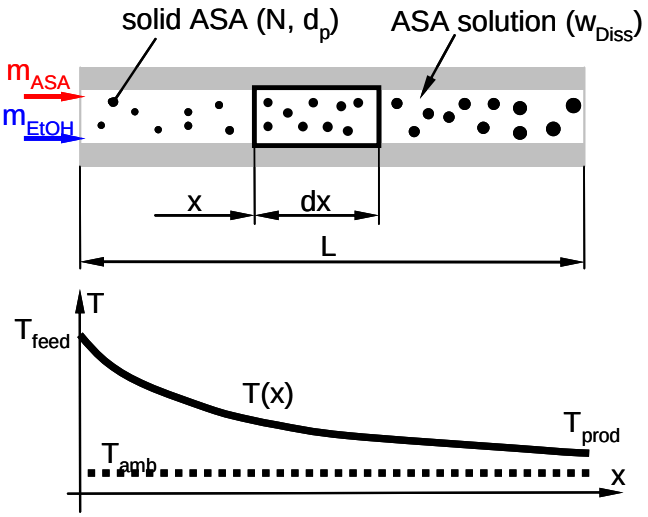

Figure 2-11. Schematic representation of the tubular crystallizer including temperature profile.

The Nývlt Model (Eq. 2-2) was used to compute the amount of dissolved ASA in the saturated solution. Tables 2-3 and 2-4 summarize the physicochemical data that have been used for the calculations. Further data are provided in the text next to the corresponding equations.

Table 2-3. Molar mass M, density ρ, fusion enthalpy Δh_f and heat capacity of ASA $c_{p,ASA}$

M_{ASA} [g/mol]	ρ_{ASA} [kg/m^3]	Δh_f[34;36] [J/mol]	$c_{p,ASA}$[36] [J/kgK]
180.16	1350	29 800	1260

Table 2-4. Molar mass M, density ρ, heat conductivity, λ and heat capacity of EtOH $c_{p,EtOH}$

M_{EtOH} [g/mol]	ρ_{EtOH} [kg/m^3]	λ_{EtOH} [W/mK]	$c_{p,EtOH}$ [J/kgK]
46.07	790	0.1676	2400

The fusion enthalpy Δh_f of ASA is shown in Table 2-4. The negative value of Δh_f is assumed to be the heat of crystallization Δh_{cryst}. The second assumption concerning Δh_{cryst} is that the value is constant over the range of temperatures and concentrations in the crystallizer. The heat conductivity of ethanol λ_{EtOH} is provided in Table 2-4 and assumed to be the heat conductivity of the ASA-EtOH suspension in the crystallizer. The ASA and EtOH masses in the ASA-EtOH solution and the seed suspension ($m_{EtOH,solution}$, $m_{EtOH,seeds}$, $m_{ASA,solution}$, $m_{ASA,seeds}$ [kg]) and the flow rates ($Q_{solution}$, Q_{seed} [m^3/s]) have been chosen according to the experiments. The temperature of the seeds T_{seeds} is 24.6 [°C] and the solution temperature $T_{solution}$ [°C] is adjusted to get T_{feed} [°C] (Table 2-2). The particle diameter of the seeds $d_{p,0}$ = 114 [µm] is an average value of the volume mean diameters of the seeds from the experiments (Table 2-1). The shape factor F_{shape} of the seeds used in the calculations is 1 [-].

Table 2-5. Length L, inner and outer diameter $d_{inner,outer}$, the heat conductivity of the tubing λ_{tubing}, the inner and outer heat transfer coefficient $\alpha_{inner,outer}$ and the ambient temperature T_{amb}

L [m]	d_{inner} [m]	d_{outer} [m]	λ_{tubing} [W/mK]	α_{inner} [W/m^{2}K]	α_{outer} [W/m^{2}K]	T_{amb} [°C]
15	0.002	0.004	0.3	306	70	24.3

Table 2-5 shows the length L, as well as the inner and outer diameter $d_{inner,outer}$ of the crystallizer, the heat conductivity of the tubing λ_{tubing}, the ambient temperature T_{amb} as well as the inner and outer heat transfer coefficient $\alpha_{inner,outer}$. Due to the low Re-number the Nusselt number (Nu) is constant and equal to 3.651.[37] The density of the suspension (ρ_{susp}) used in the calculations in this chapter was assumed to be constant and calculated as an average of the densities of EtOH and ASA and the corresponding mass fractions. Using the heat conductivity of pure EtOH (equal to

0.1676 [W/mK] at 300 [K])[37] for the suspension in the crystallizer, α_{inner} is equal to 306 [W/m^{2}K] for a pipe inner diameter of 0.002 [m].

2.4.1 Basic Calculations

Mass Fraction of Solid Particles and Dissolved ASA in the Feed Stream

The mass fraction w_{solid} of undissolved solid ASA particles can be easily calculated from the total ASA mass fraction w_{ASA} and the equilibrium mass fraction w_{Diss}. The dissolved mass fraction of ASA in the feed suspension can be calculated from the seed suspension properties and the mass fraction w_{EtOH} of ASA in the ASA-EtOH solution.

The particle concentration N/V in the feed stream can be calculated from the solid mass fraction and the seed particle size $d_{p,seed}$.

Heat Conduction through the Pipe

The total heat transfer rate $\dot{Q}$ through a pipe with length L can be calculated from

$$\dot{Q} = 2 \cdot \pi \cdot r_{outer} \cdot L \cdot k \cdot \left(T - T_{amb}\right).$$

Here, the total heat transfer coefficient k related to the outer pipe diameter is given by:

$$k = \frac{1}{r_{outer} \cdot \left(\frac{1}{r_{inner} \cdot \alpha_{inner}} + \frac{\ln\left(r_{outer} / r_{inner}\right)}{\lambda_{tubing}} + \frac{1}{r_{outer} \cdot \alpha_{outer}} \right)}$$

In this equation α_{inner} and α_{outer} are the heat transfer coefficient on the inside and the outside of the pipe in [W/m^{2}K], respectively. λ_{tubing} denotes the heat conductivity of the pipe material in [W/mK] and r_{inner}, r_{outer}, as well as L, are the inner and outer radius, as well as the length of the pipe, respectively.

Governing Equations

Here we present the heat and mass balance equations for the tubular crystallizer, i.e., a pipe reactor. The underlying assumptions for these equations are:

- the crystallizer operates in a steady-state,
- the suspension has a constant density ρ_{susp},
- there is no axial mixing but perfect radial mixing in the crystallizer,

- the value of the specific heat of crystallization Δh_{cryst} is constant along the reactor and equal to the heat of fusion of ASA,
- the suspension, i.e., the particles and the liquid phase, have locally the same temperature T,
- the ambient air has a constant temperature T_{amb} and the heat transfer coefficient from the suspension to the pipe, as well as to the ambient air, are constant,
- the suspension has a constant heat capacity which can be calculated as $\dot{m}_{tot} \cdot c_{p,tot} = \dot{m}_{ASA} \cdot c_{p,ASA} + \dot{m}_{EtOH} \cdot c_{p,EtOH}$.

Here, $\dot{m}_{tot}$, $\dot{m}_{ASA}$ and $\dot{m}_{EtOH}$ denote the total mass flow rate, as well as the mass flow rate of solid ASA and the EtOH solution in the feed stream, respectively. $c_{p,tot}$, $c_{p,ASA}$ and $c_{p,EtOH}$ are the specific heat capacities of the feed stream, the solid ASA and the EtOH solution.

Estimation of the Overall Mass Transfer Coefficient to ASA Crystals

The growth of ASA particles can be controlled by mass transfer (i.e., diffusion of ASA to the crystal's surface) or surface integration. Both phenomena are complex and a wide range of models for the overall growth rate, i.e., the growth rate considering both diffusion and surface integration of ASA, can be found in literature (see for example Lindenberg et al.[3]). It is typically modeled using a power law model (see Lindenberg et al.[3] and Granberg et al.[38] for further details). Here we assume as a model for the growth rate G_L, i.e., the increase in particle diameter with time, the following:

$$G_L = \frac{d\left(d_p\right)}{dt} = K_{g,L} \cdot \Delta w$$

The parameter $K_{g,L}$ is in the order of 10^{-5} to 10^{-4} [m/s] as shown by Granberg et al.[38] for paracetamol crystallized from an acetone-water mixture. It is expected that $K_{g,L}$ is in the same order of magnitude for the ASA-EtOH system. The parameter $K_{g,L}$ and the overall mass transfer coefficient K_g are related as follows:

$$K_{g,L} = 2 \cdot \frac{\rho_{sol,sat}}{\rho_{ASA}} \cdot K_g$$

For the ASA/EtOH-system, the ratio of the saturated solution density $\rho_{sol,sat}$ (assumed to be equal to the density of EtOH) and the density of solid ASA is 0.59.

The literature data of Lindenberg et al. indicate that $K_{g,L}$ follows the following relationship for ASA:

$$K_{g,L} = K_{g,L1} \cdot \exp\left[-\frac{K_{g,L2}}{R \cdot T}\right],$$

with the parameters $K_{g,L1}$ = 0.321 [m/s] (taking into account that they used [g/kg] as a measure for the solubility of ASA) and $K_{g,L2}$ = $2.58 \cdot 10^4$ [J/mol]. This yields $K_{g,L}$ = $1.2 \cdot 10^{-5}$ [m/s] and consequently K_g = $1.0 \cdot 10^{-5}$ [m/s] for a mean temperature in the tubular crystallizer of 305 [K]. A somewhat higher value for $K_{g,L}$ is found by Granberg et al.,[38] i.e., 2-25$\cdot 10^{-5}$ [m/s]. Note, the particle growth rate G_L depends on the supersaturation Δw and is in the range of 10^{-8} - 10^{-7} [m/s].

Energy Balance Equation

The volumetric rate of crystallization $\dot{m}_{cryst}$ can be calculated as:

$$\dot{m}_{cryst} = \frac{d\dot{M}_{cryst}}{dV} = \frac{4 \cdot N \cdot d_p^2 \cdot F_{shape} \cdot K_g \cdot \left(\frac{w_{Diss}}{1/\rho_{EtOH} + w_{Diss}/\rho_{ASA}} - \rho_{ASA,sat}(T) \right)}{L \cdot d_{inner}^2}$$

Here $d\dot{M}_{cryst}$ is the total rate of crystallization in the differential volume dV, F_{shape} is the shape factor of the particles (assumed to be equal to unity), and K_g is the mass transfer coefficient of ASA in the EtOH solution. ρ_{EtOH} is the density of pure EtOH and $\rho_{ASA,sat}(T)$ denotes the partial saturation density of ASA at temperature T. The final differential equation for the temperature profile is:

$$\frac{dT}{dx} = \frac{d_{outer} \cdot \pi}{\dot{m}_{tot} \cdot c_{p,tot}} \cdot k \cdot \left(T(x) - T_{amb}\right) \cdot$$

$$\left(d_p^2 \cdot \frac{N \cdot F_{shape} \cdot K_g \cdot \Delta h_{crist} \cdot \left(\frac{w_{Diss}}{1/\rho_{EtOH} + w_{Diss}/\rho_{ASA}} - \rho_{ASA,sat}(T) \right)}{L \cdot d_{outer}} \Big/ \left[k \cdot \left(T(x) - T_{amb}\right)\right] - 1 \right)$$

The initial condition for this equation is the feed temperature, which can be easily calculated from the temperature and flow rate of the seed and the EtOH solution.

Mass Balance Equation for the Dissolved ASA

The mass balance equation for dissolved ASA is:

$$\frac{dw_{Diss}}{dx} = -\frac{1}{\dot{m}_{EtOH}} \cdot \frac{N}{L} \cdot d_p^{\,2} \cdot \pi \cdot F_{shape} \cdot K_g \cdot \left[\frac{w_{Diss}}{1/\rho_{EtOH} + w_{Diss}/\rho_{ASA}} - \rho_{ASA,sat}(T) \right]$$

The initial condition for this equation is the dissolved ASA mass fraction in the feed stream, as described in the section “Basic Calculations”.

Mass Balance Equation for Solid ASA Particles

Neglecting breakage and agglomeration, the differential change of the particle diameter is:

$$\frac{d\left(d_p\right)}{dx} = \frac{2 \cdot F_{shape} \cdot K_g \cdot \left[\frac{w_{Diss}}{1/\rho_{EtOH} + w_{Diss}/\rho_{ASA}} - \rho_{ASA,sat}\left(T\right) \right]}{Q_{feed} / \left({d_{inner}}^2 \cdot \pi/4 \right) \cdot \rho_{ASA}}$$

Here, Q_{feed} denotes the volumetric flow rate of the feed suspension into the reactor. The initial condition for this differential equation is given by the seed particle diameter $d_{p,0}$.

Results for a Negligibly Small Heat of Crystallization

For Δh_{cryst} = 0 we obtain an analytical expression for the temperature profile T(x):

$$\Phi\left(x\right) = \frac{T_{feed} - T\left(x\right)}{T_{feed} - T_{amb}} = 1 - \exp\left[-\frac{k \cdot x \cdot d_{outer} \cdot \pi}{\dot{m}_{tot} \cdot c_{p,tot}} \right]$$

Here $\Phi\left(x\right)$ denotes the dimensionless temperature difference between the feed temperature T_{feed} and the temperature of the suspension at the axial distance x from the inlet. Here T_{prod} is the temperature of the product exiting the tubular crystallizer.

2.5 Summary and Conclusion

A novel, continuously operated tubular crystallizer system with an inner diameter of 2.0 [mm] has been developed and tested for various flow rates, hence for diverse residence times. This tubular crystallizer allows the crystallization of active pharmaceutical ingredients (APIs) under controlled conditions, as flow rate, seed loading, temperature trajectory, etc. can be varied *independently*. Acetylsalicylic acid (ASA) which was crystallized from ethanol (EtOH), was used as the model substance. An ethanol suspension of ASA-seeds was fed into the tubular crystallizer system, where it was mixed with a slightly under-saturated ASA-EtOH solution that was kept at an elevated temperature in its storage vessel. Super-saturation was created via cooling. This work mainly focused on a proof of concept and on varying the residence times of the suspension and its impact on product crystal size distributions (CSD).

Comparative studies were performed using different ASA-EtOH suspension flow rates (11.4 [ml/min], 17.2 [ml/min], 22.8 [ml/min], 25.2 [ml/min]) in a 15 m long continuously seeded, continuously operated tubular crystallizer. The main results are:

- The concept of a continuously operated tubular crystallizer is feasible, since effects such as pipe plugging can be managed in a straightforward way. Only seed feed flows of 2.5 [ml/min] or less resulted in crystallizer blockage at rare occasions. The reason for the blockage was nucleation in all cases due to the lack of seeds in the crystallizer and the high supersaturations.
- The difference between the results for mean particle sizes provided by the model (chapter 2-4) and the experiments is apparently due to agglomeration effects which have been quantified in Table 2-2.
- Scale-up can be simply achieved via numbering up, i.e., industry-relevant quantities (e.g., for pharmaceutical companies) can be achieved by multiple tubes, which can be individually cleaned (or unplugged if necessary) by flushing it with a hot solvent. For a flow rate of 22.8 [ml/min] ~ 4.6 kg of the API can be produced in 24 h per pipe. It has to be pointed out that an excessive number of parallel pipes should be avoided due to the complexity in the operation.
- All experiments showed an increase of the mean diameter and a shift of the volume density distributions towards significantly larger values for the product crystals.
- Steady state conditions in the crystallizer were reached rapidly according to masses and CSDs of the product samples 1 and 2 of each experiment.

In summary, an industrially feasible system for continuous crystallization has been developed. Typically, slow crystal growth is desirable in order to yield high purity products.[28] Thus, this tubular crystallizer should be applied preferably for the last crystallization step.

In this work the seed-suspension has been produced batch wise. Clearly, continuous seed production is advantageous. Thus, it is our aim to implement a recycling stream that would recycle a fraction of the product crystals and then, after milling and classifying, feed the recycle stream back into the tubular crystallizer. Future work will address this new set-up as well as issues related to coating of the particles. Another issue addressed in future work will be polymorphism control during the continuous crystallization in a continuously seeded and operated tubular crystallizer.

2.6 References

(1) Tavare, N. S.; Matsuoka, M.; Garside, J.; Modelling a continuous column crystallizer: Dispersion and growth characteristics of a cooling section. *Journal of Crystal Growth* **1990**, 1151-1155.

(2) Chen, L. A.; Li, J.; Matsuoka, M.; Experimental and theoretical investigation of the purification process of organic materials in a continuous inclined column crystallizer. *Industrial & Engineering Chemistry Research* **2006**, *45*, 2818-2823.

(3) Lindenberg, C.; Krattli, M.; Cornel, J.; Mazzotti, M.; Brozio, J.; Design and Optimization of a Combined Cooling/Antisolvent Crystallization Process. *Crystal Growth & Design* **2009**, *9*, 1124-1136.

(4) Myerson, A. S.; Handbook of Industrial Crystallization 2nd ed.; Butterworth-Heinemann: Boston Oxford Johannesburg Melbourne New Delhi Singapore, 2002.

(5) Mullin, J. W.; Crystallization; Butterworth-Heinemann 3rd ed.: Oxford Boston Johannesburg Melbourne New Delhi Singapore, 1992.

(6) Barrett, P.; Smith, B.; Worlitschek, J.; Bracken, V.; O'Sullivan, B.; O'Grady, D.; A review of the use of process analytical technology for the understanding and optimization of production batch crystallization processes. *Organic Process Research & Development* **2005**, *9*, 348-355.

(7) Hammond, R. B.; Pencheva, K.; Ramachandran, V.; Roberts, K. J.; Application of grid-based molecular methods for modeling solvent-dependent crystal growth morphology: Aspirin crystallized from aqueous ethanolic solution. *Crystal Growth & Design* **2007**, *7*, 1571-1574.

(8) Togkalidou, T.; Braatz, R. D.; Johnson, B. K.; Davidson, O.; Andrews, A.; Experimental design and inferential modeling in pharmaceutical crystallization. *Aiche Journal* **2001**, *47*, 160-168.

(9) Ulrich, J.; Solution crystallization - Developments and new trends. *Chemical Engineering & Technology* **2003**, *26*, 832-835.

(10) Doki, N.; Yokota, M.; Kido, K.; Sasaki, S.; Kubota, N.; Reliable and selective crystallization of the metastable alpha-form glycine by seeding. *Crystal Growth & Design* **2004**, *4*, 103-107.

(11) Chow, K.; Tong, H. H. Y.; Lum, S.; Chow, A. H. L.; Engineering of pharmaceutical materials: An industrial perspective. *Journal of Pharmaceutical Sciences* **2008**, *97*, 2855-2877.

(12) Kim, S. J.; Wei, C. K.; Kiang, S.; Crystallization process development of an active pharmaceutical ingredient and particle engineering via the use of ultrasonics and temperature cycling. *Organic Process Research & Development* **2003**, *7*, 997-1001.

(13) Oullion, M.; Puel, F.; Fevotte, G.; Righini, S.; Carvin, P.; Industrial batch crystallization of a plate-like organic product. In situ monitoring and 2D-CSD modelling. Part 2: Kinetic modelling and identification. *Chemical Engineering Science* **2007**, *62*, 833-845.

(14) Oullion, M.; Puel, F.; Fevotte, G.; Righini, S.; Carvin, P.; Industrial batch crystallization of a plate-like organic product. In situ monitoring and 2D-CSD modelling: Part 1: Experimental study. *Chemical Engineering Science* **2007**, *62*, 820-832.

(15) Winn, D.; Doherty, M. F.; Modeling crystal shapes of organic materials grown from solution. *Aiche Journal* **2000**, *46*, 1348-1367.

(16) Shekunov, B. Y.; Chattopadhyay, P.; Tong, H. H. Y.; Chow, A. H. L.; Particle size analysis in pharmaceutics: Principles, methods and applications. *Pharmaceutical Research* **2007**, *24*, 203-227.

(17) Sarkar, D.; Rohani, S.; Jutan, A.; Multi-objective optimization of seeded batch crystallization processes. *Chemical Engineering Science* **2006**, *61*, 5282-5295.

(18) Eggers, J.; Kempkes, M.; Mazzotti, M.; Measurement of size and shape distributions of particles through image analysis. *Chemical Engineering Science* **2008**, *63*, 5513-5521.

(19) Gros, H.; Kilpio, T.; Nurmi, J.; Continuous cooling crystallization from solution. *Powder Technology* **2001**, *121*, 106-115.

(20) Midler, M. Jr.; Liu, P. D.; Paul, E. L.; Futran, M.; Whittington, E. F.; A crystallization method to improve crystal structure and size. EP 0461930A1, 1991

(21) Brenek, S. J.; AM Ende, D. J.; Crystallization method and apparatus using and impinging plate assembly. US Patent 0040098839, 2004

(22) Variankaval, N.; Cote, A. S.; Doherty, M. F.; From form to function: Crystallization of active pharmaceutical ingredients. *Aiche Journal* **2008**, *54*, 1682-1688.

(23) Myerson, A. S.; Molecular crystals of controlled size. US Patent 0030170999, 2003

(24) Su, Y. F.; Kim, H.; Kovenklioglu, S.; Lee, W. Y.; Continuous nanoparticle production by microfluldic-based emulsion, mixing and crystallization. *Journal of Solid State Chemistry* **2007**, *180*, 2625-2629.

(25) Dombrowski, R. D.; Litster, J. D.; Wagner, N. J.; He, Y.; Crystallization of alpha-lactose monohydrate in a drop-based microfluidic crystallizer. *Chemical Engineering Science* **2007**, *62*, 4802-4810.

(26) Gerdts, C. J.; Tereshko, V.; Yadav, M. K.; Dementieva, I.; Collart, F.; Joachimiak, A.; Stevens, R. C.; Kuhn, P.; Kossiakoff, A.; Ismagilov, R. F.; Time-controlled microfluidic seeding in nL-volume droplets to separate

nucleation and growth stages of protein crystallization. *Angewandte Chemie-International Edition* **2006**, *45*, 8156-8160.

(27) Schiewe, J.; Zierenberg, B.; Process and apparatus for producing inhalable medicaments. *US Patent 0015194A1*, 2003

(28) Méndez del Rio, J. R.; Rousseau, R. W.; Batch and tubular-batch crystallization of paracetamol: Crystal size distribution and polymorph formation. *Crystal Growth & Design* **2006**, *6*, 1407-1414.

(29) Lawton, S.; Steele, G.; Shering, P.; Zhao, L. H.; Laird, I.; Ni, X. W.; Continuous Crystallization of Pharmaceuticals Using a Continuous Oscillatory Baffled Crystallizer. *Organic Process Research & Development* **2009**, *13*, 1357-1363.

(30) Vishweshwar, P.; McMahon, J. A.; Oliveira, M.; Peterson, M. L.; Zaworotko, M. J.; The predictably elusive form II of aspirin. *Journal of the American Chemical Society* **2005**, *127*, 16802-16803.

(31) Bond, A. D.; Boese, R.; Desiraju, G. R.; On the polymorphism of aspirin: Crystalline aspirin as intergrowths of two "polymorphic" domains". *Angewandte Chemie-International Edition* **2007**, *46*, 618-622.

(32) Faria, N.; Pons, M. N.; de Azevedo, S. F.; Rocha, F. A.; Vivier, H.; Quantification of the morphology of sucrose crystals by image analysis. *Powder Technology* **2003**, *133*, 54-67.

(33) Vivier, H.; Pons, M. N.; BernardMichel, B.; Rolland, T.; Voignier, L.; Vucak, M.; Quantification of particle morphology in powder process technology. *Microscopy Microanalysis Microstructures* **1996**, *7*, 467-475.

(34) Maia, G. D.; Giulietti, M.; Solubility of acetylsalicylic acid in ethanol, acetone, propylene glycol, and 2-propanol. *Journal of Chemical and Engineering Data* **2008**, *53*, 256-258.

(35) Su, J. W.; Gu, Z. L.; Li, Y.; Feng, S. Y.; Xu, X. Y.; Solution of population balance equation using quadrature method of moments with an adjustable factor. *Chemical Engineering Science* **2007**, *62*, 5897-5911.

(36) Kirklin, D. R.; Enthalpy of combustion of acetylsalicylic acid. *Journal of Chemical Thermodynamics* **2000**, *32*, 701-709.

(37) Bird, R. B.; Steward, W. E.; Lightfood, E. N.; Transport Phenomena; John Wiley and Sons, Inc.: 2002.

(38) Granberg, R. A.; Bloch, D. G.; Rasmuson, A. C.; Crystallization of paracetamol in acetone-water mixtures. *Journal of Crystal Growth* **1999**, *199*, 1287-1293.

3 Seed Loading Effects on the Mean Crystal Size of Acetylsalicylic Acid in a Continuous-Flow Crystallization Device[d]

This study investigates the effects of seed loading on the mean crystal size of the model substance, acetylsalicylic acid, crystallized from ethanol in a continuously seeded tubular crystallizer. A hot, highly concentrated ethanolic acetylsalicylic acid solution was mixed with an acetylsalicylic acid-ethanol seed suspension. Subsequent cooling of the slurry in the tubing promoted supersaturation and hence crystal growth. The tubular shape of the 15 m-long crystallizer with an inner diameter of 2 mm enabled narrow residence time distributions of the crystals in the pipe and excellent temperature control in the radial direction and along the tubing. Crystals entering the crystallizer had both identical growth conditions in each section and about the same time for crystal growth. Narrow crystal size distributions were achieved with decreasing differences in the volume-mean-diameter sizes of the seed and product crystals as seed loadings increased. Decreasing the seed size had a similar effect as increasing the seed loading, since in that case the same amount of seed mass resulted in more individual seed particles. Altering the arrangement of the coiled crystallizer with respect to spatial directions (horizontal, vertical) did not lead to a significantly different outcome. All experiments produced considerably larger product crystals in comparison to the seeds despite relatively short crystallization times of less than 3 min. Moreover, product mass gains of a few hundred percent at a g/min-scale were achieved. Similarities in product crystal samples taken at different times at the outlet of the crystallizer showed that steady-state conditions were rapidly reached in the continuous flow crystallization device.

3.1 Introduction

Since more than 90% of all active pharmaceutical ingredients (APIs) are crystals of small organic molecules[1] crystallization from solution is extensively employed as the final step in the production of bulk APIs, allowing relatively inexpensive phase separation and purification.[2-4] Moreover, critical process parameters, such as temperature, energy input, concentration of target compounds, surfactants, additives or antisolvents, can be manipulated to affect the product's quality with respect to the

[d] This chapter is based on the journal article by Eder et al. in Crystal Research and Technology 2011.

crystal shape and size distribution (CSSD).[5-8] These bulk properties greatly affect downstream processes (filtration, washing, drying, etc.)[1;9;10] and further handling of the crystals, since flowability, storage characteristics, dusting,[11] segregation phenomena, compactibility and tabletability[12] are functions of the aforementioned CSSD. In the context of APIs, this has a major impact on disintegration and dissolution rates[2] and hence on the bioavailability of the compound.[13;14] Polymorphism control is another critical objective during crystallization operations.[15;16] Different crystal modifications are likely to produce crystals of varying shapes[6;17] and solid materials with varying physical properties (melting point, density, hardness, solubility).[18-20] Consequently, the morphology directly affects downstream operations, handling of the bulk particles and the bioavailability of the drug substance.[21;22] This is also true for solvates, salts and amorphous solids.[8] Furthermore, polymorphism, salt and solvate formation are important concerns with regard to patent issues.[15;23] Thus, tight control of critical process parameters during a crystallization step is of utmost importance for obtaining high yields and good quality products in terms of purity, shape and size distribution, as well as distinct crystal modification. These are necessary to satisfy the customers' safety needs and the strict requirements of regulatory bodies, such as the Food and Drug Administration (FDA) and the European Medicines Agency (EMA).

Due to the economic importance of crystalline substances, a vast number of products is manufactured using diverse crystallization methods and a wide range of crystallizer types.[2;24] They can be classified based on the creation of supersaturation, the driving force of crystallization[25] (i.e., cooling, evaporation, change of solvent composition and reaction) or based on the process mode (i.e., continuous, semi-batch or batch operation).[2] The pharmaceutical industry strongly relies on batch processes, particularly concerning crystallization operations.[26] The advantages of batch crystallizations include easy implementation and maintenance, suitability for viscous and toxic substances and the ability to obtain larger crystals for systems with slow crystal growth than those produced via continuous processes.[27] Furthermore, with regard to industrial crystallization, continuous operations have some crystallization-specific disadvantages, namely incrustation problems, slow attainment of a steady-state and potential operational instability.[24] However, the advantages of continuous processes are significant and include shorter down times, fewer scale-up issues, better control potential for optimal process conditions, improved process safety and

economy,[26] good reproducibility of results[28] and smaller equipment size, which reduce capital and operating costs.[24] Although additional facilities and instrumentation may be required, they offer a high level of automatization and therefore cost efficiency.

The benefits of continuous manufacturing have been exploited in other industrial fields for several decades, but the pharmaceutical industry is still in a transitional phase. Yet the interest in continuous manufacturing of pharmaceutical products has recently increased significantly. Novartis, for example, provided the Massachusetts Institute of Technology (MIT) a 10-year grant of $ 65 million to establish a Novartis-MIT Center for Continuous Manufacturing.[26] Other centers for pharmaceutical manufacturing (e.g., at Rutgers University) have for many years focused on continuous process design, and the number of publications on continuous API fabrication, including reports on continuous crystallization methods, is steadily increasing.

In the area of crystallization, several innovative continuous techniques based on precipitation via impinging jets or tubular devices (with and without static mixers) have been reported. Impinging jet precipitation, for example, has been applied to API micro-particle formation as described by Brenek et al.[29] and Midler et al.[30] Fast precipitation is especially used for improving bioaviability by generating small particles with high specific surface areas.[31] Micro-reactor technology has been adopted for the production of solid products, since it has shown several benefits (e.g., tight reaction control and numbering up instead of scale-up[26]) in other areas of chemical engineering. To date, the application of micro-systems for the solids manufacturing has mostly been restricted to inorganic nanoparticles.[26] Recent exceptions include, for instance, the reports by Debuigne et al.,[32] Su et al. (2,2´dipyridylamine),[33] Dombrowski et al. (alpha-lactose monohydrate),[34] and Gerdts et al. (proteins),[35] as well as the patent of Myerson for molecular API crystals of a controlled size,[36] where organic particles were formed in micro-structured channels. Currently, the number of publications in the field of organic particle formation, including APIs, via micro reactor technology is growing rapidly.

Earlier, Raphael et al.[37] described the precipitation of sunflower proteins, Virkar et al. of soy protein,[38] Riviera and Randolph[39] of pentaerythritol tetranitrate and Stahl et al.[40] of benzoic acid in a tubular device with an inner diameter (d_{inner}) in the millimeter range. A patent by Schiewe and Zierenberg[41] describes the continuous production of

inhalable drug particles in a size range from 0.3 to 20 µm. These particles are precipitated in tube-like channels, where a stream of alternating segments of a suspension and a transport medium (e.g., gas or oil) is produced in order to achieve a very narrow residence time distribution. Similar segmented flow tubular reactors (SFTR) were described earlier in the literature.[42] In addition, Méndez del Rio and Rousseau[43] reported the use of a tubular device for tubular-batch crystallizations. The tubing was used to rapidly cool the solution and, after primary nucleation, paracetamol crystals grew in the stirred receiving vessel. Lately, new crystallization equipment for APIs has been described in the literature, such as a continuous baffled crystallizer by Lawton et al.[44] and a very recent work on a continuous plug flow crystallizer for drug compounds by Alvarez and Myerson[1] as well as a flow through crystallization device by our group.[2;45-47] This shows that continuous crystallization in pharmaceutical applications is a research area of increasing interest and a critical step for the implementation of over-all continuous API manufacturing from substance synthesis to final products.

The present study investigates the influence of seed loading on the mean particle size of a cooling crystallization in a tubular flow-through device. Moreover, the effects of the seed size on the product attributes and of the geometrical orientation of the coiled tubing (vertical or horizontal arrangement) on particle segregation phenomena along the length of the crystallizer were analyzed.

For the experiments, an ethanolic suspension of acetylsalicylic acid (ASA) seeds is fed into a tubular crystallizer, where it is mixed with a hot, highly concentrated ASA-ethanol (EtOH) solution. Supersaturation is created via cooling and the seeds grow to form the product crystals while passing through the tubing. Due to the tubular appearance and small inner dimensions (millimeter-range) of the crystallizer, the temperatures along the tubing can be adjusted depending on the crystallization needs without temporal or spatial oscillations, and narrow residence time distributions of the slurry in the pipe can be achieved. Hence, the seeds crystallize in a similar environment (concentration, temperature, etc.) and take approximately the same time to grow. Thus, a narrow crystal size distribution (CSD) can be obtained.

3.2 Experimental

Materials. ASA (Rhodine 3020, pharmaceutical grade 100.0%, monoclinic) was provided from GL-Pharma. EtOH (99.8% denaturized with 1.0% methyl ethyl ketone) and cyclohexan (100.0%) were purchased from Roth (Lactan).

Equipment. Two peristaltic pumps (PI and PII) were utilized to feed the solution (PI: Ismatec BVP-Process 65-3/6; Tube: Pharmmed® d_{inner} = 1.6 mm, d_{outer} = 4.8 mm) and the seed suspension (PII: Reglo Digital MS-2/6V 1.13C; Tube: Pharmmed® d_{inner} = 2.8 mm, d_{outer} = 5.0 mm) into a tubular crystallizer. A polytetrafluorethylene (PTFE) Y-fitting (d_{inner} = 2 mm) connected the Pharmmed® tubes with a 15m long polysiloxane tubing (d_{inner} = 2.0 mm, d_{outer} = 4.0 mm), in which the seeds grew to form the product crystals. Several thermostatic baths from Lauda® were used to create the cooling sections. Crystal Size Distribution (CSD) characterizations were performed with a Quicpic® system from Sympatec® and the corresponding Oasis® dispersion unit. Pictures of the crystals were taken with a Leica® DM 4000 microscope equipped with a Leica® DFC camera.

Set-up. A schematic of the system is shown in Figure 3-1. The ASA-EtOH solution was kept at around 60.0 ± 0.2 ℃ ($T_{sol.}$) in its storage vessel, and the ASA-EtOH seed suspension was stirred at 25.0 ± 0.2 ℃ ($T_{susp.}$). Peristaltic pumps fed the solution (PI, $\dot{V}_{sol.}$ = 13.1 ml/min) and the suspension (PII, $\dot{V}_{susp.}$ = 3.8 ml/min) streams into the crystallizer.

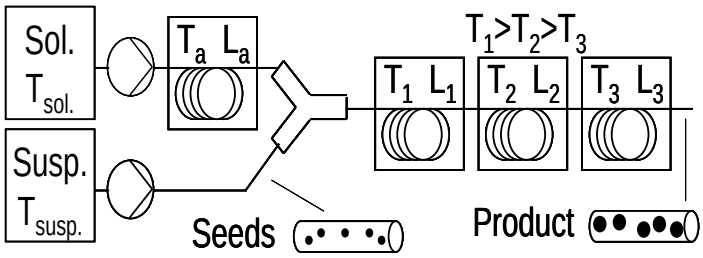

Figure 3-1. Schematic of the process.

Before entering the Y-fitting, a thermostatic bath was employed to bring the solution to 40.0 ± 0.2 ℃ (T_a). The minimum length of L_a (Figure 3-1) was determined by the flow rate of the solution given that T_a, $T_{sol.}$, the concentration and the properties of the tubing (material, d_{inner} and d_{outer}) were constant. T_a guaranteed a slightly supersaturated solution feed stream, leading to crystal growth after mixing the solution with the cooler suspension feed (25.0 ℃). A relatively low supersaturation ratio (S) of the solution feed minimized the risks of ASA nucleation before mixing of

solution and suspension. After mixing the solution and the suspension in the Y-fitting, the supersaturation ratio was still low enough to avoid excessive nucleation events in the tubular crystallizer. S results from the actual concentration (conc.) and the equilibrium concentration (conc.*) at a given temperature according to Eq. (3-1):

$$S = \frac{conc.}{conc.^*} \tag{3-1}$$

The tubular crystallizer was placed in three successive thermostatic baths with decreasing temperatures (T_1 = 32.0, T_2 = 27.0 and T_3 = 22.0 ± 0.2 °C) in order to create a temperature gradient. In general, a tubular crystallizer is highly flexible, as the number of cooling sections, their respective temperatures and their lengths can be changed independently, thus allowing the tailoring of the temperature gradient and the residence time (within bounds). In our case the lengths were L_1 = 5.0, L_2 = 3.0 and L_3 = 7.0 m, respectively. All these parameters were kept constant throughout the experiments.

The tubular crystallizer was coiled on 3 cylinders (d_{outer} = 0.1 m) made from grid-structured material in order to ensure good heat transfer. The geometry of the tubular crystallizer was kept constant for a set of experiments with varying seed loads (Exps. 1-3). As shown in Figures 3-1 and 3-2a, the axis of the cylinder (height) was arranged horizontally. Thus, the coils were vertical, and the slurry in the tubing had subsequent up- and down-flow sections.

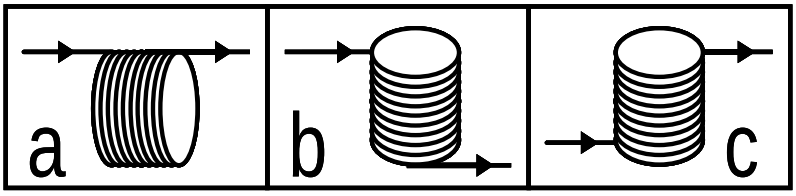

Figure 3-2. Arrangement of coiled crystallizer: a vertically, b horizontally with feed on the top and c horizontally with feed at the bottom.

Another set of experiments was performed with differently-sized seeds to investigate the influence of seed size on the product properties (Exps. 4-6). In the first experiment with the altered seed size, the coils of the tubing were placed in the cooling sections as described above (Figures 3-1 and 3-2a). Then, the coiled crystallizer was arranged horizontally so that for one experiment the feed end in each cooling section were on the top (Figure 3-2b) and, for a follow-up experiment, at the bottom of each cylinder (Figure 3-2c).

In Figure 3-3 the growth of the particles is shown schematically. Heat removal ($\dot{Q}$) due to cooling of the slurry from T_{feed} to the product temperature ($T_{prod.}$) via the temperature trajectory (T_x) towards the ambient temperature ($T_{amb.}$) is responsible for the supersaturation generation.

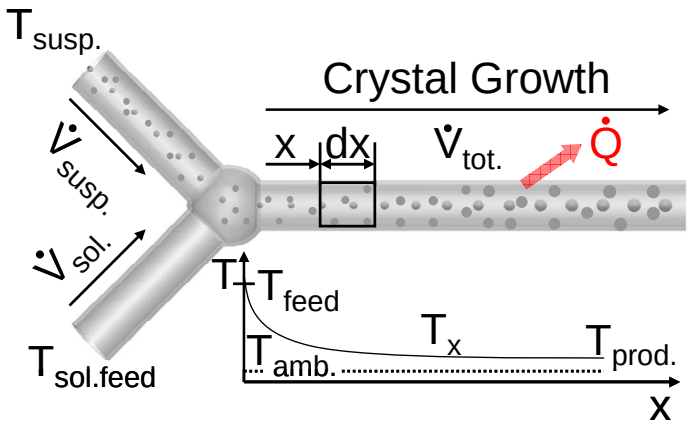

Figure 3-3. Schematic of crystal growth upon cooling.

Figure 3-4 presents a schematic of temperature trajectories for natural (uncontrolled), linear and controlled cooling policies.

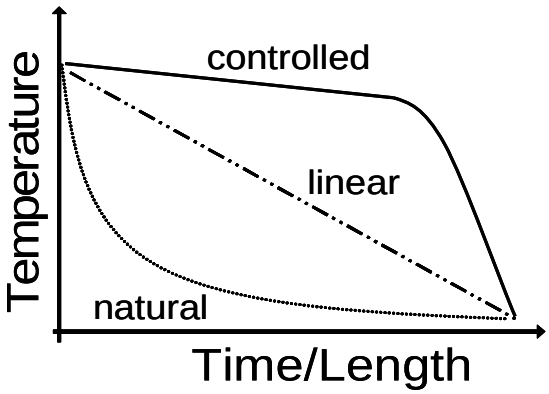

Figure 3-4. Schematic profiles of natural, linear and controlled cooling policies.

In natural cooling with no temperature control, the slurry approaches the ambient temperature with a constant heat transfer coefficient. Due to a significant initial temperature decrease, the elevated supersaturation can cause nucleation[48] whenever the metastable limit is exceeded, which is undesirable. Linear cooling is defined by constant heat removal over time, reducing the potential for excessive nucleation. However, a controlled policy that allows crystallization at almost constant supersaturation is even more favorable[49] for several reasons (e.g., polymorphism control). Under a controlled cooling policy, the cooling trajectory is flat in the beginning and increases towards the end. As crystals and their surface areas grow,

the cooling rate can be increased and, thus, the crystallization process can be accelerated without significantly altering the supersaturation. This concept can be applied to keep supersaturation values below the limit over which excessive nucleation occurs and, at the same time, allows reasonably fast crystal growth. Thus, we adopted a controlled cooling approach by using three cooling sections with different temperatures (see Figure 3-1) in order to perform the experiments at relatively low supersaturation levels to avoid excessive nucleation, with S still high enough for reasonably fast crystal growth rates.

Model. A model reported earlier[2] was used to asses the temperature trajectory, the particle growth and the supersaturation ratio S. Adaptations were made in order to reflect the current experiments. A value of α_{outer} = 1494 [W/m^{2}K] was used for the outer heat transfer coefficient, since water baths were used for cooling. For crystal growth the model assumes a single particle size for each position along the tubing and no axial, but perfect radial mixing. Furthermore, agglomeration, breakage and nucleation events were neglected, and hence, the particle number was constant.[2]

Procedure. A highly concentrated ASA-EtOH solution with an ASA wt-% of 33.3 (e.g., 100 g ASA in 200 g EtOH; conc.$_{ASA}$ ~ 2.19 mol/l) was prepared by dissolving the substance at 62.0 ± 0.2 ℃ under vigorous stirr ing for 30 min. This ensured that no solid ASA was left. Additionally, the solution was sufficiently undersaturated since a wt-% of around 48.6 could theoretically be achieved at this temperature according to the Nývlt model (Eq. 3-2).

$$\log(X^{*}_{ASA} = N_1 + \frac{N_2}{T} + N_3 \log(T) \qquad (3\text{-}2)$$

The parameters $N_{1,2,3}$ have the values of 22.769, -2500.906 and -8.323[50] for the system ASA-EtOH and the temperature (T) is expressed in Kelvin. Maia and Giulietti[50] showed that experimental solubility data excellently agree with equilibrium solubility values (X^*_{ASA}) obtained from Equation 3-2.

The molar fraction of dissolved ASA (X_{ASA}) is given by Eq. 3-3. Here n denotes the moles of either ASA or EtOH according to the indices. (The molecular weight of ASA and EtOH are 180.16 g/mol and 46.07 g/mol respectively).

$$X_{ASA} = \frac{n_{ASA}}{n_{ASA} + n_{EtOH}} \qquad (3\text{-}3)$$

The ASA-EtOH seed suspensions were prepared by dissolving different amounts of ASA at 62.0 ± 0.2 ℃ followed by precipitation thro ugh cooling at ~ 4 ℃ and vigorous

stirring. Because of friction, breakage, dissolution and re-crystallization effects, the suspension was stirred at 25 ± 0.2 ℃ for 48 hours in order to reach equilibrium conditions between the solid and the liquid phase, as well as steady CSDs of the seeds between 30 and 300 µm (seed loading experiments No. 1-3), or for 24 hours for the fraction between 30 and 400 µm (different seed size and crystallizer coil orientation experiments No. 4-6).

Prior to each experiment the crystallizer was placed in the thermostatic baths and flushed with EtOH in order to rinse the tubing with the help of PI and PII, before PII was switched to the seed suspension supply vessel. Subsequently, PI was switched from pure EtOH to the ASA-EtOH solution in order to start the crystallization process. This start-up procedure ensured that seed crystals were present in the tube at any time when the solution entered the tubing. (In preliminary studies it was observed that the absence of seeds led to uncontrolled primary nucleation events that ultimately resulted in the blockage of the tubular crystallizer.) Throughout the experiments that lasted about 15 to 20 min, two product samples were taken at different times at the outlet of the crystallizer. Seeds were sampled in the beginning and at the end of each run. Samples were collected via filtration, followed by washing the crystals with cyclohexane, a solvent in which ASA does not dissolve. Before assessing weight and CSDs, the samples were vacuum-dried. The dissolved ASA in the product stream was determined by removing the solid ASA via filtration, followed by weighing the solution and the ASA-residue after complete evaporation of the ethanol.

In the first set of experiments the solid ASA loading in the seed suspension (m_{seed}) vessel was varied in order to feed different seed loadings (solid ASA per ml slurry) into the tubular crystallizer (m_{seed}/ml_{slurry} =. 0.02, 0.04 and 0.05 g/ml). An alternative approach would be to alter the seed suspension flow rate. In this case, an adjustment of the solution feed temperature would be necessary in order to keep T_{feed} constant. All other parameters that affect crystallization, including the solution properties (temperature, $conc._{ASA}$), cooling trajectory and residence time were kept constant. This allowed us to specifically determine the effect of the seed loading on the mean product particle size.

A further set of experiments was performed with different-sized seeds to study the influence of the seed size on the product property. Furthermore, the orientation of the tubular crystallizer was varied (Figure 3-2) to observe if differences in the product CSDs are caused by segregation phenomena. All experiments were performed twice.

3.3 Results and Discussion

Table 3-1 summarizes experimental data with regard to three different seed loadings (Exps. 1-3). Here the seed loading describes the mass of particles per ml of slurry entering the crystallizer. In contrast, the seed loading fraction x_{seed} is defined as the mass flow rate of solid seeds over the mass flow rate of dissolved ASA before entering the crystallizer (not shown in the Table):

$$x_{seed} = \frac{\dot{m}_{seed}}{\dot{m}_{solute}} \tag{3-4}$$

$\dot{m}_{solute}$ and $\dot{m}_{seed}$ denote the mass flow rate of dissolved ASA and the mass flow rate of seeds, respectively, at the crystallizer inlet. The seed loading fractions for the Exps. 1-3 were $x_{seed,1}$ = 0.07, $x_{seed,2}$ = 0.14 and $x_{seed,3}$ = 0.16. All other parameters were kept constant, including the flow rate ($\dot{V}_{tot.}$ (16.9 ml/min) = $\dot{V}_{susp.}$ (3.8 ml/min) + $\dot{V}_{sol.}$ (13.1 ml/min)), and thus the mean residence time of the slurry was $t_{res.}$ ~ 161 s (2.7 min) in the tubing. A mass gain r_m, according to Eq. 3-5

$$r_m = \frac{\dot{m}_{prod.}}{\dot{m}_{seed}}.100\% , \tag{3-5}$$

was achieved during all experiments and was almost as high as 800%. The total product ASA mass flow ($\dot{m}_{prod.}$) increased with the seed loading, as more solid ASA was present in the feed. However, r_m decreased as expected with the increasing seed loadings, as the dissolved amount of ASA in the solution remained constant.

Similar product sample masses and CSDs of the product crystals in each experiment imply that steady-state conditions were rapidly reached in the tubular crystallizer. Differences between volume mean diameters ($d_{p,vol.}$) of the seed and product crystals suggest that crystal growth took place. Microscopic pictures of the product crystals in Figure 3-5 (seed loading of 0.04 g_{seed}/ml_{slurry}) show that product crystals increased in size due to crystal growth and not only due to the aggregation and agglomeration of smaller crystallites, which always take place during bulk crystallization processes.[51]

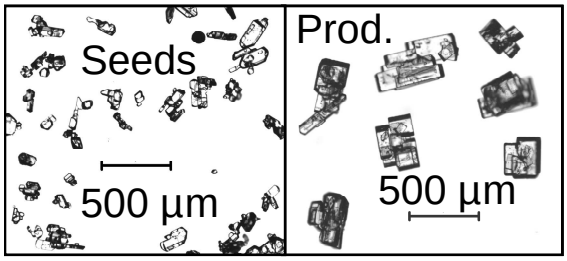

Figure 3-5. Photos of seed and product crystals (0.04 g_{seed}/ml_{slurry}).

To assess the width of the size distributions $\chi_{vol.10/90}$ was computed, $\chi = 1$ corresponding to uniform crystal size. As can be seen χ of the product increased as expected for similar growth rates of small and larger crystals.

Table 3-1. Experiments 1-3: seed loading (m_{seed}/ml_{slurry}), sampling time (t), solid ASA mass ($\dot{m}_{ASA}$), volume mean diameter ($d_{p,vol.}$), $\chi_{vol.10/90}$ and mass gain (r_m).

m_{seed}/ml_{slurry} [g/ml]*	Sample	t [min]**	$\dot{m}_{ASA}$ [g/min]	$d_{p,vol.}$ [µm]	$\chi_{vol.10/90}$ [µm/µm]	r_m [%]
0.02	$Seeds_1$	-	0.35***	136	73/206 = 0.35	779
	$Prod._{1-1}$	5	2.73	260	173/347 = 0.50	
	$Prod._{1-2}$	10	2.72	265	178/357 = 0.50	
0.04	$Seeds_2$	-	0.70***	143	79/233 = 0.34	407
	$Prod._{2-1}$	8	2.86	256	168/350 = 0.48	
	$Prod._{2-2}$	14	2.84	259	171/352 = 0.49	
0.05	$Seeds_3$	-	0.84***	132	72/201 = 0.36	348
	$Prod._{3-1}$	5	2.90	232	150/317 = 47	
	$Prod._{3-2}$	12	2.94	232	149/304 = 0.49	

* Solid ASA-seed mass per ml slurry entering the tubing. ** Sampling time t of products after startup. *** Arithmetic mean values of two seed samples.

Figure 3-6 shows volume density distributions $q_3(x)$ of the seed and two product samples. It should be noted that the volume density distributions $q_3(x)$ in the Figures 3-6 and 3-8 are plotted on a linear and not on a log-normal scale, thus appearing broader. Evidently, the product sample distributions are shifted to the right, towards larger crystal sizes compared to the seeds. The almost-identical volume density distribution of the product samples 1 and 2 supports the assumption that a steady-state condition was reached rapidly and sustained throughout the experiment. The discrepancy was well within the limits of statistical fluctuations that are observed when repeatedly characterizing the same sample. The experiments with seed loadings of 0.02 or 0.05 g_{seed}/ml_{slurry} in the crystallizer yielded comparable results, which led to the same conclusions concerning crystal growth and steady-state conditions. However, increasing the seed loading resulted in smaller differences between mean seed and product sample sizes.

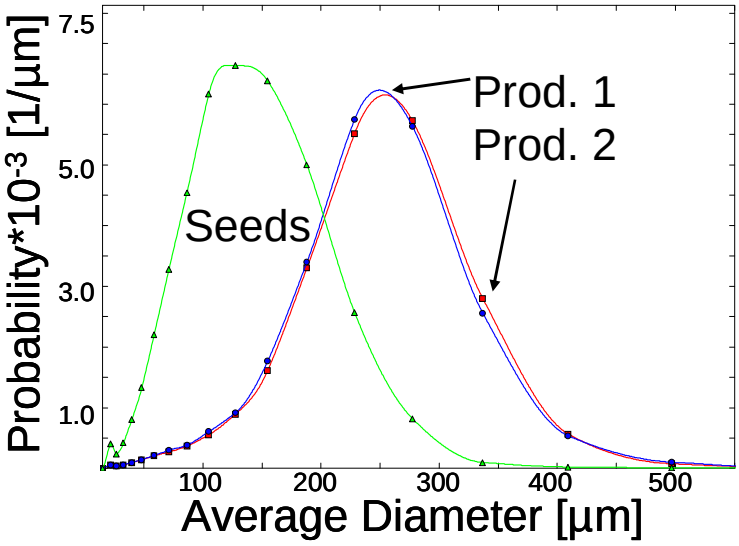

Figure 3-6. Volume-density distributions of seed and product samples (0.04 g_{seed}/ml_{slurry})

In Figure 3-7 the differences between mean seed and product crystal samples ($\Delta d_{p,vol.}$) of the experiments and theoretical calculations are plotted against the seed loadings of the slurry, showing an inversely proportional relationship between seed loading and $\Delta d_{p,vol.}$. This was to be expected, since increased seed loading results in a higher number of individual particles available as crystallization sites. This can also be observed in Figure 3-8 showing the product size distributions $q_3(x)$ for experiments 1-3. In this case, the volume density distributions with higher seed loadings shifted to smaller sizes. Note that during the experiments with 0.04 gseed/mlslurry the seeds were slightly larger, thus explaining the shift of the $q_3(x)$ distribution to higher diameters than expected.

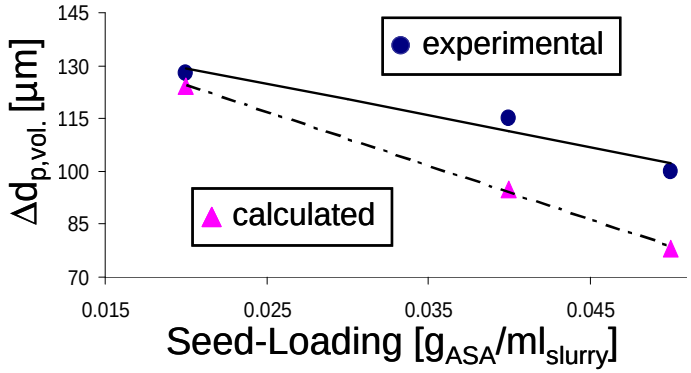

Figure 3-7. Seed loading versus $\Delta d_{p,vol.}$. (The lines are drawn to aid the eye.)

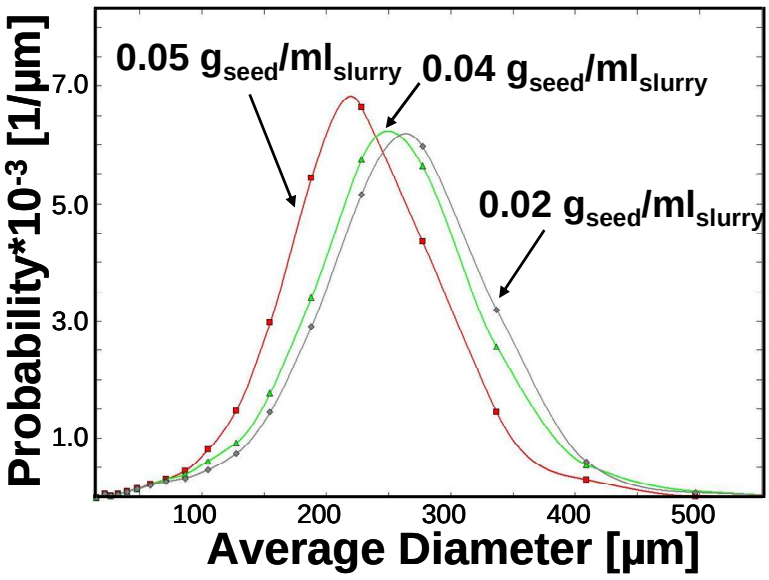

Figure 3-8. Product volume-density distributions of experiments with different seed loadings.

As pointed out above in the model section, agglomeration, breakage and nucleation were neglected.[2] Agglomeration effects and non-idealities in the system (e.g., residence time distribution of crystals), however, might explain the deviation between $\Delta d_{p,vol.}$ of the experiments and the model (Figure 3-7). The growing differences between computed and experimental values with increasing seed-loadings may be attributed to increasing agglomeration effects due to larger numbers of smaller crystals.[52]

Figures 3-9 and 3-10 show the modeled results for the temperature, the particle size and the supersaturation profile in the crystallizer. As can be seen, in each cooling section, the temperature dropped quickly to reach a plateau corresponding to the bath temperature. Due to the chosen bath temperature trajectory the maximum S increased slightly in each subsequent cooling section since the supersaturation was not consumed fast enough for the system to reach equilibrium conditions. However, this allowed for fast crystal growth and S was still low enough to suppress nucleation. More cooling sections and increasing the length of the cooling sections (or decreasing the flow rate) could lead to an optimal cooling policy with a flatter cooling profile with respect to the maximum of S. This, however, is a question of process optimization.

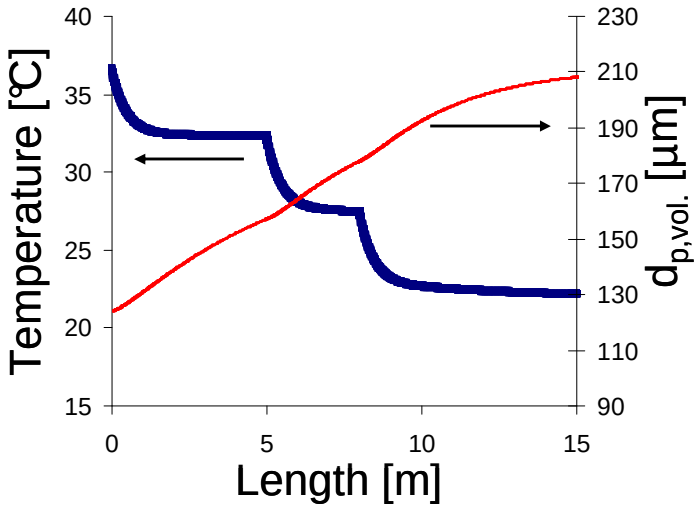

Figure 3-9. Increase in particle size and temperature course.

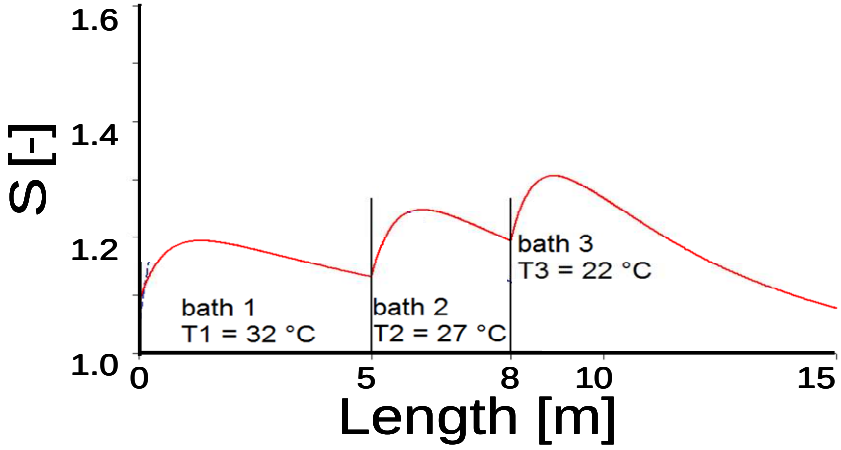

Figure 3-10. Supersaturation ratio S observed in 3 cooling sections along the crystallizer length (Exp. 1).

The modeled supersaturation ratios of the experiments with increasing seed loadings Exps. 1-3 show that the liquid phase of the slurry at the outlet was for all cases close to equilibrium solubility conditions ($S_{Exp.1}$ = 1.14, $S_{Exp.2}$ = 1.06, $S_{Exp.3}$ = 1.03). Only the experiment with the lowest seed loading resulted in a supersaturation of ~ 14%. This is because lower amounts of seeds provide less surface area and result additionally in larger crystals growing in the crystallizer with less surface area per mass to consume the supersaturation.

For the experiments No. 4-6, data are shown in Table 3-2. The total flow rate of the slurry was again kept at 16.9 ml/min and the solid content of seeds at the feed end was 0.05 g_{seed}/ml_{slurry}. Thus, the seed loading fraction (Eq. 3-4) of Exps. 4-6 was comparable to Exp. 3 ($x_{seed,3}$ ~ $x_{seed,4\text{-}6}$ ~ 0.16). However, the seeds were larger than those used in the experiments above (Exps. 1-3) and the geometrical orientation of the coiled tubing (vertical or horizontal arrangement) was altered in order to assess

particle segregation phenomena along the length of the crystallizer. In all experiments a mass increase between seed and product samples was observed. Product volume mean diameters shifted to larger sizes indicating crystal growth. Product samples taken at different times were comparable with respect to mass, volume mean size and χ, showing that the system operated in steady-state conditions and that a relatively narrow CSD was achieved. The modeled supersaturation ratio ($S_{Exp.4-6}$ = 1.08) at the outlet was slightly higher than for Exp. 3, because increased seed sizes resulted in a decreased crystal surface area per mass.

Table 3-2. Experiments 4-6: sampling time (t), solid ASA mass ($\dot{m}_{ASA}$), volume mean diameter ($d_{p,vol.}$), $\chi_{vol.10/90}$ and mass gain (r_m).*

Coil Orientation	Sample	t [min]	$\dot{m}_{ASA}$ [g/min]	$d_{p,vol.}$ [µm]	$\chi_{vol.10/90}$	r_m [%]
Figure 2a	$Seeds_4$	-	0.86	184	96/271 = 0.35	
vertical	$Prod._{4-1}$	5	3.08	330	200/452 = 0.44	362
	$Prod._{4-2}$	9	3.15	329	197/458 = 0.43	
Figure 2b	$Seeds_5$	-	0.85	186	96/280 = 0.34	
horizontal	$Prod._{5-1}$	12	3.19	334	204/461 = 0.44	376
top-feed	$Prod._{5-2}$	16	3.21	325	197/441 = 0.45	
Figure 2c	$Seeds_6$	-	0.89	183	93/276 = 0.34	
horizontal	$Prod._{6-1}$	4	3.17	327	204/444 = 0.46	355
bottom-feed	$Prod._{6-2}$	12	3.15	325	203/436 = 0.47	

* For details on abbreviations see Table 3-1.

Generally, no significant differences between experiments 4, 5 and 6 were apparent with respect to average crystal size and CSD according to the cumulative volume fractions $Q_3(x)$ shown in Figure 3-11.

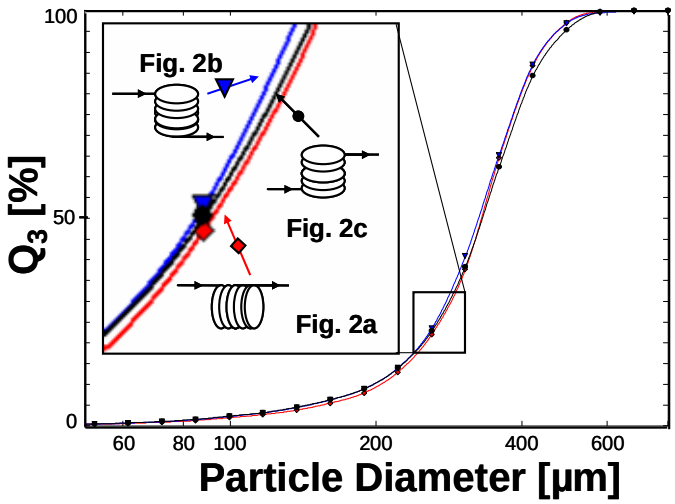

Figure 3-11. Cumulative volume fractions (Exps. 4-6).

Data presented in Table 3-2 show slightly narrower CSDs for horizontal coil arrangements. Nevertheless, no trend could be derived, since the differences were very small although the Reynolds number (Re ~ 17, Eq. 3-6) indicated laminar flow for these experiments with a mean slurry velocity of ν ~ 0.09 m/s.

$$\mathrm{Re} = \frac{\rho_{slurry} v d_{inner}}{\mu_{slurry}} \tag{3-6}$$

The density and the dynamic viscosity of the slurry at 25 °C were ρ_{slurry} ~ 950 kg/m^3 and μ_{slurry} ~ 0.01 Pa·s.[2] Density and viscosity variations due to decreasing temperatures and increasing solid contents along the crystallizer were negligible. The Stokes settling velocity (ν_{Stokes}) of individual crystals can be calculated according to Eq. (3-7).

$$v_{Stokes} = \frac{2(\rho_{ASA} - \rho_{solution})g}{9\mu}\left(\frac{d_{p,vol.}}{2}\right)^2 \tag{3-7}$$

The densities of the solid ASA and the solution are ρ_{ASA} ~ 3500 kg/m^3 and $\rho_{solution}$ ~ 865 kg/m^3 (25 °C). Thus, for a $d_{p,vol.}$ = 184 µm the settling velocity is 0.05 m/s. The particle Reynolds number (Re_p = 3) was slightly larger than the ones in the Stokes regime. Thus, modified corrections, well-known in the literature, were used to give a settling velocity of about 0.03 m/s. Furthermore, particles are non-spherical and hence, the actual velocity should be even smaller. In conclusion, the settling velocities are smaller than the flow velocity by more than a factor of 3. It thus can be expected that particles are carried with the flow in case of the vertical tube arrangement. Moreover, the up- and downward sections were of same length, thus minimizing potential particle size segregation effects over the length of the crystallizer. Additionally, the solid mass content was high, reaching almost 20% at the end of the crystallizer. Thus, hindered settling phenomena of the particles can be expected, and the particles may tend to settle *en masse* more slowly,[53] and hence, the size segregation is further reduced. In the case of the horizontal tube, particles should settle within a short distance. Yet, the small difference between the CSD for both orientations indicates that the crystals are still carried by the solution. Thus, in summary no significant segregation effects were detectable for our system. Future experiments could, however, implement segmented flows as utilized by Schiewe and Zierenberg[41] and Vacassy et al.[42] This would entirely eliminate a wide residence time distribution of the slurry in the tubing and size segregation effects of the particles. Combining a segmented flow with the vertical coil orientation (Figure 3-2a) seems to

be the best option of all possible spatial coil arrangements. The particles would change their relative position in a suspension segment from the droplet front - while moving downwards - to the back when coming up again. This would additionally enhance mixing in each droplet segment, and therefore, mass and heat transfer.

Comparing results of experiment 3 (0.05 g_{seed}/ml_{slurry}, Table 2-1) to those of experiments 4, 5 and 6 (0.05 g_{seed}/ml_{slurry}, Table 3-2) shows that, depending on the seed size, significant differences of the product crystal sizes can be observed. Reduced seed particle sizes resulted in a higher number of individual seed crystals and hence smaller product crystals, as well as in reduced differences between seed and product crystals. Generally, all seed properties including mean seed size, seed size distribution and the seed mass have a major effect on the outcome of the product.[54]

3.4 Summary and Conclusion

A continuously seeded flow-through crystallizer system with an inner diameter of 2 mm was evaluated with various seed loadings. The process parameters, including temperatures, temperature gradients, concentrations and flow rates were kept constant in order to asses the influence of seed loading on the product crystal sizes. The effects of seed crystal size differences on the product were investigated and the spatial arrangement of coiled tubular crystallizer was studied as well. The major findings are:

- All experiments resulted in mass gains of a few g/min due to crystal growth and in product crystals of considerably increased size in comparison to the seeds.
- A steady-state condition in the crystallizer was reached rapidly.
- Increasing seed loadings resulted in decreased differences between the mean seed and product crystal sizes, since more individual particles were introduced into the system to consume the same amount of supersaturation.
- Reducing seed sizes while keeping the seed mass per ml slurry constant resulted in smaller differences between the seed and product crystal sizes, since more individual crystals consumed the supersaturation.
- The orientation of the coiled crystallizer had no significant effect on particle segregation.

- Several cooling sections can be utilized to control the temperature profile, and thus, the supersaturation trajectory. The cooling curve was set to keep the supersaturation high enough to obtain reasonable crystal growth rates but low enough to avoid the formation of new nuclei.

Concluding Remarks. The continuous crystallizer presented in this study has several advantages. First, a narrow inner diameter provides excellent process parameter control; however, the formation of crusts in the narrow tubing presents the risk of blockage. The choice of the surface material and the cooling policy can have positive effects on the crust reduction, as recently demonstrated by Abohamra and Ulrich.[55]

Product masses of around 2.70 g/min (about 3.88 kg/day) and more were harvested during the experiments. Increasing the throughput via higher flow rates and numbering up could thus be effective for producing industrial quantities of pharmaceutical materials. To perform a numbering-up approach would guarantee identical time scales (e.g., for reaching steady state conditions, heat and mass transfer etc.). Hence, there would be no need for a traditional scale up, i.e., an increase in the size of the equipment. Using multiple pipes would require appropriate distribution and collection devices, as well as equipment to efficiently clean the crystallizer. Therefore, a large number of parallel pipes would increase the complexity of the operation. These challenges will be addressed in future work.

Generally slow crystallization (at low supersaturation) is key to yielding pure crystals with little impurity incorporations into the crystal lattice and mother liquor inclusions. This implies a long crystallization time and, ultimately, long tubular crystallizers. By adjusting the temperature trajectory, an optimum between sufficiently fast crystal growth, high purity, length of crystallizer and flow rate can be established. In the current study the residence time was around 3 min. However, doubling the length of the crystallizer and/or reducing the flow rate could effectively increase the residence time. We successfully tested residence times of up to 15 minutes. Clearly, for practical reasons, the length of the crystallizer is to some degree limited, and excessively slow flow rates would increase the risk of crust build up and blockage of the tubing. Nonetheless, this concept might be applicable to final (re-) crystallization steps from almost pure solvents with the aim to achieve narrow CSDs.

Evidently, a continuously seeded tubular crystallizer appears to be an interesting tool for crystallization operations. Earlier it was established that tight control of operating parameters can be effective for engineering crystal sizes and shapes.[2] The current study shows that modification of the product crystal sizes can be performed by simple means, such as controlling the seed loading or seed size variations.

At present, the seeds are fed into the tubing from a stirred storage vessel. Recycling, milling and classifying product crystals for seed generation is a possibility for generating the seeds continuously.

3.5 References

(1) A. J. Alvarez and A. S. Myerson, Cryst. Growth Des. **10**, 2219 (2010).

(2) R. J. P. Eder, S. Radl, E. Schmitt, S. Innerhofer, M. Maier, H. Gruber-Woelfler, and J. G. Khinast, Cryst. Growth Des. **10**, 2247 (2010).

(3) P. Barrett, B. Smith, J. Worlitschek, V. Bracken, B. O'Sullivan, and D. O'Grady, Org. Proc. Res. Dev. **9**, 348 (2005).

(4) Y. Ma, K. Chen, Y. Wu, J. Zhu, and Y. Sheng, Cryst. Res. Technol. **45**, 1021 (2010).

(5) K. Chow, H. H. Y. Tong, S. Lum, and A. H. L. Chow, J. Pharm. Sci. **97**, 2855 (2008).

(6) R. Beck, R. Heskestad, D. Malthe-Sørenssen, A. Häkkinen, M. Louhi-Kultanen, and J. P. Andreassen, Cryst. Res. Technol. **45**, 204 (2010).

(7) C. Lindenberg, M. Krattli, J. Cornel, M. Mazzotti, and J. Prozio, Cryst. Growth Des. **9**, 1124 (2009).

(8) R. G. Iacocca, C. L. Burcham, and L. R. Hilden, J. Pharm. Sci. **99**, 51 (2010).

(9) M. Fujiwara, Z. K. Nagy, J. W. Chew, and R. D. Braatz, J. of Process Control **15**, 493 (2005).

(10) C. Borchert, N. Nere, D. Ramkrishna, A. Voigt, and K. Sundmacher, Chem. Eng. Sci. **64**, 868 (2009).

(11) M. Oullion, F. Puel, G. Fevotte, S. Righini, and P. Carvin, Chem. Eng. Sci. **62**, 833 (2007).

(12) D. Winn and M. F. Doherty, AIChE J. **46**, 1348 (2000).

(13) M. A. Lovette, A. R. Browning, D. W. Griffin, J. P. Sizemore, R. C. Snyder, and M. F. Doherty, Ind. .Eng. Chem. Res. **47**, 9812 (2008).

(14) D. W. Griffin, D. A. Mellichamp, and M. F. Doherty, Chem. Eng. Sci. **65**, 5770 (2010).

(15) J. Ulrich, Chem. Eng. Technol. **26**, 832 (2003).

(16) B. O'Sullivan and B. Glennon, Org. Proc. Res. Dev. **9**, 884 (2005).

(17) R. Spruijtenburg, Org. Proc. Res. Dev. **4**, 403 (2000).

(18) D. Mangin, F. Puel, and S. Veesler, Org. Proc. Res. Dev. **13**, 1241 (2009).

(19) W. Beckmann, Org. Proc. Res. Dev. **4**, 372 (2000).

(20) A. Llinas and J. M. Goodman, Drug Discov. Today **13**, 198 (2008).

(21) S. L. Morissette, O. Almarsson, M. L. Peterson, J. F. Remenar, M. J. Read, A. V. Lemmo, S. Ellis, M. J. Cima, and C. R. Gardner, Adv. Drug Deliv. Rev. **56**, 275 (2004).

(22) M. Müller, U. Meier, D. Wieckhusen, R. Beck, S. Pfeffer-Hennig, and R. Schneeberger; Cryst. Growth Des. **6**, 946 (2006).

(23) M. E. Auer, U. J. Griesser, and J. Sawatzki, J. Mol. Struct. **661**, 307 (2003).

(24) H. Gros, T. Kilpio, and J. Nurmi, Powder Technol. **121**, 106 (2001).

(25) W. Omar and J. Ulrich, Cryst. Res. Technol. **41**, 431 (2006).

(26) N. Variankaval, A. S. Cote, and M. F. Doherty, AIChE J. **54**, 1682 (2008).

(27) M. Oullion, F. Puel, G. Fevotte, S. Righini, and P. Carvin, Chem. Eng. Sci. **62**, 820 (2007).

(28) T. L. LaPorte and C. Wang, Curr. Opin. Drug Discov. Devel. **10**, 738 (2007).

(29) S. J. Breneck and D. J. AM Ende, US Patent 0040098839 (2004).

(30) M. Jr. Midler, P. D. Liu, E. L. Paul, M. Futran, and E. F. Whittington, EP 0461930A1 (1991).

(31) C. Beck, S. V. Dalvi, and R. N. Dave, Chem. Eng. Sci. **65**, 5669 (2010).

(32) F. Debuigne, L. Jeunieau, M. Wiame, and J. B. Nagy, Langmuir **16**, 7605 (2000).

(33) Y. F. Su, H. Kim, S. Kovenklioglu, and W. Y. Lee, J. Solid State Chem. **180**, 2625 (2007).

(34) R. D. Dombrowski, J. D. Litster, N. J. Wagner, and Y. He, Chem. Eng. Sci. **62**, 4802 (2007).

(35) C. J. Gerdts, V. Tereshko, M. K. Yadav, I. Dementieva, F. Collart, A. Joachimiak, R. C. Stevens, P. Kuhn, A. Kossiakoff, and R. F. Ismagilov, Angew. Chem. Int. Ed. **45**, 8156 (2006).

(36) A. S. Myerson, US Patent 0030170999 (2003).

(37) M. Raphael, S. Rohani, and F. Sosulski, Can. J. Chem. Eng. **73**, 470 (1995).

(38) P. D. Virkar, M. Hoare, M. Y. Y. Chan, and P. Dunnill, Biotechnol. Bioeng. **24**, 871 (1982).

(39) T. Rivera and A. D. Randolph, Ind. Eng. Chem. Process Des. Dev. **17**, 182 (1978).

(40) M. Stahl, B. L. Alund, and A. C. Rasmuson, AIChE J. **47**, 1544 (2001).

(41) J. Schiewe and B. Zierenberg, US Patent 0015194A1 (2003).

(42) R. Vacassy, J. Lemaitre, H. Hofmann, and J. H. Gerlings, AIChE J. **46**, 1241 (2000).

(43) J. R. Méndez del Rio and R. W. Rousseau, Cryst. Growth Des. **6**, 1407 (2006).

(44) S. Lawton, G. Steel, P. Shering, L. H. Zhao, I. Laird, and X. W. Ni, Org. Proc. Res. Dev. **13**, 1357 (2009).

(45) R. J. P. Eder, H. Gruber-Woelfler, and J. G. Khinast, CIT **81**, 1171 (2009).

(46) R. J. P. Eder, E. Schmitt, J. Grill, S. Radl, H. Gruber-Woelfler, and J. G. Khinast, CIT **82**, 1469 (2010).

(47) R. J. P. Eder, E. Schmitt, J. Grill, M. Maier, S. Innerhofer, S. Radl, H. Gruber-Woelfler, and J. G. Khinast, Sci. Pharm. **78**, 664 (2010).

(48) J. B. Rawlings, S. M. Miller, and W. R. Witkowski, Ind. Eng. Chem. Res. **32**, 1275 (1993).

(49) H. Hojjati and S. Rohani, Chem. Eng. Process. **44**, 949 (2005).

(50) G. D. Maia and M. Giulietti, J. Chem. Eng. Data **53**, 256 (2008).

(51) O. D. Linnikov, Cryst. Res. Technol. **43**, 1268 (2008).

(52) J. W. Mullin, Crystallization, 3rd ed. (Elsevesier Butterworth-Heinemann, Oxford, UK, 1997 paperback ed.), p. 24.

(53) T. Allen, in: Particle Size Measurement, edited by B. Scarlet and G. Jimbo, Powder Sampling and Particle Size Measurement, Vol. 1 (Chapman and Hall, London, 1997), chap. 6.

(54) S. H. Chung, D. L. Ma, and R. D. Braatz, Can. J. of Chem. Eng. **77**, 590 (1999).

(55) E. Abohamra and J. Ulrich, CIT **82**, 1081 (2010).

4 Continuous Sonocrystallization of ASA: Control of Crystal Size[e]

ABSTRACT: A continuous tubular crystallizer system with an inner diameter of 2.0 mm and an overall length of 27 m was used to directly precipitate acetylsalicylic acid from ethanolic solution via cooling and ultrasound irradiation and to grow the crystals in the tubing with a controlled temperature trajectory. In order to minimize the residence time distribution air bubbles were introduced into the system to generate a segmented gas-slurry flow. The narrow residence time distribution and the tight temperature control in the small tubing due to the large surface to volume ratio resulted in relatively narrow crystal size distributions of the product. Generally, all experiments clearly demonstrated significant crystal growth for the product crystals in comparison to the seeds and yielded product masses on the g/min scale. Furthermore, it was demonstrated that the size of the product can be easily controlled via fines removal by dissolution due to rapid heating and varying the mass of seeds per ml of solution.

4.1 Introduction

Background. The final form of 90% of active pharmaceutical ingredients (APIs) are crystals of small organic molecules.[1,2] Therefore, crystallization from the mother liquor is an important separation and purification process in the pharmaceutical industry.[1,3-7] Next to crystal purity, other critical quality attributes exist for bulk crystals. These include crystal shape[8] and size, the corresponding distributions,[9-12] surface properties and the polymorphism of the crystals.[13,14] Crystal size and shape distribution (CSSD) directly affects downstream process operations, such as filtration, washing, drying and milling.[14-16] Furthermore, the ease of particle handling greatly depends on the CSSD, since flowability, dust formation,[17] mixing properties, segregation phenomena, storage characteristics and compactability are direct functions of the aforementioned characteristics.[18] Finally, the CSSD affects the performance of the final drug,[19,20] since dissolution rates, for example, depend on the specific surface area.

[e] This chapter is based on a journal paper by Eder et al. submitted to Crystal Growth and Design.

Moreover, the distinct crystal form might directly affect its physical properties[21,22] (i.e., melting point, density, hardness, solubility[23-26]) and shape and may impact adversely the bioavailability[27,28] if not controlled carefully. Additionally, polymorphs, solvates and salts are sensitive issues with respect to intellectual property rights[29,30] that frequently lead to patent disputes. In order to meet the strict requirements of regulatory bodies, such as the Food and Drug Administration (FDA), the Japan Pharmaceutical Manufacturers Association (JPMA) and the European Medicines Agency (EMA), critical process parameters (e.g., levels of impurities, supersaturation, etc.) that affect the product quality must be tightly controlled during a crystallization process.

Since a wide range of crystalline substances is manufactured with diverse physical-chemical properties and for various purposes, numerous crystallization techniques and crystallizer types have been developed. The method used to create supersaturation (i.e., cooling, evaporation, change of solvent composition and reaction[31,32]) and the mode of process operation (i.e., batch, semi-batch or continuous) may be used to classify crystallization processes. In the pharmaceutical industry, unit operations are most commonly run in batch mode, particularly during crystallization processes,[16] in part due to regulatory requirements and several benefits offered by batch operations, such as easy implementation and maintenance. Further advantages of batch processing include its suitability for viscous slurries and substances with slow crystal growth rates[33] and the possibility to clean the equipment after each batch to avoid encrustation problems. Fouling, slow attainment of steady state and potential operation instabilities are the main downsides of continuous crystallizers.[32] In contrast, continuous processes offer benefits that are readily used in many industrial areas. Shorter downtimes,[32] fewer scale-up issues, better control potential for optimal process conditions[32] and enhanced reproducibility of results[16,34] are typical features of continuous processes. Furthermore, continuous crystallizers require smaller equipment size[32] and, consequently, reduced capital investment.[16] Additional facilities and instrumentation that may be required for continuous processes[35] offer a high level of automatization and, as a result, reduce operating costs.[36]

In the last decade the interest in continuous manufacturing has grown significantly in the pharmaceutical industry. In the field of crystallization several continuous systems were suggested. Semi-batch and continuous processes employing high

intensity mixers such as vortex mixers, and confined impinging jets for API precipitation were described by Beck et al.,[37] Dalvi et al.,[38] Dong et al.,[39] Brenek et al.,[40] Midler et al.,[41] Ferguson et al.,[42] and others.[43] Small particles with a large specific surface area to increase the dissolution rate of poorly soluble drugs were successfully produced using the above methods due to the high mixing rates.[37,38] Fast mixing can also be achieved via micro-reactors that also allow tight process control.[28] Moreover, miniaturized channels may serve as tools for high throughput screening to crystallize organic molecules and proteins.[44] To date, the majority of publications on particle formation in micro-structures have focused on inorganic nano-particles.[28] However, the number of reports on organic solid substances, including APIs, is steadily increasing (e.g., Su et al.,[45] Dombrowski et al.,[46] Gerdts et al.[47] and a patent of Myerson[48]).

Precipitation of organic molecules in tubular devices with larger inner diameters operated in a plug-flow mode was described, for example, by Raphael et al.,[49] Virkar et al.,[50] Riviera and Randolph[51] and Stahl et al.[52] Recently, Alvarez and Myerson[2] reported a continuous plug flow crystallization process with additional injection points for antisolvent along the pipe to promote crystal growth after precipitation of solid particles.

Lawton et al.[53] implemented oscillating baffles in a tubular crystallizer in order to maintain narrower residence time distribution of crystals in the tubing and to achieve longer crystallization time, compared to plug flow devices of similar length. Mendez del Rio and Rousseau[54] used a semi-batch laminar flow tubular crystallizer device to precipitate paracetamol.

Eder et al. reported growth of crystals upon cooling in a continuous laminar tubular crystallizer.[35,36,55,56] Low flow rates (laminar flow) provided sufficient time for significant crystal growth. However, for these cases a segmented flow is required to reduce the residence time distribution of the slurry. This is demonstrated in the current study where air bubbles were introduced into the system to achieve a segmented gas-slurry flow. Segmented flow tubular reactors were described earlier in the literature, including particulate systems (e.g., ref.[57-59]) and API precipitation/crystallization processes.[60,61] The segmented flow is typically achieved by introducing gas bubbles or drops of liquids that are immiscible with the solution.

In our past work seeds were prepared batch wise in a vessel and then used as starting material for a continuous crystallization process. In our current study, seeds

were generated continuously by exposing an ethanolic acetylsalicylic acid (ASA) solution to ultrasonic irradiation in a narrow tubing to enhance nucleation for *in situ* seed generation.

In general, ultrasonic energy can have a strong influence on crystallization,[62,63] such as induction of primary nucleation[64-69], reduction of crystal size,[38,70] inhibition of agglomeration,[65] reduction or elimination of the need for seed crystals[71] and even control of polymorphism.[72] Therefore, the use of ultrasound for crystallization, including APIs, has received substantial attention.[73] Ruecroft et al.[74] summarized the use of ultrasonic irradiation in industrial crystallization processes, including reports on pharmaceuticals. One of the applications is a patent of Boehringer Ingelheim on crystallization of inhalable products in a continuous crystallization process in a micro-reactor with a segmented flow.[61] Kim et al.[70], Guo et al.[68], Miyasaka et al.[65,66], Dalvi et al.[38] and Li et al.[75] provide further examples of ultrasonic irradiation in API crystallization. Furthermore, the crystallization behaviour under sonication has been studied for excipients and other substances.[62,72,76,77]

Current Study. The model substance ASA was crystallized from a corresponding ethanol solution in a narrow tubular continuous crystallizer. A side stream of the solution was treated with ultrasonic irradiation to enhance nucleation. The product was harvested either directly after particles with a volume mean diameter (VMD) of ~20 µm had been formed, after they had further grown in the tube along a temperature trajectory (VMD ~50 µm) or after mixing the nuclei with a corresponding hot, highly-concentrated solution that led to even larger particle sizes (VMD ~80-190 µm).

In order to achieve a narrow residence time distribution in the tubing, air bubbles were introduced into the system to create a segmented gas-slurry flow. The small inner diameter of the tubing together with the narrow residence time distribution allowed the crystals to grow for a comparable amount of time in a similar environment without significant spatial temperature differences in radial direction. Therefore, relatively narrow crystal size distributions (CSDs) were achieved, even though precipitation of the seeds resulted in a wide CSD and the crystals in the pipe may have been affected by growth rate dispersion phenomena,[2] as described by other groups including Zumstein and Rousseau,[78] Bohlin and Rasmuson,[79] Larson and White,[80] Patience et al.[81] and Haseltine et al.[82]

By varying seed loading (mass of solid ASA per ml of slurry) crystals were grown in the size range between 50 to 190 µm. In order to obtain crystals with VMD larger than ~120 µm, a temperature cycle for fines control was implemented.

4.2 Experimental

Materials. G. L. Pharma GmbH provided the ASA (Rhodine 3020, pharmaceutical grade, monoclinic, M = 180.16 g/mol). EtOH (99.8% denaturized with 1% methyl ethyl ketone, M = 46.07 g/mol) was purchased form Roth (Lactan).

Equipment. Polysiloxane tubing with an inner diameter (d_{in}) of 2.0 mm and an outer diameter (d_{out}) of 4.0 mm of varying lengths was used for the (1) crystallizer (l = 27 m), (2) the pre-cooling section of the solution (l = 3 m), (3) the section where seeds were generated in situ with ultrasound irradiation and (4) the temperature cycle for fines control. The lengths of tubing for seed generation and temperature cycling varied in order to keep residence times for varying flow velocities comparable (for details see “Procedure”).

Two peristaltic pumps (PI and PII) were used to pump the solution to the pre-cooling section of the solution or to the sonicated zone, respectively (Ismatec Reglo MS 2/6V 1.13C; tubing: PHARMED d_{in} = 2.8 mm, d_{out} = 5.0 mm). Another peristaltic pump supplied the air bubbles into the crystallizer (PIII: BVP- Process IP 65 - 3/6; tubing: PHARMED d_{in} = 1.6 mm, d_{out} = 4.8 mm). The air was saturated with the solvent at room temperature since it was obtained from a vessel with an ethanol-covered bottom. Therefore, it can be assumed that little ethanol evaporated from the slurry.

Straight-, Y- and T-fittings (PTFE, d_{in} = 2.0 mm) were used to connect the PHARMED with the polysiloxane tubing (straight), to mix the solution with the seed suspension (Y) and to introduce the air bubbles into the crystallizer (T). The sonication was performed in an ultrasonic bath (Elma Transonic 460; 35 kHz). Temperatures were regulated via thermostatic baths.

CSDs were measured with the Helos (Sympatec) system. Pictures of the crystals were taken with a Leica DM 4000 microscope equipped with a DFC 290 camera.

Set-Up. The equipment was assembled in a similar manner as described in earlier publications.[35,36]

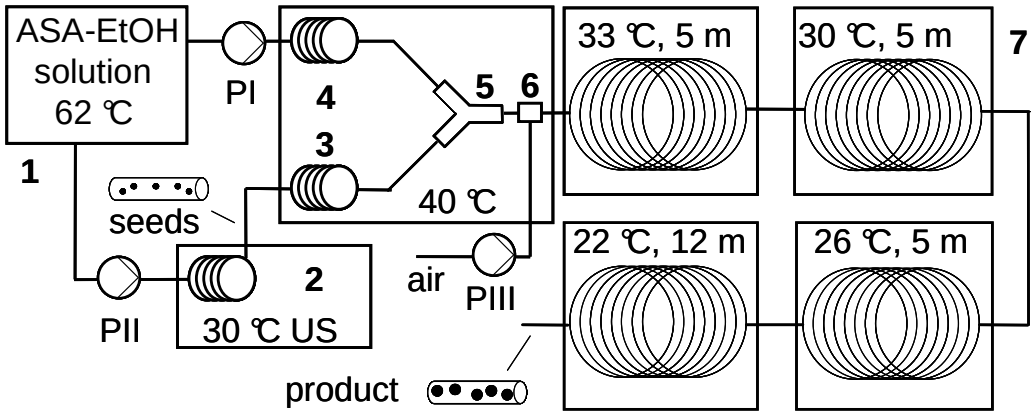

Figure 4-1. The schematic shows the process with (1) solution storage tank, (2) seed generation via ultrasound (US), (3) temperature cycle for fines destruction, (4) cooling of the solution feed, (5) Y-fitting, (6) air bubble inlet for the segmented flow, (7) coiled tubular crystallizer in four cooling sections and pumps (PI-III).

Figure 4-1 shows the experimental set-up. The ASA-EtOH solution was kept in a storage vessel at 62 ± 0.2 ℃. Depending on the exper iment, two peristaltic pumps were used to feed one fraction of the solution into the thermostatic bath at 40 ± 0.2 ℃ and the other one into the ultrasonic bath at 30 ± 1 ℃ or 28 ± 1 ℃ to yield a suspension via *in situ* seed generation. To keep the temperature in the ultrasonic bath constant heat generated by the US irradiation had to be removed via a heat exchanger. For fines destruction, the seed suspension was briefly heated to 40 ± 0.2 ℃ during a temperature cycle to remove (dissolve) the smallest crystals.

In order to achieve a segmented flow, a peristaltic pump was used to feed air bubbles into the crystallizer via a T-fitting that was placed 20 mm after mixing the seed suspension and the solution.

The 27 m long silicone tubing (d_{in} = 2 mm) was coiled on four grid structured cylinders such that the magma in the coils could flow up and down. The first 5 m were kept at 33 ± 0.2 ℃, followed by 5 m at 30 ± 0.2 ℃, 5 m at 26 ± 0.2 ℃ and 12 m at 22 ± 0.2 ℃.

Experimental data from the literature[83] and the Nývlt-Model (Eq. 4-1) were used to establish the solubility of ASA in EtOH at a given temperature.

$$\log X_{ASA} = N_1 + \frac{N_2}{T} + N_3 \log(T) \tag{4-1}$$

For ethanol the parameters in equation (4-1) are N_1 = 27.769, N_2 = -2500.906 and N_3 = -8.323[83] and X_{ASA} is the mole fraction of dissolved ASA. The temperature in the equation is expressed in Kelvin.

The details on the models regarding supersaturation, based on equilibrium solubility and the growth rate of the crystals as well as considerations for defining the temperature gradient along the tubing and the solution temperature at the Y-fitting are provided elsewhere.[35,36]

Figure 4-2 shows the Y-fitting, where the seed suspension (T_{susp}, $\dot{V}_{susp}$) is mixed with the solution (T_{sol}, $\dot{V}_{sol}$), and the air bubble inlet for the segmented flow. The photo of the segmented flow was taken with a high-speed camera. In the section where the photo was taken the flow moved in an upward direction of the vertically coiled tubing.

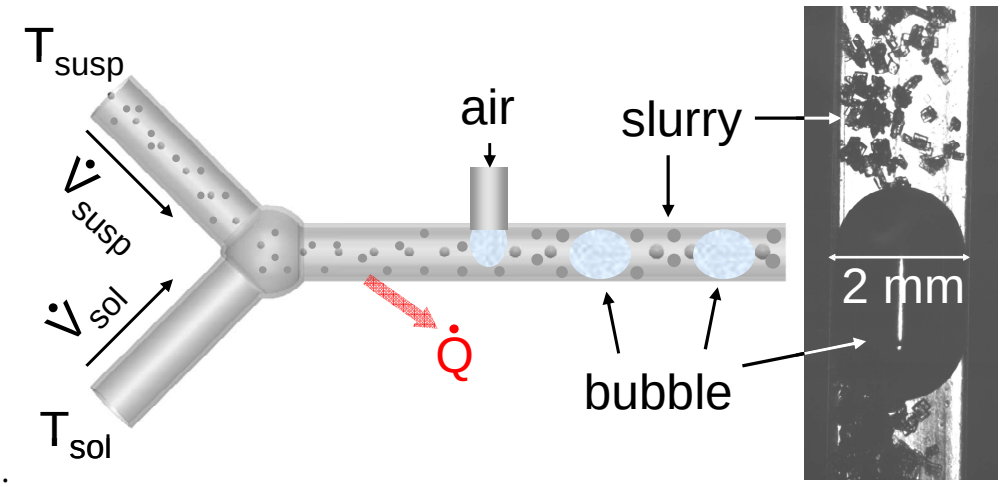

Figure 4-2. Schematic of the Y-fitting where solution is mixed with the seed suspension and of the air bubble inlet. The photo shows an air bubble taken with a high-speed camera.

Procedure. An ASA-EtOH solution with an ASA mole fraction of X_{ASA} = 0.113 (c_{ASA} ~2.19 mol/l) was prepared by dissolving 50 g ASA per 100 g ethanol at 62.0 ± 0.2 ℃.

Prior to each experiment, the tubing was rinsed with ethanol before the seed suspension was fed into the crystallizer inlet. To generate the seeds *in situ* the solution was partly pumped through a separate tube, in which it was exposed to ultrasound irradiation. At the beginning of the experiment, the continuously generated seed suspension was mixed in the Y-fitting with pure ethanol in which the seeds dissolved, since saturation was not reached in the mixed inlet stream. Next, the pure solvent was switched to the ASA-EtOH solution that was cooled to 40 ℃ in order to reach close-to-equilibrium saturation conditions before being mixed with the seed suspension. Thereafter, further crystal growth upon cooling was observed. This start-up procedure guaranteed that the seeds were inside the crystallizer when the solution was fed into the inlet. Direct nucleation without ultrasound irradiation always

resulted in blockage of the tubing for the investigated experimental parameters. With ultrasonic irradiation, nucleation occurred at higher temperatures and hence less solid ASA was formed. Additionally, the particles may have been less aggregated due to the energy input of the ultrasonic bath. Thus, blockage of the tubing was effectively avoided.

The air bubbles were introduced via a T-fitting approximately 20 mm past the mixing point of the solution with the *in situ* generated seed suspension.

Seed samples were taken during the experiments in order to assess the mass flow and CSD directly after the ultrasonic bath, the temperature cycle and mixing the seed suspension with the solution. Several product samples were taken at the crystallizer's outlet. The particles were separated via filtration and the crystals were washed with cyclohexane (an antisolvent for ASA). The crystal samples were dried in vacuum, weighted and the CSD was measured.

Experiments. (**a**) In the first set of experiments, it was investigated if seeds can be precipitated with approximately constant CSDs over the period of time required for the experiments (~25 min). Furthermore, the consistency of results between different experiments was studied. For this purpose, 1.5 m of the polysiloxane tubing were placed in the ultrasonic bath (US) at T_{US}=28 ± 1 °C and the solution was fed at 6.0 ml/min into the tubing. During each experiment four seed samples were taken to measure CSD and mass.

(**b**) To obtain preliminary results on the crystal size increase, the seed suspension (6.0 ml/min, T_{US} = 28 ± 1 °C) was mixed with additional solution (10.0 and 20.0 ml/min) before the slurry was segmented via air bubbles and further cooled step by step to 22 °C for crystal growth. Furthermore, 5 ml/min of the seed suspension were mixed with 16 ml/min of the solution, including and excluding the temperature cycle for fines removal. These results formed the basis for the design of the subsequent experiments.

For handling reasons, the temperature of the ultrasonic bath was changed to 30 ± 1 °C. The thermostatic bath at 30 °C used as cooling section along the crystallizer provided the cooling water for the ultrasonic bath and hence no additional thermostatic bath was necessary.

(**c**) Two series of experiments with three different seed loadings each were performed, which focused on products achieved with and without fines control (i.e., heating the seed suspension from 30 to 40 °C to dissolve the smallest crystals).

These experiments were all conducted with a total flow rate of 15 ml/min. To generate the seed suspension 15, 10 or 5 ml/min were pumped (PII) into the sonicated zone. The remaining amount of solution that was necessary to reach 15 ml/min of feed stream was fed by PI into the crystallizer inlet (i.e., 0, 5 or 10 ml/min). To obtain comparable residence times in the sonicated zone (US) and the temperature cycle (TC), the corresponding lengths of the tubing were altered according to the flow rate (see Table 4-2).

(**d**) A further experiment was performed with an even smaller ratio of seed-mass to the liquid phase to obtain even larger product. Additionally, the throughput was increased to enhance the product mass yield per minute. 5.0 ml/min of the seed suspension (PII) were mixed with 15.0 ml/min of the solution (PI). Additionally, 0.15 m of the crystallizer at the outlet was placed in an ultrasonic bath (Elma Transonic 310; 35 kHz) at 21 ± 1 ℃ for taking extra samples to dete rmine if sonication would have an effect on the product crystals.

4.3 Results and Discussion

(**a**) Direct sonication-assisted precipitation of ASA crystals in the tubing resulted in constant CSDs of the samples taken consecutively during each experiment and for different experiments as shown in Figure 4-3 presenting the cumulative volume density distributions (Q_3).

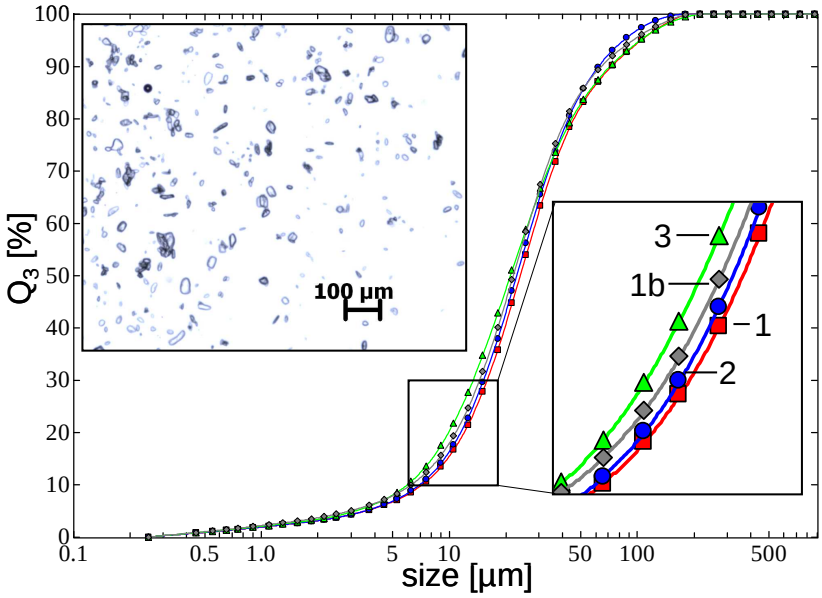

Figure 4-3. Q_3 distributions of seed crystals sampled at different times during an experiment (1-3) and after re-starting the process (1b). Inset = crystals precipitated in the tubing at 28 ± 1 ℃.

The crystal mass yield from the sonication-assisted precipitation was around 0.12 g of solid ASA per ml suspension (PII = 6.0 ml/min → $\dot{m}_{ASA}$ ~ 0.72 g/min). It remained constant throughout the experiments, which supported the observation based on CSDs that the process led to reproducible results of the seed precipitator. Moreover, the tubular crystallizer proved to be ideally suited for sonication applications, since energy dissipation does not pose a problem due to the small inner dimensions. Additionally, heat generated by the sonication energy input can immediately be removed due to the high surface-to-volume ratio of the tubing.

(**b**) Table 4-1 summarizes the process parameters and the results of the experiments during which additional solution was mixed into the seed suspension before the slurry was segmented via air bubbles and further cooled step by step to 22 °C to generate supersaturation for crystal growth. On e experiment (1.4_{TC}) included a rapid temperature increase to T_{TC} = 40 °C (l_{Tc} = 0.5 m) for fines control. Although several seed and product samples were taken for each experiment, only one value is presented in Table 4-1 since the results were very consistent. Steady-state conditions were rapidly reached in the tubular crystallizer and remained constant over the course of earlier reported experiment.[35,36]

The mass gain r_m according to Equation 4-2

$$r_m = \frac{\dot{m}_{prod}}{\dot{m}_{seed}} \cdot 100\% \qquad (4\text{-}2)$$

strongly depended on the seed loading at the crystallizer's inlet and varied from 380% to over 700%. Here $\dot{m}$ denotes the solid mass flow of either the seed or the product ASA, as indicated by the indices. The seed loading (m_{seed}/ml_{slurry}) refers to the solid ASA content per ml of slurry in the pipe at the inlet where the seed suspension is, for example, mixed with the fresh solution.

The residence time τ in the crystallizer was measured by following air bubbles from the crystallizer's inlet to its end.

Table 4-1. Pump flow rates, residence time τ, seed loading, solid ASA production rate $\dot{m}_{ASA}$ and mass gain r_m. (PI = solution, PII = suspension)

No.	PI [ml/min]	PII [ml/min]	τ [s]	m_{seed}/ml_{slurry} [g/ml]	$\dot{m}_{ASA}$ [g/min]	r_m [%]
1.1_{seed}	10.0	6.0	260	0.04	0.71	380
1.1_{prod}					2.70	
1.2_{seed}	20.0	6.0	180	0.03	0.70	572
1.2_{prod}					4.01	
1.3_{seed}	16.0	5.0	200	0.03	0.70	550
1.3_{prod}					3.85	
$1.4_{seed,TC}$	16.0	5.0	200	0.02	0.50	722
$1.4_{prod,TC}$					3.61	

As can be seen from the Table, the product yield per minute increased with higher throughput. Clearly, an increase in r_m was observed when more solution at constant seed feed rate was supplied to the crystallizer. A comparison between experiments 1.4_{TC} and 1.3 shows a decreased seed mass after the temperature cycle, since solid ASA dissolved. Therefore, r_m increased for experiment 1.4_{TC} in comparison to experiment 1.3 as approximately the same amount of ASA was harvested at the outlet.

Clearly, the cooling trajectory of the slurry is dependent on the flow rate. However, earlier work of our group indicated that at the outlet close-to-equilibrium conditions were typically achieved, even with shorter residence times.[36] For the experiments presented in this paper close-to-equilibrium conditions are observed at the crystallizer's outlet as well.

Figure 4-4 shows Q_3 curves of the seeds (exp. 1.1) and product crystals for experiments 1.1 and 1.2.

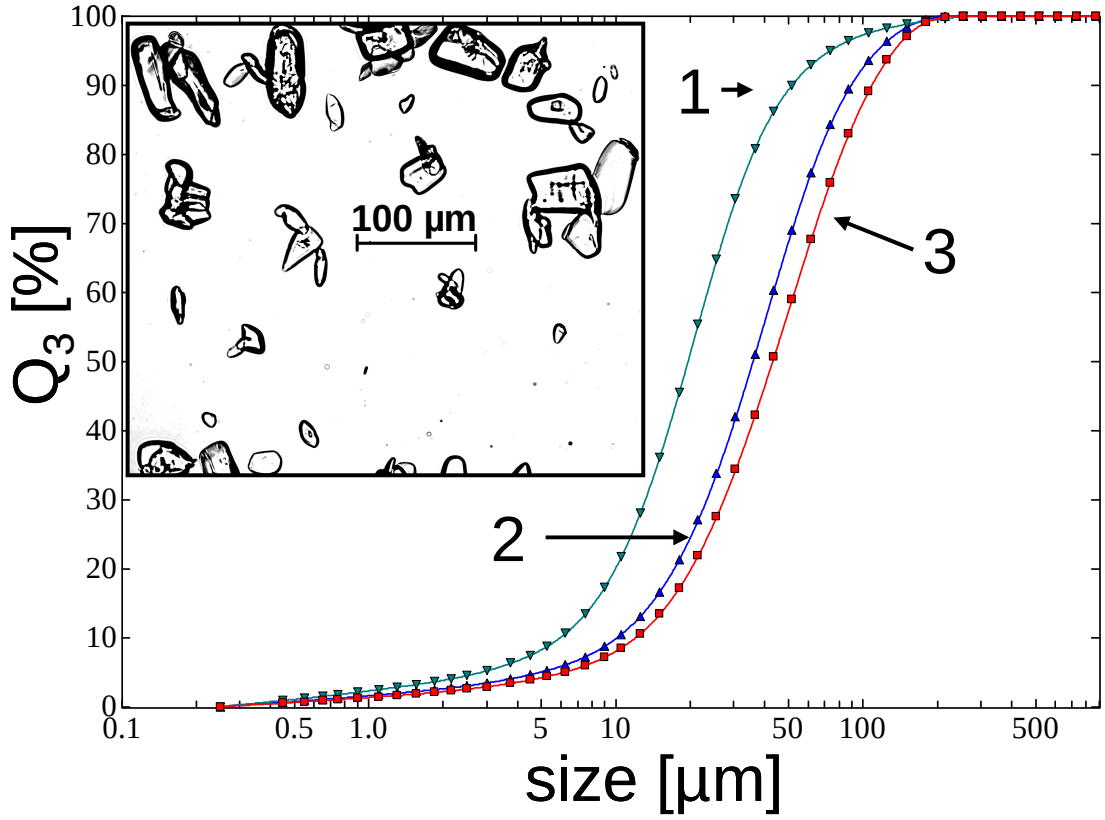

Figure 4-4. Q_3 curves of seeds (1) and product crystals for 10 ml/min (2) and 20 ml/min (3) of additional solution. Image corresponds to curve 3.

The product crystals were significantly larger than the seed crystals at the inlet. As the seed loading decreased (exp. 1.2), larger product crystals were observed, as fewer individual seed crystals consumed the supersaturation. Similar observations for the tubular crystallizer have already been published.[36]

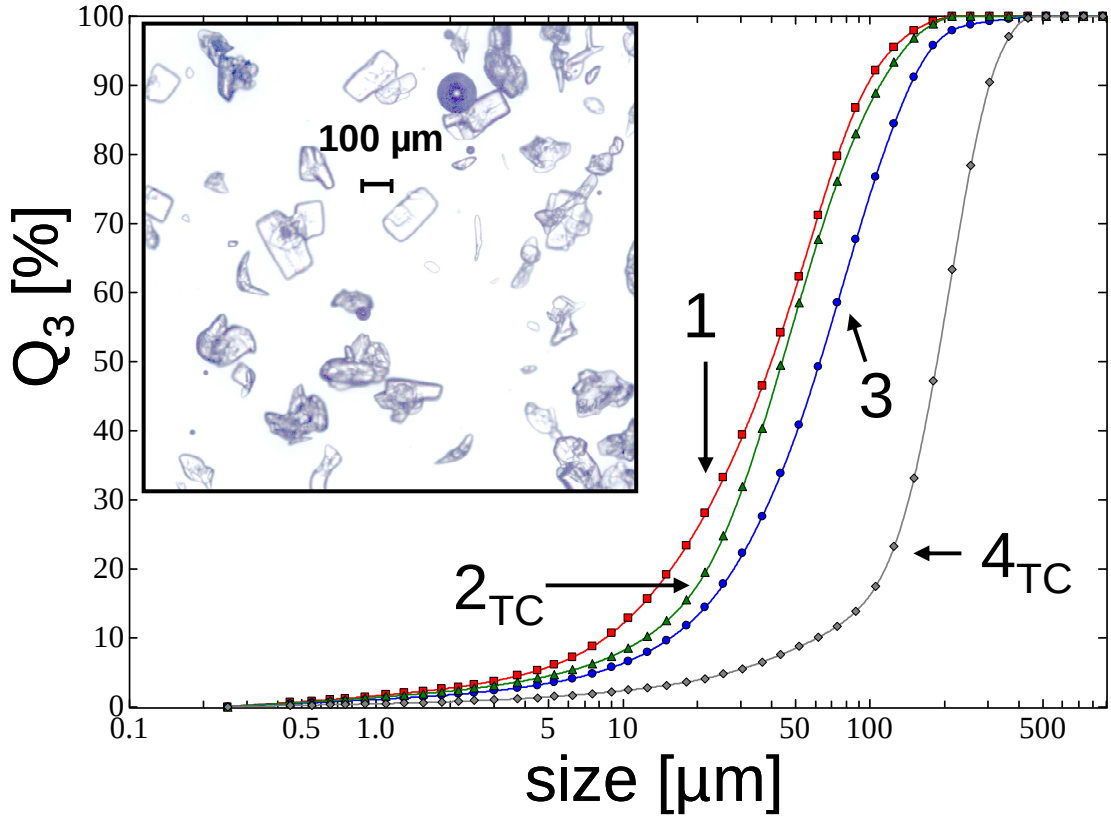

Figure 4-5. Q_3 curves of seeds (1) without a temperature cycle, (2) with a temperature cycle (2_{TC}), and corresponding products (3 and 4_{TC}). Image corresponds to 4_{TC}.

Figure 4-5 shows the results of experiments 1.3 and 1.4_{TC}. The Q_3 curve of the seeds after the temperature cycle shifted to the right towards larger crystal sizes in comparison to the seeds sampled right after the precipitation. Since small crystals dissolve faster due to their larger surface to volume ratio, it may be assumed that a considerable amount of fines was removed (dissolved), which ultimately resulted in less and larger seeds, which should yield larger product crystals. The fact that less seeds (or less seed mass) entered the crystallizer can also be observed in Table 4-1, which shows that the seed mass flow entering the crystallizer is 0.5 g/min for a system with temperature cycle versus 0.7 g/min without. Figure 4-5 shows that - as expected - significantly larger product crystals were obtained for the experiment with the temperature cycle, due to reduced amounts of fines and therefore fewer and bigger particles that increased their size at the expense of the available supersaturation.

The seed crystals sampled after the temperature cycle may have had slightly increased sizes than those of the seeds fed directly into the crystallizer, since the

additional ASA of the dissolved fine crystals may have crystallized on the remaining seeds while being harvested. However, the effect is negligible.

In summary it was shown that seed loading and fines removal are excellent strategies to control the final product size.

(**c, d**) Results from above led to two sets of experiments with and without temperature cycles with different flow rates, in order to assess if product crystal sizes between the seed size and the maximum product crystal size in experiment 1.4_{TC} can be obtained in a controlled way. Table 4-2 summarizes the process parameters and product mass yields for the experiments, all with constant residence times in the crystallizer (τ ~ 265 s), in the sonication zone (30 ± 1 ℃) and – if in use – in the temperature cycle (experiments 2.1-3.3). Furthermore, one experiment (4.1_{TC}) with an increased solution feed (τ ~ 215 s) was performed.

Table 4-2. Pump flow rates, lengths of US and TC, seed loading, solid ASA production rate $\dot{m}_{ASA}$ and mass gain r_m. (PI = solution, PII = suspension)

No.	PI [ml/min]	PII [ml/min]	l [m]	m_{seed}/ml_{slurry} [g/ml]	$\dot{m}_{ASA}$ [g/min]	r_m [%]
2.1_{seed}	0.0	15.0	US: 3	0.10	1.42	172
2.1_{prod}					2.44	
2.2_{seed}	5.0	10.0	US: 2	0.06	0.89	311
2.2_{prod}					2.77	
2.3_{seed}	10.0	5.0	US: 1	0.03	0.52	506
2.3_{prod}					2.63	
$3.1_{seed,TC}$	0.0	15.0	US: 3	0.05	0.81	299
$3.1_{prod,TC}$			TC: 1.5		2.42	
$3.2_{seed,TC}$	5.0	10.0	US: 2	0.42	0.63	435
$3.2_{prod,TC}$			TC: 1		2.74	
$3.3_{seed,TC}$	10.0	5.0	US: 1	0.03	0.46	572
$3.3_{prod,TC}$			TC: 0.5		2.63	
$4.1_{seed,TC}$	15.0	5.0	US: 1	0.03	0.45	744
$4.1_{prod,TC}$			TC: 0.5		3.35	

All experiments showed a significant mass increase of solid ASA for the product samples. As can be seen the series of experiments No. 2 and 3_{TC} (with temperature cycle for fines removal) yielded very similar amounts of product production rates, as in all cases the same amount of ASA was fed to the crystallizer and since the solution was close to equilibrium at the outlet. The highest difference between crystal production rates (3.1_{TC} and 2.2) was still less than 15%. As can be seen the smallest production rates (about 2.4 g/min of product) were obtained when only one pump was used to deliver 15ml/min. Even though the calibration of the pumps with respect to mass and volume per minute was performed at the outlet of the crystallizer, the pressure drop in the ~ 27 m long crystallizer (d_{in} = 2mm), plus 3 m in the ultrasonic bath, may have been high enough that one pump (plus the air pump) could not keep the flow rate constant during the course of the experiments. This effect became less significant when all pumps were in use, since three rather than two pumps provided the energy input. Thus, the 27 m of crystallizer length appeared to be the practical limit for the set of equipment used in our work.

With the decreasing flow rates of the seed suspension (PII) less seed mass per time was obtained for experiments 2.1-2.3. The same trend was observed for experiments 3.1_{TC}-3.3_{TC}, although the seed mass flow rate was lower due to fines dissolution in the temperature cycle. However, with the decreasing seed suspension flow rates the differences in the seed mass between the experiments with and without the temperature cycle diminished. The reason was the significant cooling of the seed suspension that resulted in crystal growth during sampling, since the suspension had to be pumped through an additional cooler piece of tubing. As a consequence, the seed mass values at higher flow rates of PII were more accurate, since the time that the slurry needed to pass through the sample tube was shorter, and thus, the temperature loss was smaller. Generally, the seed sample values of the experiments without the temperature cycle were more accurate, since the difference between the precipitation temperature and the room temperature was smaller. Obviously, r_m-values were also affected by this systematic sampling inaccuracy. However, the expected trend of increasing r_m-values with decreasing seed loadings was clearly observed. The product crystals were harvested close to room temperature and at nearly equilibrium solubility conditions directly at the crystallizer outlet. Hence, the sampling was straightforward.

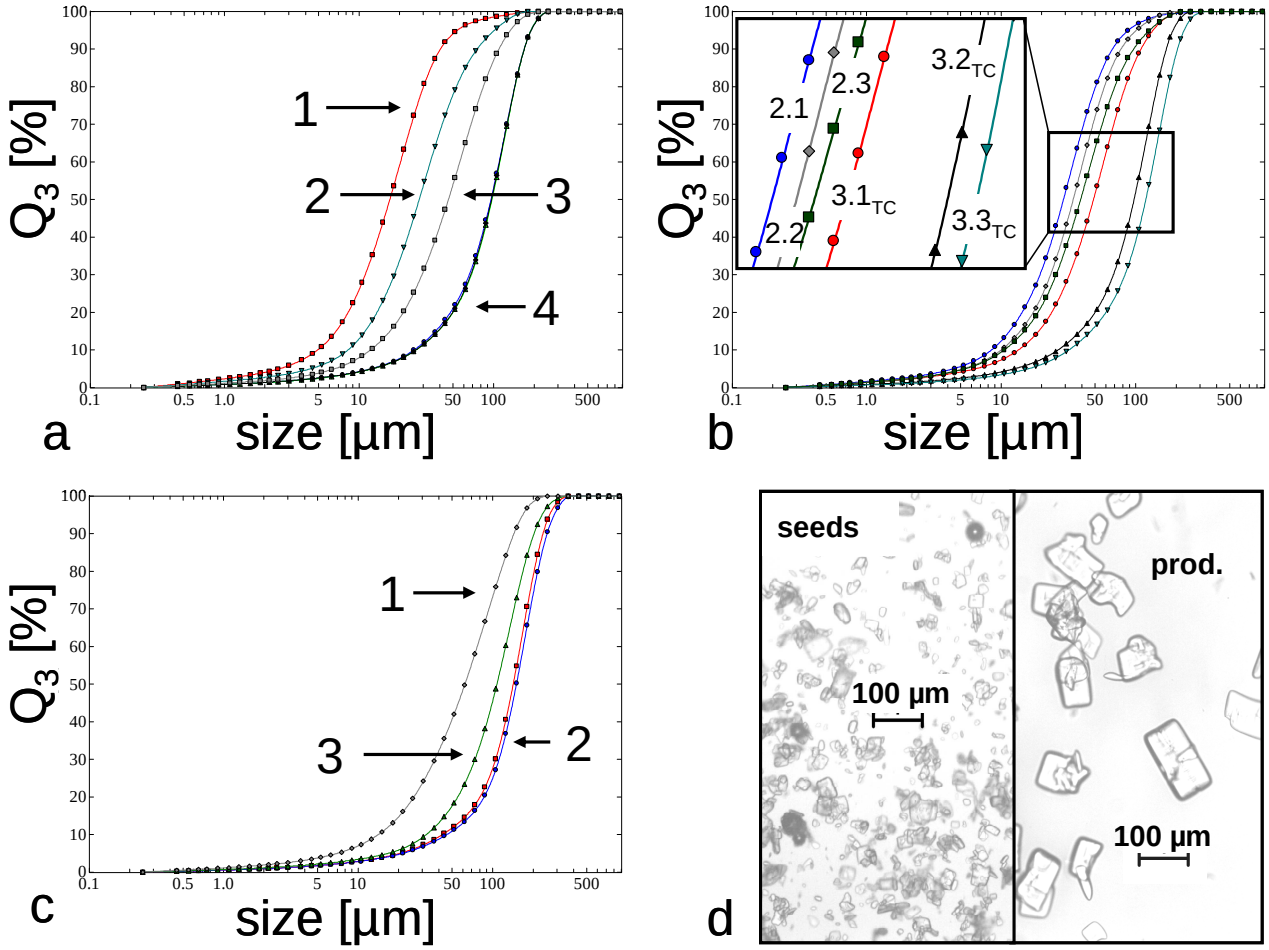

Figure 4-6. (a) Q_3 curves of exp. 3.2_{TC} for (1) the seeds directly after precipitation, (2) the seeds after the temperature cycle, (3) the seeds after addition of fresh solution and (4) three product samples. (b) Product Q_3 curves for the exps. 2.1, 2.2 and 2.3 as well as 3.1_{TC}, 3.2_{TC} and 3.3_{TC}. (c) Q_3 curves of exp. 4.1_{TC} for (1) the seeds after the temperature cycle and addition of fresh solution, (2) two product samples and (3) a product sample with ultrasound irradiation at the crystallizer outlet. (d) Seed and product crystals of exp. 4.1_{TC}.

Figure 4-6a shows the CSDs of experiment 3.2_{TC} (Table 4-2) for seed and product crystals. The smallest particles were harvested directly after precipitation, and the size increased after the temperature cycle, as shown above. The size increased even further after mixing the seed suspension with fresh solution. The shift of CSD towards larger sizes after the temperature cycle in comparison to the directly precipitated ASA was – as established earlier – the result of dissolving the finest particles. Due to the high surface-to-volume ratio of the small crystals their dissolution rate was higher than that of the larger particles.[84,85] Thus, a lot of fine particles dissolved in favor of larger seed crystals that consumed the additional ASA in the liquid phase later on in the process. The seeds that were harvested after adding fresh solution were larger than the seeds at an earlier stage in the process along the tubing, since in the liquid

phase additional ASA was present that grew on the seeds as the slurry cooled while being sampled.

The three product samples that were consecutively taken at the crystallizer's outlet had significantly larger crystal sizes in comparison to all types of seeds. The Q_3 curves of the product samples are on top of each other, indicating that the process was operated in a steady state. CSDs were relatively narrow, which was generally the case for the crystals that our experiments yielded.

Figure 4-6b shows the product CSD for experiments 2.1-2.3 and 3.1_{TC}-3.3_{TC}. CSD for the process with and without the temperature cycle shifted towards larger sizes with the decreasing seed loadings, as less seeds were available to serve as nuclei for crystal growth. In the exps. 3.1_{TC}-3.3_{TC} fines control with temperature cycling shifted the size distribution towards larger crystals, again as less seeds were available and this effect was – as indicated above – further amplified by adding increasing amounts of fresh ASA-EtOH solution.

Generally, seed properties such as mass, size and shape have a significant impact on the outcome of the product[36,86-92] and fines control has regularly been applied to crystallization processes[70,93-96] to engineer the product characteristics.

Figure 4-6c shows the seed and product CSDs of experiment 4.1_{TC}. Again, the increase of the product crystal sizes can be observed. The corresponding samples harvested at different times after the start-up of the process were nearly identical. The product CSD of the sample where the last 0.15m of the crystallizer were exposed to ultrasonic irradiation was smaller in comparison. This is due to the reduction of aggregates and agglomerates and possibly due to the breakage of crystals due to energy input.[62,69,97]

Figure 4-6d shows the seed and product crystals of experiment 4.1_{Tc}. As can be seen there was a significant growth of crystals in the crystallizer. The product crystals are clearly larger, and the size increase may be attributed to a great extent to crystal growth and not only to the aggregation and agglomeration of smaller crystallites, which always takes place during bulk crystallization processes.[98]

4.4 Summary and Conclusion

A continuously seeded flow-through crystallizer system with an inner diameter of 2 mm and an overall length of 27 m was demonstrated in this study. The seeds were generated *in situ* via the cooling of the stock solution and ultrasonic irradiation. The

seed loadings were changed in order to yield a different-sized bulk product. Optionally, a temperature cycle was used to dissolve the fines in order to grow larger product crystals. To provide sufficient time for significant crystal growth the flow rate was kept low below the critical Reynolds number (Re_{crit} ~ 2200). Thus, a laminar flow regime was obtained in earlier experiments.[35,36] In order to minimize the residence time distribution of the slurry in the tubing, air bubbles were introduced into the system to generate a segmented flow.

The findings were:

- Seed generation via ultrasound-assisted precipitation resulted in constant seed quantity and quality.
- Air-bubbles successfully yielded a segmented gas-slurry flow and minimized the residence time distribution of the slurry in the crystallizer.
- All experiments resulted in product yields of a few g/min and in crystals with relatively narrow CSDs and considerably increased sizes in comparison to the seeds.
- Steady-state conditions were rapidly reached in the tubing according to the crystal mass yield and CSDs.
- Increasing seed loadings resulted in decreased product crystal sizes, since more individual particles were introduced into the system to consume the same amount of supersaturation.
- Fines control via rapid heating of the seed suspension in the tubing resulted in larger product crystals than those obtained without the temperature cycle.

In general, the current study showed how the continuous tubular flow crystallizer yielded a product with a volume-mean diameter size from ~20 to 190 µm in a controlled way via altering the seed loading and fines removal. If an online tool were in use to measure (for example) the x_{50} or the cord length distribution (CLD) of the product crystals, a controlled increase of the size can be easily achieved by increasing the solution feed rate or by enhancing the fines removal (e.g., by increasing the temperature of the temperature cycle bath). Simon and Myerson[99] recently presented the use of an FBRM probe that was implemented perpendicularly on the flow in a tubular crystallizer to measure the CLD and Borchert and Sundmacher[12] followed the size and the shape of particles in a flow through cell (QicPic-Lixell, Sympatec).

Traditional scale-up via increasing the diameter of the tubular crystallizer appears to be difficult, since air bubbles were observed to move above the slurry as soon as the inner diameter was altered to 3mm.

To increase the product mass higher throughput or parallel pipes may be applicable. To perform a numbering-up approach would guarantee identical time scales (e.g., for reaching steady state conditions, heat and mass transfer etc.).

Rammeloo suggested to frequently introduce pure solvent between air bubbles into the system in order to establish an in process cleaning procedure. Pressure drop could be an indicator for launching the cleaning cycle.

The choice of crystallizer surface material and the cooling policy can reduce the tendency of crust formation, as recently demonstrated by Abohamra and Ulrich.[100] Thus, a relatively low frequency for cleaning cycles may be achieved.

Generally, slow crystallization (at low supersaturation) yields pure crystals with little impurity incorporations into the crystal lattice and mother liquor inclusions. This implies a long crystallization time and, ultimately, long tubular crystallizers. By adjusting the temperature trajectory, and hence the supersaturation, an optimum between sufficiently fast crystal growth, high purity, length of crystallizer and flow rate can be established.

Therefore, this concept might be applicable to final (re-) crystallization steps from almost pure solvents with the aim to achieve narrow CSDs. In cases where rapid cooling results in supersaturation that exceeds the metastable limit and hence promotes nucleation, additional temperature cycles for fines removal between each cooling step could be used to obtain bulk product with narrow CSDs.

4.5 References

(1) Shekunov, B. Y.; York, P., *J. Cryst. Growth* **2000,** *211* (1-4), 122-136.

(2) Alvarez, A. J.; Myerson, A. S., *Cryst. Growth Des.* **2010,** *10* (5), 2219-2228.

(3) O'Sullivan, B.; Barrett, P.; Hsiao, G.; Carr, A.; Glennon, B., *Org. Process Res. Dev.* **2003,** *7* (6), 977-982.

(4) Paul, E. L.; Tung, H.-H.; Midler, M., *Powder Technol.* **2005,** *150* (2), 133-143.

(5) Simon, L. L.; Nagy, Z. K.; Hungerbuhler, K., *Org. Process Res. Dev.* **2009,** *13* (6), 1254-1261.

(6) Simon, L. L.; Oucherif, K. A.; Nagy, Z. K.; Hungerbuhler, K., *Ind. Eng. Chem. Res.* **2010,** *49* (20), 9932-9944.

(7) Simon, L. L.; Abbou Oucherif, K.; Nagy, Z. K.; Hungerbuhler, K., *Chem. Eng. Sci.* **2010,** *65* (17), 4983-4995.

(8) Borchert, C.; Nere, N.; Ramkrishna, D.; Voigt, A.; Sundmacher, K., *Chem. Eng. Sci.* **2009,** *64* (4), 686-696.

(9) Gadewar, S. B.; Doherty, M. F., *J. Cryst. Growth* **2004,** *267* (1-2), 239-250.

(10) Steyer, C.; Sundmacher, K., *J. Cryst. Growth* **2009,** *311* (9), 2702-2708.

(11) Simon, L. L.; Nagy, Z. K.; Hungerbuhler, K., *Chem. Eng. Sci.* **2009,** *64* (14), 3344-3351.

(12) Borchert, C.; Sundmacher, K., *Chem. Eng. Technol.* **2011,** *34* (4), 545-556.

(13) Fujiwara, M.; Nagy, Z. K.; Chew, J. W.; Braatz, R. D., *J. Process Control* **2005,** *15* (5), 493-504.

(14) Chow, K.; Tong, H. H. Y.; Lum, S.; Chow, A. H. L., *J. Pharm. Sci.* **2008,** *97* (8), 2855-2877.

(15) Kadam, S. S.; van der Windt, E.; Daudey, P. J.; Kramer, H. J. M., *Cryst. Growth Des.* **2010,** *10* (6), 2629-2640.

(16) Chen, J.; Sarma, B.; Evans, J. M. B.; Myerson, A. S., *Cryst. Growth Des.* **2011,** *11* (4), 887-895.

(17) Oullion, M.; Puel, F.; Fevotte, G.; Righini, S.; Carvin, P., *Chem. Eng. Sci.* **2007,** *62* (3), 833-845.

(18) Winn, D.; Doherty, M. F., *AIChE J.* **2000,** *46* (7), 1348-1367.

(19) Lovette, M. A.; Browning, A. R.; Griffin, D. W.; Sizemore, J. P.; Snyder, R. C.; Doherty, M. F., *Ind. Eng. Chem. Res.* **2008,** *47* (24), 9812-9833.

(20) Griffin, D. W.; Mellichamp, D. A.; Doherty, M. F., *Chem. Eng. Sci.* **2010,** *65* (21), 5770-5780.

(21) Veesler, S.; Lafferrere, L.; Garcia, E.; Hoff, C., *Org. Process Res. Dev.* **2003,** *7* (6), 983-989.

(22) Iacocca, R. G.; Burcham, C. L.; Hilden, L. R., *J. Pharm. Sci.* **2010,** *99* (1), 51-75.

(23) Beckmann, W., *Org. Process Res. Dev.* **2000,** *4* (5), 372-383.

(24) Blagden, N.; de Matas, M.; Gavan, P. T.; York, P., *Adv. Drug Delivery Rev.* **2007,** *59* (7), 617-630.

(25) Llinas, A.; Goodman, J. M., *Drug Discovery Today* **2008,** *13* (5-6), 198-210.

(26) Mangin, D.; Puel, F.; Veesler, S., *Org. Process Res. Dev.* **2009,** *13* (6), 1241-1253.

(27) Müller, M.; Meier, U.; Wieckhusen, D.; Beck, R.; Pfeffer-Hennig, S.; Schneeberger, R., *Cryst. Growth Des.* **2006,** *6* (4), 946-954.

(28) Variankaval, N.; Cote, A. S.; Doherty, M. F., *AIChE J.* **2008,** *54* (7), 1682-1688.

(29) Auer, M. E.; Griesser, U. J.; Sawatzki, J., *J. Mol. Struct.* **2003,** *661-662* (0), 307-317.

(30) Bernstein, J., *Cryst. Growth Des.* **2011,** *11* (3), 632-650.

(31) Lindenberg, C.; Krattli, M.; Cornel, J.; Mazzotti, M.; Brozio, J. r., *Crystal Growth & Design* **2009,** *9* (2), 1124-1136.

(32) Gros, H.; Kilpiö, T.; Nurmi, J., *Powder Technol.* **2001,** *121* (1), 106-115.

(33) Oullion, M.; Puel, F.; Fevotte, G.; Righini, S.; Carvin, P., *Chem. Eng. Sci.* **2007,** *62* (3), 820-832.

(34) Alvarez, A. J.; Singh, A.; Myerson, A. S., *Cryst. Growth Des.* **2011,** *11* (10), 4392-4400.

(35) Eder, R. J. P.; Radl, S.; Schmitt, E.; Innerhofer, S.; Maier, M.; Gruber-Woelfler, H.; Khinast, J. G., *Cryst. Growth Des.* **2010,** *10* (5), 2247-2257.

(36) Eder, R. J. P.; Schmitt, E. K.; Grill, J.; Radl, S.; Gruber-Woelfler, H.; Khinast, J. G., *Cryst. Res. Technol.* **2011,** *46* (3), 227-237.

(37) Beck, C.; Dalvi, S. V.; Dave, R. N., *Chem. Eng. Sci.* **2010,** *65* (21), 5669-5675.

(38) Dalvi, S. V.; Dave, R. N., *Ind. Eng. Chem. Res.* **2009,** *48* (16), 7581-7593.

(39) Dong, Y.; Ng, W. K.; Shen, S.; Kim, S.; Tan, R. B. H., *Int. J. Pharm.* **2011,** *410* (1-2), 175-179.

(40) Brenek, S. J.; Am Ende, D. J. Crystallization Method and Apparatus Using an Impinging Plate Assembly US Patent 0040098839, 2004.

(41) Midler, M.; Liu, P. D.; Paul, E. L.; Futran, N.; Whittington, E. F. A Crystallization Method to Improve Crystal Structure and Size. EP Patent 0461930A1, 1991.

(42) Ferguson, S.; Morris, G.; Barrett, M.; Hao, H.; Glennon, B. ISIC 18. In *Design and Optimization of Plug Flow Crystallizers* Zurich, 2011.

(43) Panagiotou, T.; Mesite, S. V.; Fisher, R. J., *Ind. Eng. Chem. Res.* **2009,** *48* (4), 1761-1771.

(44) Ildefonso, M.; Candoni, N.; Veesler, S., *Cryst. Growth Des.* **2011,** *11* (5), 1527-1530.

(45) Su, Y. F.; Kim, H.; Kovenklioglu, S.; Lee, W. Y., *J. Solid State Chem.* **2007,** *180* (9), 2625-2629.

(46) Dombrowski, R. D.; Litster, J. D.; Wagner, N. J.; He, Y., *Chem. Eng. Sci.* **2007,** *62* (17), 4802-4810.

(47) Gerdts, C. J.; Tereshko, V.; Yadav, M. K.; Dementieva, I.; Collart, F.; Joachimiak, A.; Stevens, R. C.; Kuhn, P.; Kossiakoff, A.; Ismagilov, R. F., *Angewandte Chemie International Edition* **2006,** *45* (48), 8156-8160.

(48) Myerson, A. S. Molecular Crystals of Controlled Size US Patent 0030170999, 2003.

(49) Raphael, M.; Rohani, S.; Sosulski, F., *The Canadian Journal of Chemical Engineering* **1995,** *73* (4), 470-483.

(50) Virkar, P. D.; Hoare, M.; Chan, M. Y. Y.; Dunnill, P., *Biotechnol. Bioeng.* **1982,** *24* (4), 871-887.

(51) Rivera, T.; Randolph, A. D., *Ind. Eng. Chem. Process Des. Dev.* **1978,** *17* (2), 182-188.

(52) Ståhl, M.; Åslund, B. L.; Rasmuson, Å. C., *AIChE J.* **2001,** *47* (7), 1544-1560.

(53) Lawton, S.; Steele, G.; Shering, P.; Zhao, L.; Laird, I.; Ni, X.-W., *Org. Process Res. Dev.* **2009,** *13* (6), 1357-1363.

(54) Mendez del Rio, J.; Rousseau, R. W., *Cryst. Growth Des.* **2006,** *6* (6), 1407-1414.

(55) Eder, R. J. P.; Gruber-Wölfler, H.; Khinast, J. G., *CIT* **2009,** *81* (8), 1171-1171.

(56) Eder, R. J. P.; Schmitt, E.; Grill, J.; Radl, S.; Gruber-Wölfler, H.; Khinast, J. G., *CIT* **2010,** *82* (9), 1469-1470.

(57) Vacassy, R.; Lemaître, J.; Hofmann, H.; Gerlings, J. H., *AIChE J.* **2000,** *46* (6), 1241-1252.

(58) Khan, S. A.; Guenther, A.; Schmidt, M. A.; Jensen, K. F., *Langmuir* **2004,** *20* (20), 8604-8611.

(59) Jones, A.; Rigopoulos, S.; Zauner, R., *Comput. Chem. Eng.* **2005,** *29* (6), 1159-1166.

(60) Schiewe, J.; Zierenberg, B. Process and Apparatus for Producing Inhalable Medicaments. US Patent, 0015194A1, 2003.

(61) Jongen, N.; Lemaître, J.; Bowen, B.; Donnet, M.; Schiewe, J.; Zierenberg, B.; Soare, B. Process and Reactor for the Manufacture of Powders of Inhalable Medicaments. WO 04/304943, 2004.

(62) Devarakonda, S.; Evans, J. M. B.; Myerson, A. S., *Cryst. Growth Des.* **2004,** *4* (4), 687-690.

(63) de Castro, M. D. L.; Priego-Capote, F., *Ultrason. Sonochem.* **2007,** *14* (6), 717-724.

(64) Lyczko, N.; Espitalier, F.; Louisnard, O.; Schwartzentruber, J., *Chem. Eng. J.* **2002,** *86* (3), 233-241.

(65) Miyasaka, E.; Kato, Y.; Hagisawa, M.; Hirasawa, I., *J. Cryst. Growth* **2006,** *289* (1), 324-330.

(66) Miyasaka, E.; Ebihara, S.; Hirasawa, I., *J. Cryst. Growth* **2006,** *295* (1), 97-101.

(67) Kim, Y. H.; Lee, K.; Koo, K. K.; Shul, Y. G.; Haam, S., *Cryst. Res. Technol.* **2002,** *37* (9), 928-944.

(68) Guo, Z.; Zhang, M.; Li, H.; Wang, J.; Kougoulos, E., *J. Cryst. Growth* **2005,** *273* (3-4), 555-563.

(69) Zeiger, B. W.; Suslick, K. S., *J. Am. Chem. Soc.* **2011,** *133* (37), 14530-14533.

(70) Kim, S.; Wei, C.; Kiang, S., *Org. Process Res. Dev.* **2003,** *7* (6), 997-1001.

(71) McCausland, L. J.; Cains, P. W.; Martin, P. D., *Chem. Eng. Prog.* **2001,** *97*, 56-61.

(72) Gracin, S.; Uusi-Penttila, M.; Rasmuson, A. C., *Cryst. Growth Des.* **2005,** *5* (5), 1787-1794.

(73) Ambrus, R.; Amirzadi, N. N.; Sipos, P.; Szabó-Révész, P., *Chem. Eng. Technol.* **2010,** *33* (5), 827-832.

(74) Ruecroft, G.; Hipkiss, D.; Ly, T.; Maxted, N.; Cains, P. W., *Org. Process Res. Dev.* **2005,** *9* (6), 923-932.

(75) Li, H.; Wang, J.; Bao, Y.; Guo, Z.; Zhang, M., *J. Cryst. Growth* **2003,** *247* (1-2), 192-198.

(76) Narducci, O.; Jones, A. G.; Kougoulos, E., *Chem. Eng. Sci.* **2011,** *66* (6), 1069-1076.

(77) Narducci, O.; Jones, A. G.; Kougoulos, E., *Cryst. Growth Des.* **2011,** *11* (5), 1742-1749.

(78) Zumstein, R. C.; Rousseau, R. W., *AIChE J.* **1987,** *33* (1), 121-129.

(79) Bohlin, M.; Rasmuson, A. C., *AIChE J.* **1992,** *38* (12), 1853-1863.

(80) Larson, M. A.; White, E. T.; Ramanarayanan, K. A.; Berglund, K. A., *AIChE J.* **1985,** *31* (1), 90-94.

(81) Patience, D. B.; Dell'Orco, P. C.; Rawlings, J. B., *Org. Process Res. Dev.* **2004,** *8* (4), 609-615.

(82) Haseltine, E. L.; Patience, D. B.; Rawlings, J. B., *Chem. Eng. Sci.* **2005,** *60* (10), 2627-2641.

(83) Maia, G. D.; Giulietti, M., *J. Chem. Eng. Data* **2008,** *53* (1), 256-258.

(84) Jinno, J.-i.; Kamada, N.; Miyake, M.; Yamada, K.; Mukai, T.; Odomi, M.; Toguchi, H.; Liversidge, G. G.; Higaki, K.; Kimura, T., *J. Controlled Release* **2006,** *111* (1-2), 56-64.

(85) Mosharraf, M.; Nyström, C., *Int. J. Pharm.* **1995,** *122* (1-2), 35-47.

(86) Chung, S. H.; Ma, D. L.; Braatz, R. D., *The Canadian Journal of Chemical Engineering* **1999,** *77* (3), 590-596.

(87) Jagadesh, D.; Kubota, N.; Yokota, M.; Doki, N.; Sato, A., *J. Chem. Eng. Jpn.* **1999,** *32* (4), 514-520.

(88) Kubota, N.; Doki, N.; Yokota, M.; Jagadesh, D., *J. Chem. Eng. Jpn.* **2002,** *35* (11), 1063-1071.

(89) Kubota, N.; Doki, N.; Yokota, M.; Sato, A., *Powder Technol.* **2001,** *121* (1), 31-38.

(90) Lung-Somarriba, B. L. M.; Moscosa-Santillan, M.; Porte, C.; Delacroix, A., *J. Cryst. Growth* **2004,** *270* (3-4), 624-632.

(91) Aamir, E.; Nagy, Z. K.; Rielly, C. D., *Cryst. Growth Des.* **2010,** *10* (11), 4728-4740.

(92) Huang, D. C.; Liu, W.; Zhao, S. K.; Shi, Y. Q.; Wang, Z. X.; Sun, Y. M., *Chem. Eng. J.* **2010,** *156* (2), 360-365.

(93) Rawlings, J. B.; Miller, S. M.; Witkowski, W. R., *Ind. Eng. Chem. Res.* **1993,** *32* (7), 1275-1296.

(94) Rohani, S.; Paine, K., *The Canadian Journal of Chemical Engineering* **1991,** *69* (1), 165-172.

(95) Tadayyon, A.; Rohani, S., *The Canadian Journal of Chemical Engineering* **2000,** *78* (4), 663-673.

(96) Tavare, N. S., *AIChE J.* **1986,** *32* (5), 705-732.

(97) Devarakonda, S.; Evans, J. M. B.; Myerson, A. S., *Cryst. Growth Des.* **2003,** *3* (5), 741-746.

(98) Linnikov, O. D., *Cryst. Res. Technol.* **2008,** *43* (12), 1268-1277.

(99) Simon, L. L.; Myerson, A. S. ISIC 18. In *Continuous Antisolvent Plug-Flow Crystallization of a Fast Growing API* Zurich, 2011.

(100) Abohamra, E.; Ulrich, J., *CIT* **2010,** *82* (7), 1081-1084.

5. Summary of Major Findings

Chapter two to four are based on partially already published journal papers by Eder et al. in which several parameters and strategies to tailor the crystal size and to get narrow size distributions of the bulk product in the tubular crystallization device are detailed.

In chapter two comparative studies were performed using different ASA-EtOH suspension flow rates (11.4 [ml/min], 17.2 [ml/min], 22.8 [ml/min], 25.2 [ml/min]) in a 15 m long continuously seeded, continuously operated tubular crystallizer. The findings are:

- The concept of a continuously operated tubular crystallizer is feasible, since effects such as pipe plugging can be managed in a straightforward way. Only seed feed flows of 2.5 [ml/min] or less resulted in crystallizer blockage at rare occasions. The reason for the blockage was nucleation in all cases due to the lack of seeds in the crystallizer and the supersaturation of the feed stream.
- All experiments showed an increase of the mean diameter and a shift of the volume density distributions towards significantly larger values for the product crystals.
- Steady state conditions in the crystallizer were reached rapidly according to masses and CSDs of the product samples 1 and 2 of each experiment.
- Increasing flow rates at constant crystallizer design (i.e., length & diameter) rendered the crystals less time to grow and hence the final crystal size decreased. This effect was certainly amplified by reduced agglomeration tendencies due to higher shear rates that are associated with the increasing flow rates.

In chapter three the tubing was 15 m long and the temperature trajectory was flattened by putting three cylinders on which the crystallizer was coiled into temperature bathes at defined temperatures. The amount of individual seed crystals was altered by increasing the seed loading (i.e., seed mass per ml of slurry) or increasing the seed size at constant seed loading. Additionally, the spatial orientation of the coils was altered in order to find out if this would have an influence on size segregation of the crystals in the tubing.

The major findings were:

- Again, all experiments resulted in mass gains of a few g/min due to crystal growth and in product crystals of considerably increased size in comparison to the seeds.
- As established in the first experiments a steady-state condition in the crystallizer was reached rapidly.
- Increasing seed loadings resulted in decreased differences between the mean seed and product crystal sizes, since more individual particles were introduced into the system to consume the same amount of supersaturation.
- Reducing seed sizes while keeping the seed mass per ml slurry constant resulted in smaller differences between the seed and product crystal sizes, since more individual crystals consumed the supersaturation.
- The orientation of the coiled crystallizer had no significant effect on particle segregation.
- Several cooling sections can be utilized to control the temperature profile, and thus, the supersaturation trajectory. The cooling curve was set to keep the supersaturation high enough to obtain reasonable crystal growth rates but low enough to avoid the formation of new nuclei.

In chapter four the crystallizer was 27 m long. This time the crystallizer was coiled on four cylinders and put into four thermostatic bathes to define a relatively flat cooling trajectory. Additionally, seeds were generated in situ in the tubing via cooling and ultrasonic irradiation. Furthermore, temperature cycling was employed for fines removal via dissolution. In addition air-bubbles were introduced into the system in order to get defined, narrow residence time distributions.

The major findings were:

- Seed generation via ultrasound-assisted precipitation resulted in constant seed quantity and quality.
- Air-bubbles successfully yielded a segmented gas-slurry flow and minimized the residence time distribution of the slurry in the crystallizer.
- All experiments resulted in the product yields of a few g/min and in crystals with relatively narrow CSDs and considerably increased sizes in comparison to the seeds.
- Steady-state conditions were rapidly reached in the tubing according to the crystal mass yield and CSDs.

- Increasing seed loadings resulted in the decreased product crystal sizes, since more individual particles were introduced into the system to consume the same amount of supersaturation.
- Fines control via rapid heating of the seed suspension in the tubing resulted in larger product crystals than those obtained without the temperature cycle.

5. Outlook

Generally, a capable, very versatile crystallization system has been designed and tested and detailed in this thesis. Simple measures, such as varying seed loading, seed size, flow rates and employing fines removal are very effective to tailor the mean crystal size.Product with a volume-mean diameter size from ~20 to 190 µm in a controlled way was generated.

Online tools could be uses to measure (for example) the x_{50} or the cord length distribution (CLD) of the product crystals. Thus, a controlled increase of the size can be easily achieved by increasing the solution feed rate or by enhancing the fines removal (e.g., by increasing the temperature of the temperature cycle bath). Simon and Myerson[f] recently presented the use of an FBRM probe that was implemented perpendicularly on the flow in a tubular crystallizer to measure the CLD and Borchert and Sundmacher[g] followed the size and the shape of particles in a flow through cell (QicPic-Lixell, Sympatec).

To further develope the simulation models together with the implementation of Process Analytical Technology (PAT) tools as mentioned above could form the basis for feed-back and forward control of the crystallization with respect to the CSD. This may enable the process to quickly adjust parameters to keep product quality attributes as the mean crystal size and the corresponding distribution constant even with altering seed size and quantity.

Traditional scale-up via increasing the diameter of the tubular crystallizer appears to be difficult, since air bubbles were observed to move above the slurry as soon as the inner diameter was altered to 3mm.

To increase the product mass higher throughput or parallel pipes may be applicable. To perform a numbering-up approach would guarantee identical time scales (e.g., for reaching steady state conditions, heat and mass transfer etc.).

[f] Simon, L. L.; and Myerson, A. S. ISIC 18. In Continuous Antisolvent Plug-Flow Crystallization of a fast Growing API Zurich, 2011.
[g] Borchert, C.; Sundmacher, K., *Chem. Eng. Technol*. **2011**, 34 (4), 545-556

To establish an in process cleaning procedure pure solvent can be frequently introduced into the system between air bubbles. Pressure drop could be an indicator for launching the cleaning cycle.

The choice of crystallizer surface material and the cooling policy can reduce the tendency of crust formation, as recently demonstrated by Abohamra and Ulrich.[h] Thus, a relatively low frequency for cleaning cycles may be achieved.

In cases where rapid cooling results in supersaturation that exceeds the metastable limit and hence promotes nucleation, additional temperature cycles for fines removal between each cooling step could be established to obtain bulk product with narrow CSDs.

The excellent temperature control and the possibility to attain short residence times may aid in polymorphism control, which is one of the most important issues in API crystallization, as different polymorphs exhibit different physical properties (e.g., solubility) and therefore altered bioavailability.

One of the approaches for controlling crystal modifications is to use seeds of the desired target polymorph and to create, depending on the individual substance (e.g., Paracetamol, abecarnil, etc.), an environment in the continuous tubular crystallizer that allows crystallization but not transformation of seeds into other polymorphs, or hydrates and other solvates. This is usually straightforward when the desired polymorph is the most stable one at given conditions; however, also seeding a metastable form can be successful. For the latter case solvent-mediated transformation is the main problem. The possibility to operate the continuous tubular crystallizer with short residence times provides the opportunity to harvest the metastable polymorph before solvent-mediated transformation occurs. Transformation in the dry state is less commonly observed due to the decreased mobility of molecules in the solid state.[i] Mendez del Rio and Rousseau[j] provided strong evidence for the presence of the less stable polymorph form II of paracetamol by employing a laminar flow tubular-batch crystallization device. In their conclusion they suggested that fast extraction of unstable form II could be effective to preserve that form. The possibility for rapid sequestration and drying of product is one of the inherent characteristics of the continuous tubular crystallizer. Thus, it can be expected that it is possible to extract metastable forms of target substances via

[h] Abohamra, E.; Ulrich, J., *CIT* **2010**, 82 (7), 1081-1084.
[i] Beckmann, W.; *Org. Proc. Res. Dev.* **2000**, 4 (5), 372-383
[j] Méndez del Rio, J. R.; Rousseau, R. W.; *Cryst. Growth Des.* **2006**, 6 (6), 1407-1414

seeding techniques and direct nucleation of a less stable polymorph due to e.g., rapid cooling. Often the least stable polymorph is formed first via nucleation and might be transformed step-wise into more stable forms (Ostwald rules of stages).

In short, seeding with a metastable or a stable crystal form, direct nucleation and creating an environment to favor the formation of a certain crystal modification, may be effective measures to obtain targeted crystal modifications in the tubular crystallizer.

Thus the field of research can be considerably broadened into several directions. On the long range it even appears to be achievable to directly modify the crystals at the outlet with additional tubular devices in which a coating is deposited on the crystal core to tailor the particle characteristics. This is a step towards multifunctional engineered particles. Several commercially aqueous polymer dispersions are suitable for the coating of pharmaceutical dosage forms to modify and control drug release (e.g., prolonging time of activity or enteric coating) or simply for taste masking.

THE END

6. Publications

Publications in refereed journals

- R. J. P. Eder, S. Schrank, M. O. Besenhard, E. Roblegg, H. Gruber-Wölfler, J. G. Khinast, Continuous Sonocrystallization of ASA: Control of Crystal Size, *Crystal Growth and Design*, **2012**, submitted
- R. J. P. Eder, E. K. Schmitt, J. Grill, S. Radl, H. Gruber-Wölfler, J. G. Khinast, Seed Loading Effect on the Mean Crystal Size of Acetylsalicylic Acid in a Continuous-Flow Crystallization Device, *Crystal Research and Technology*, **2011**, 46, 227-237
- R. J. P. Eder, S. Radl, E. Schmitt, S. Innerhofer, M. Maier, H. Gruber-Wölfler, J. G. Khinast, Continuously Seeded Continuously Operated Tubular Crystallizer for the Production of Active Pharmaceutical Ingredients, *Crystal Growth and Design*, **2010**, 10 (5), 2247-2257
- C. Jeanquartier, G. Schider, S. Feichtenhofer, H. Schwab, R. Schennach, J. Stettner, A. Winkler, H. Gruber-Woelfler, G. Schitter, R. J. P. Eder, J. G. Khinast, A Two-step Method to Covalently Bind Biomolecules to Group-IV Semiconductors: Si(111)/1,2-Epoxy-9-decene/Esterase, *Langmuir*, **2008**, 24, 13957-13961

Conference proceedings

- R. J. P. Eder, M. Besenhard, S. Schrank, E. Roblegg, H. Gruber-Woelfler, J. Khinast. API Crystallization in a Continuous-Flow Equipment. Book of Abstracts ISIC18, **2011**, 74-75
- R. J. P. Eder, J. Grill, E. K. Schmitt, M. O. Besenhard, S. Schrank, E. Roblegg, S. Radl, H. Gruber-Wölfler, J. Khinast. API-Kristallisation in einem Rohr. Tagungsband 7. Minisymposium der Verfahrenstechnik, **2011**, 81-82
- M. O. Besenhard, A. Eitzlmayr, R. J. P. Eder, D. Suzzi, J. G. Khinast, Theory and Application of Population Balance Equations in Chemical Engineering. Tagungsband Minisymposium der Verfahrenstechnik 7, **2011**, 11-13
- R. J. P. Eder, J. Grill, E. K. Schmitt, S. Schrank, R. Roblegg, M. Besenhard, S. Radl, H. Gruber-Wölfler, J. G. Khinast, Continuous Flow

Crystallization of Active Pharmaceutical Ingredients. Pharmaceutical Sciences for the Future of Medicines 3, EUFEPS, **2011**, 137 – 138

– R. J. P. Eder, J. Grill, E. K. Schmitt, S. Radl, M. Maier, S. Innerhofer, H. Gruber-Wölfler, J. G. Khinast, Kontinuierliches Wachstum von pharmazeutischen Impf- zu Produktkristallen in einem Rohr. Tagungsband Minisymposium der Verfahrenstechnik 6, **2010**, 121 – 122

– R. J. P. Eder, E. K. Schmitt, J. Grill, S. Radl, H. Gruber-Wölfler, J. G. Khinast, Kontinuierliches Wachstum von API Impf- zu Produktkristallen in einem Rohrkristallisator, *Chemie-Ingenieur-Technik*, **2010**, 82 (9), 1469 - 1470

– R. J. P. Eder, S. Radl, E. K. Schmitt, S. Innerhofer, M. Maier, H. Gruber-Wölfler, J. G. Khinast, Preparation of APIs in a continuously seeded, continuously operated tubular crystallizer. International Congress of Chemical and Process Engineering Summaries 5 System and technology, **2010**, 1899 – 1900

– R. J. P. Eder, E. K. Schmitt, J. Grill, M. Maier, S. Innerhofer, S. Radl, H. Gruber-Wölfler, J. G. Khinast, Crystallization of APIs in a continuously seeded tubular Crystallizer. Central European Symposium on Pharmaceutical Technology 8, Scientia Pharmaceutica, **2010**, 664

– R. J. P. Eder, H. Gruber-Wölfler, J. G. Khinast, Kontinuierliche Kristallisation in einem Rohrkristallisator, *Chemie Ingenieur Technik*, **2009**, 81, 1171

– H. Gruber-Wölfler, R. J. P. Eder, P. Feenstra, P. Radaschitz, V. Cappello, J. G. Khinast, Funktionalisierte Oberflächen für heterogene Katalyse, *Chemie Ingenieur Technik*, **2009**, 81, 1169-1170

– R. J. P. Eder, M. Maier, S. Innerhofer, S. Radl, H. Gruber-Wölfler, J. G. Khinast, Kontinuierliche Kristallisation von pharmazeutischen Wirkstoffen. Tagungsband Minisymposium Verfahrenstechnik 5, **2009**, 112 – 113

– H. Gruber-Woelfler, R. J. P. Eder, B. Wilding, I. Pflüger, G. Schider, E. Polo, J.G. Khinast, Development of Heterogeneous Organometallic Catalysts by Functionalisation of Silicon-based Solid Supports, *Chemie Ingenieur Technik*, **2008**, *80,* 1249

– H. Wölfler, R. J. P. Eder, G. Schitter, S. Rivillon, J. Khinast, Entwicklung von heterogenen Metallocen-Katalysatoren*, Chemie Ingenieur Technik*, **2007**, *79 (9),* 1367-1368

Presentations and talks

- R. J. P. Eder, J. Grill, E. K. Schmitt, S. Schrank, E. Roblegg, M. Besenhard, S. Radl, H. Gruber-Wölfler, J. G. Khinast. API-Crystal Preparation in a Continuously Seeded Tubular Crystallizer, AIChE Meeting, 16.10.-21.10., Minneapolis, USA, **2011**
- R. J. P. Eder, J. Grill, E. K. Schmitt, S. Schrank, E. Roblegg, M. Besenhard, S. Radl, H. Gruber-Wölfler, J. G. Khinast. Continuous-Flow API Crystallization. 5th International Congress on Pharmaceutical Engineering, Graz Austria, 29.09.-30.09., **2011**
- R. J. P. Eder, J. Grill, E. K. Schmitt, S. Radl, H. Gruber-Wölfler, J. G. Khinast. API-Crystallization in a Continuous-Flow Device. ProcessNet Annual Meeting, Berlin Germany, 26.09.-28.09., **2011**
- R. J. P. Eder, M. Besenhard, S. Schrank, E. Roblegg, H. Gruber-Woelfler, J. Khinast. API Crystallization in a Continuous-Flow Equipment. ISIC18, Zurich Swizerland, 12.09.-16.09., **2011**
- M. O. Besenhard, A. Eitzlmayr, R. J. P. Eder, D. Suzzi, J. G. Khinast:Theory and Application of Population Balance Equations in Chemical Engineering. Minisymposium der Verfahrenstechnik 7, Graz, 30.06.-01.07., **2011**
- R. J. P. Eder, E. K. Schmitt, J. Grill, S. Radl, H. Gruber-Wölfler, J. G. Khinast: Crystallization of API-crystals in a continuously seeded tubular crystallizer. AIChE, Salt Lake City, UT, USA, 06.11.-12.11., **2010**
- R. J. P. Eder, S. Radl, E. K. Schmitt, S. Innerhofer, M. Maier, H. Gruber-Wölfler, J. G. Khinast: Preparation of APIs in a continuously seeded, continuously operated tubular crystallizer. CHISA, Praha, 29.08.-01.09., **2010**
- R. J. P. Eder, E. K. Schmitt, J. Grill, S. Radl, H. Gruber-Wölfler, J. G. Khinast: Kontinuierliches Wachstum von API Impf- zu Produktkristallen in einem Rohrkristallisator. ProcessNet DECHEMA, Aachen 21.09.-23.09., **2010**
- R. J. P. Eder, S. Innerhofer, M. Maier, S. Radl, H. Gruber-Woelfler, J. G. Khinast Continuous Preparation of APIs in a Tubular Crystallizer, AIChE Annual Meeting, Nashville, TN, USA, November 8-13, **2009**
- H. Gruber-Woelfler, R. J. P. Eder, B.Wilding, I. Pflüger, P. Feenstra, P. Radaschitz, G. Schider, E. Polo, J. G. Khinast, Development of Heterogeneous

Catalysts for the Continuous Production of Pharmaceutical Substances, ACHEMA, Frankfurt, 11.-15. Mai, **2009**

– H. Gruber-Woelfler, R. J. P. Eder, B.Wilding, I. Pflüger, P. Feenstra, P. Radaschitz, V. Cappello, E. Polo, J. G. Khinast, Hybrid Organic-Inorganic Materials for Heterogeneous Catalysis: Development of supported Ti and Pd-Catalysts, 13. Österreichische Chemietage, Wien, 25.-28. August. **2009**

– H. Gruber-Wölfler, R. J. P. Eder, B. Wilding, I. Pflüger, G. Schider, E. Polo, J. G. Khinast, Controlled Immobilization of Organometallic Catalysts on Solid Supports and Their Application for Pharmaceutical Synthesis, International Graz Workshop for Pharmaceutical Engineering, Graz, May 15-16, **2008**

– H. Gruber-Woelfler; R. J. P. Eder; B. Wilding, I. Pflüger, G. Schider, J. G. Khinast, Development of Chiral Heterogeneous Titanocenes for the Synthesis of Pharmaceutical Intermediates, CHISA, Prague, August 24 – 28, **2008**

– H. Gruber-Woelfler, R. J. P. Eder, B. Wilding, I. Pflüger, G. Schider, E. Polo, J.G. Khinast, Development of Heterogeneous Organometallic Catalysts by Functionalization of Silicon-based Solid Supports, ProcessNet, Karlsruhe, October 7-9, **2008**

– H. Gruber-Woelfler, R. J. P. Eder, B. Wilding, I. Pflüger, P. Feenstra, G. Schider, A. Muhr, C. Kutschera, J. G. Khinast**,** Development of Continuous Processes for the Production of Pharmaceutical Substances Using Heterogeneous Catalysis, AIChE Annual Meeting, Philadelphia, USA, November 16 – 21, **2008**

– H. Gruber-Woelfler, R. J. P. Eder, B. Wilding, I. Pflüger, G. Schider, A. Muhr, P. Feenstra, E. Polo**,** J. G. Khinast, Design of Smart Heterogeneous Catalysts by Controlled Immobilization of Organometallic Compounds, AIChE Annual Meeting, Philadelphia, USA, November 16 – 21, **2008**

– H. Woelfler, G. Schitter, R. J. P. Eder, C. Jeanquartier, J. Khinast, Synthesis and Immobilization of Covalently Tethered Group 4 Metallocenes, 12. Österreichische Chemietage, September 10-13, Klagenfurt, **2007**

– H. Woelfler, G.Schitter, R. J. P. Eder, C. Jeanquartier, J. G. Khinast, Development of New Covalently Tethered Group 4 Metallocenes, AIChE Annual Meeting, Salt Lake City, USA, November 4-9, **2007**

Posters:

– M. Besenhard, R. J. P. Eder, D. Suzzi, A Quantitative Process Model for a Continuous-Flow API Crystallization, 5th International Congress on Pharmaceutical Engineering, Graz, 29.09.-30.09., **2011**

– R. J. P. Eder, J. Grill, E. K. Schmitt, M. Besenhard, S. Schrank, E. Roblegg, S. Radl, H. Gruber-Wölfler, J. G. Khinast, API-Kristallisation in einem Rohr, 7. Minisymposium der Verfahrenstechnik, Graz, AT, 30.06.-01.07., **2011**

– R. J. P. Eder, J. Grill, E. K. Schmitt, S. Schrank, R. Roblegg, M. Besenhard, S. Radl, H. Gruber-Wölfler, J. G. Khinast, Continuous Flow Crystallization of Active Pharmaceutical Ingredients. PharmSciFAir, Prag, CZ, 13.06-17.06., **2011**

– R. J. P. Eder, E. K. Schmitt, J. Grill, M. Maier, S. Innerhofer, S. Radl, H. Gruber-Wölfler, J. G. Khinast, Crystallization of APIs in a continuously seeded tubular crystallizer. International Graz Congress for Pharmaceutical Engineering, Graz, Austria, 16.09.-18.09., **2010**

– R. J. P. Eder, E. Schmitt, J. Grill, S. Radl, M. Maier, S. Innerhofer, H. Gruber-Wölfler, J. G. Khinast, Kontinuierliches Wachstum von pharmazeutischen Impf- zu Produktkristallen in einem Rohr, VT Minisymposium, Tulln, 25.06., **2010**

– R. J. P. Eder, S. Innerhofer, M. Maier, S. Radl, H. Gruber-Woelfler, J. G. Khinast Kontinuierliche Kristallisation von pharmazeutischen Wirkstoffen, 5. Minisymposium der Verfahrenstechnik, Wien, 24.-25.6., **2009**

– R. J. P. Eder, H. Gruber-Wölfler, J. G. Khinast, Kontinuierliche Kristallisation in einem Rohrkristallisator, *ProcessNet,* **2009**, 8.-10. September, Mannheim

– R. J. P. Eder, S. Innerhofer, M. Maier, S. Radl, H. Gruber-Wölfler, J. G. Khinast, Crystallization of APIs in a Continuously Operated Tubular Crystallizer, International Graz Congress for Pharmaceutical Engineering, Graz, 17.-18.9., **2009**

– H. Gruber-Wölfler, R. J. P. Eder, P. Feenstra, P. Radaschitz, V. Cappello, J. G. Khinast, Funktionalisierte Oberflächen für heterogene Katalyse, *ProcessNet,*, Mannheim, 8.-10. September **2009**

– H. Gruber-Woelfler, R. J. P. Eder, B. Wilding, I. Pflüger, V. Cappello, E. Polo, J. G. Khinast, Supported Titanocenes for the Heterogeneous

Hydrosilylation of Imines, AIChE Annual Meeting, Nashville, TN, USA, November 8-13, **2009**

– Eder, R. J.; Feenstra, P.; Gruber-Wölfler, H.; Khinast, J.: Heterogenization of Organometallic Catalysts and their Application in Pharmaceutical Engineering, 4 Minisymposium der Verfahrenstechnik, Montanuniversität Leoben, 03.07.**2008**

– H. Gruber-Wölfler, G. Schitter, R. J. P. Eder, C. Jeanquartier, G. Schider, J. G. Khinast, Development of Heterogeneous Group 4 Metallocenes. Pharmaceutical Engineering Meeting, Graz, Technische Universität, 01.06, **2007**

– G. Schitter, H. Gruber-Woelfler, C. Jeanquartier, R. J. P. Eder, G. Schider, J. Khinast, Funktionalisierung von Oberflächen mit katalytisch aktiven Molekülen, Minisymposium Verfahrenstechnik, Linz, 13. Juni, **2007**

– H. Woelfler, R. J. P. Eder, G. Schitter, S. Rivillon, Entwicklung von heterogenen Metallocen-Katalysatoren, ProcessNet-Jahrestagung, Aachen, Deutschland, 16. – 18. Oktober **2007**

Innovation:

– R. J. P. Eder, J. G. Khinast, H. Gruber-Wölfler, M. Maier, Continuous tubular crystallizer with a seed feed supply. Technische Universität Graz, Austria, **2009**

Funding and grants:

– J. G. Khinast, R. J. P. Eder, C. Kutschera, Development of a Versatile Continuous-Flow Crystallizer. FWF, Austria, **2010**, erteilt: Entscheidung steht aus

– J. G. Khinast, R. J. P. Eder, C. Kutschera, Kontinuierliche Kristallisation von pharmazeutischen Wirkstoffen in einem neuartigen Energie- und Stoffstrom-optimierten Rohrkristallisator. Zukunfdsfonds des Landes Steiermark, Austria, **2009**, erteilt: € 5000

Diploma-thesis (Eder):

– R. J. P. Eder, Development of Heterogeneous Group 4 Metallocenes for the Synthesis of Active Pharmaceutical Ingredients, J. G. Khinast, H. Gruber-Wölfler, Technische Universität Graz, Austria, **2007**

Diploma-thesis (supervised):

– S. Innerhofer, Development of a Continuously Operated Tubular Crystallizer for the Production of Active Pharmaceutical Ingredients and Fine Chemicals; J. G. Khinast, R. J. P. Eder, H. Gruber-Wölfler, Technische Universität Graz, Austria, **2010**

– E. K. Schmitt, Continuously Seeded Tubular Crystallizer: Influence of Seed-Loading, Flow Rates and Cooling Trajectory on the Crystal Size Distribution of APIs and Fine Chemicals; J. G. Khinast, R. J. P. Eder, Technische Universität Graz, Austria, **2010**

– J. Grill, Continuously Seeded Tubular Crystallizer: Target Substances; J. G. Khinast, R. J. P. Eder, Technische Universität Graz, Austira, **2010**, work in progress

Bachelor thesis (supervised):

– M. Maier, Continuous Crystallization of Active Pharmaceutical Ingredients (APIs) in a tubular Reactor: Effect of Mean Residence Time on Crystal Size and Crystal Size Distribution; R. J. P. Eder, H. Gruber-Wölfler, J. G. Khinast, Technische Universität Graz, Austria, **2009**